INTERIM REPORT

Accession No.
LO-00-80-115

Contract Program or Project Title: LOFT PROGRAM

Subject of this Document: (Title) "The Effect of Cladding Surface Thermocouples on the Quench Behavior of an Electrical Heater Rod"

Type of Document: Technical R & D

Author(s): R. C. Gottula, J. A. Good

Date of Document: March 1980

Responsible NRC Individual and NRC Office or Division: G. D. McPherson



Prepared for
U.S. Nuclear Regulatory Commission
Washington, D.C. 20555

INTERIM REPORT

EG&G Idaho

# INTEROFFICE CORRESPONDENCE

R-5405

date MAR 19 1980

to DISTRIBUTION

from LOFT CDCS, TAN 602, Ext. 6177 S K Hathaway

subject DOCUMENT TRANSMITTAL

The following documents released by LOFT CDCS, are hereby transmitted for your use and information:

| DOCUMENT NO. | REV | CHG | DATE |
|---|---|---|---|
| LTR LO-00-80-115 | Ø | | 3-5-80 |
| "The Effect of Cladding Surface Thermocouples on the Quench Behavior of an Electrical Heater Rod" R. C. Gottula, J. A. Good | | | |

REMARKS: Reference A2, TREE 1334, NUREG CR 0837, will be published at a later date. No other disposition required.

DISTRIBUTION

M. Akimoto - 2
W. Amidei w/o Att.
B. O. Anderson
E. C. Anderson w/o Att.
J. G. Arendts
B. L. Chamberlain w/o Att.
G. A. Dinneen
D. B. Engelman
B. L. Freed-Orig.+7
R. T. French
R. C. Gottula - 10
R. C. Guenzler
J. C. Haire
J. Hansen
S. W. Hills
G. L. Hunt w/o Att.
F. K. Hyer w/o Att.
D. B. Jarrell
N. C. Kaufman w/o Att.
S. T. Kelppe
J. L. Liebenthal
A. S. Lockhart
J. H. Linebarger
D. W. Marshall w/o Att.
S. Matovich
G. D. McPherson
J. C. Morrow
S. A. Naff
N. E. Pace w/o Att.
T. F. Pointer
G. Rieger
P. Schally
D. G. Satterwhite w/o Att.
W. A. Spencer
J. C. Stachew w/o Att.
K. C. Sumpter
R. E. Tiller
S. R. Wagoner w/o Att.
G. Weimann
L. Winters
B. J. Yohn
J. A. Good
Tech Library - 2
W. J. Quapp WJQ/sh per telecon 3-5-80
L. P. Leach
J. V. Anderson
B. L. Barnes
T. R. Yackle
M. L. Carboneau
E. W. Coryell
R. L. Crumley
R. A. Cushman
D. J. Hanson
G. H. Hanson
J. C. Lin
P. E. McDonald
J. S. Martinell
M. G. Matras
C. L. Nalezny
C. S. Olsen
E. L. Tolman

FORM EG&G-954
(Rev. 2-77)

EG&G Idaho, Inc.

(LTR)

Report No. LO-00-80-115

Date: March 5, 1980

RELEASED BY LOFT CDCS

USNRC-P-394

# INTERNAL TECHNICAL REPORT

Title: THE EFFECT OF CLADDING SURFACE THERMOCOUPLES ON THE QUENCH BEHAVIOR OF AN ELECTRICAL HEATER ROD

Organization: LOFT TEST SUPPORT BRANCH

Author: R. C. Gottula, J. A. Good



Checked By: W. J. Quapp

Approved By: L. P. Leach

EG&G Idaho, Inc.

LOFT TECHNICAL REPORT
LOFT PROGRAM

FORM EG&G-229
(Rev. 12-78)

| TITLE | REPORT NO. |
|---|---|
| The Effect of Cladding Surface Thermocouples on the Quench Behavior of an Electrical Heater Rod | LO-00-80-115 |
| AUTHOR: R. C. Gottula and J. A. Good | SWA NO.: 53CAS01GN |
| PERFORMING ORGANIZATION: LOFT Test Support Branch | DATE: RELEASED BY LOFT CDCS March 5, 1980 |
| LOFT APPROVAL: [signature] LEPD Mgr. | |

## DISPOSITION OF RECOMMENDATIONS

Reference A2, TREE 1334, NUREG CR 0837, will be published at a later date. No other disposition required.

# THE EFFECT OF CLADDING SURFACE THERMOCOUPLES ON THE QUENCH BEHAVIOR OF AN ELECTRICAL HEATER ROD

By:

R. C. Gottula

J. A. Good

CONTENTS

TABLE OF CONTENTS (CONTINUED)

TABLES

TABLE OF CONTENTS (CONTINUED)

FIGURES

TABLE OF CONTENTS (CONTINUED)

FIGURES (CONTINUED)

## ABSTRACT

Tests have been conducted to evaluate the effect of cladding external surface thermocouples on the quench behavior of a single swaged electrical heater rod. The tests were successfully completed in the Blowdown Loop of the LOFT Test Support Facility (LTSF) at the Idaho National Engineering laboratory (INEL).

The results of the tests indicated that cladding external surface thermocouples significantly increase the cooldown rate and reduce the quench time of the swaged heater rod.

## SUMMARY

A test program is being conducted in the Blowdown Loop of the LOFT Test Support Facility (LTSF) to determine the effect of cladding external surface thermocouples on the quench behavior of electrical heater rods. The first phase of the tests, reported herein, was conducted on a single swaged electrical heater rod at both high pressure (7 MPa) and low pressure (ambient) conditions and over a wide range of flooding rates. The high pressure tests were intended to simulate the high pressure rewet conditions that occurred in the LOFT core during the blowdown phase of the LOFT L2-2 and L2-3 tests. The rod was tested both with and without cladding external thermocouples.

The results of the tests showed that on a swaged electrical heater rod, external thermocouples increase the cooldown rate of the rod during precursory cooling prior to quench and also cause the rod to quench from a higher temperature. For the tests at 7 MPa, this resulted in a reduction in the quench times for the rod with external thermocouples to approximately half those for the rod without external thermocouples. Although the results from these tests cannot be directly extrapolated to a nuclear fuel rod, due to the configuration and thermal diffusivity of the swaged heater rod, a similar effect is expected to occur on a nuclear fuel rod. However, the magnitude of the effect on a nuclear fuel rod is expected to be small since nuclear rods are anticipated to quench considerably faster than the electric rods used in these tests under the same flooding conditions. The magnitude of any thermocouple effect on the quench behavior of a nuclear fuel rod will be better evaluated during the second phase of the test program where a cartridge electrical heater rod will be used, better simulating the thermal characteristics of a nuclear fuel rod.

# 1. INTRODUCTION AND TEST OBJECTIVES

The Loss-of-Fluid Test (LOFT) facility is an integral nuclear reactor system designed to simulate, as nearly as possible, all of the important effects that are expected to occur during a loss-of-coolant accident (LOCA) in a large pressurized water reactor (LPWR) system. LOFT utilizes special experimental instrumentation which includes fuel rod cladding external surface thermocouples. The LOFT L2-2 and L2-3 tests experienced unexpected fuel rod quenching early in the blowdown of these loss-of-coolant experiments evidenced by the response of the surface thermocouples as shown in Figure 1. It has been postulated that the cladding surface thermocouples may cause premature quenching of the fuel rods to which they are attached as well as affect the thermal hydraulic environment of adjacent fuel rods.

The specific problem to be investigated was whether or not cladding external thermocouples cause premature quenching of the rods to which they are attached, as well as propagation of the quench phenomena to adjacent rods, which would otherwise not occur if cladding surface thermocouples were not present.

The purpose of the separate effects tests described herein was to investigate quench behavior under various hydraulic conditions to determine where a thermocouple effect might be significant, particularly at high pressure (7 MPa) where quenching occurred in the LOFT reactor during the L2-2 and L2-3 tests. The tests are being conducted in two phases. The first phase of testing, which has been completed and is reported herein, utilized a single swaged heater rod of the type used in the Semiscale[1], FLECHT[2] and ORNL[3] programs on LOCA testing sponsored by the United States Nuclear Regulatory Commission (USNRC). The heater rod had a 1.67 m heated length and stainless steel cladding and was placed in a 2.43 cm I.D. test vessel. The rod was tested both with and without cladding external thermocouples over a wide range of flooding conditions. Because of

the immediate availability of the swaged heater rod, the specific objectives of the first phase of testing were to: (a) provide preliminary information on the effect of cladding surface thermocouples on quench behavior, (b) to examine the method of testing and repeatability of test data in the Blowdown Loop at the LTSF, and (c) to scope the hydraulic conditions at which a thermocouple effect might occur to aid in developing a test matrix for the second phase of testing.

The second phase of testing will utilize a nine rod bundle in a 6.67 cm I.D. test vessel. The center rod in the bundle will be a German REBEKA heater rod which will be tested both with and without cladding surface thermocouples. This heater rod was chosen because its zircaloy cladding, built-in gap, and aluminum oxide pellet construction provide the closest simulation to a nuclear fuel rod of any electrical heater rod currently available. The eight peripheral heater rods will provide a geometry and thermal-hydraulic environment more typical of a nuclear rod cluster. The nine rod bundle will also incorporate grid spacers similar to those used in the LOFT core.

Included in this report is a description of the scope of the tests, the test facility, the test section, instrumentation and data processing, and the experimental procedure. This is followed by the results of the tests with plots comparing the quench times and cooldown rates of the electric heater rod with and without cladding surface thermocouples. Conclusions are then stated based on the test results.

# 2. EXPERIMENT DESCRIPTION

## 2.1 Scope of Tests

For the first phase of testing, thermal-hydraulic conditions in the LOFT core at the time the high pressure quench occurred were simulated by heating the heater rod to a high temperature in a fairly stagnant nitrogen environment, simulating film boiling on the LOFT fuel rods, and then subjecting the rod to a sudden surge of coolant as occurred during the LOFT tests.

The following test conditions were investigated:

### HIGH PRESSURE TESTS

| | |
|---|---|
| Pressure: | 7 MPa |
| Test Section Inlet Flooding Rate: | 0.4, 1.8, 3.0 and 6.0 m/sec |
| Initial Rod Temperature: | 775, 1025 and 1175 K |
| Test Section Inlet Fluid Quality: | 0 and 15 percent |

### LOW PRESSURE TESTS

| | |
|---|---|
| Pressure: | atmospheric |
| Flooding Rate: | 4 and 10 cm/sec |
| Initial Rod Temperature: | 1025 K |
| Inlet Fluid Temperature: | 300 K |

Eighteen test runs were first conducted on the rod with external thermocouples. The specified test conditions for each run are given in Table 1 and the actual test conditions are given in Appendix D. The external thermocouples were then removed from the rod and the same eighteen test runs were repeated. The test runs are listed in Appendix D in the actual sequence in which they were conducted. Run No. 11 was repeated 3 times (Runs 11A, 11B, and 24) during the course

of the testing to determine the repeatability of the tests and to determine any change in quench behavior from the beginning to the end of the test program.

TABLE 1. NOMINAL TEST CONDITIONS FOR PHASE 1 QUENCH TESTS

| Run No. | Test Section Pressure (Mpa) | Test Section Inlet Quality (Percent) | Average Test Section Inlet Fluid Velocity (m/sec) | Rod Hot Spot Initial Temperature (K) | Test Section Mass Flow Rate (Kg/sec) |
|---|---|---|---|---|---|
| 1 | 0.1 (ambient) | 69°C subcooled | 0.04 | 1025 | 0.015 |
| 3 | 0.1 (ambient) | 69°C subcooled | 0.1 | 1025 | 0.037 |
| 6 | 7 | 0 | 0.4 | 775 | 0.11 |
| 7 | 7 | 0 | 0.4 | 1025 | 0.11 |
| 8 | 7 | 11 | 1.3 | 1025 | 0.11 |
| 10 | 7 | 0 | 1.8 | 775 | 0.5 |
| 11 | 7 | 0 | 1.8 | 1025 | 0.5 |
| 11A | 7 | 0 | 1.8 | 1025 | 0.5 |
| 11B | 7 | 0 | 1.8 | 1025 | 0.5 |
| 24 | 7 | 0 | 1.8 | 1025 | 0.5 |
| 12 | 7 | 5 | 3.5 | 1025 | 0.5 |
| 13 | 7 | 15 | 7.5 | 1025 | 0.5 |
| 14 | 7 | 0 | 1.8 | 1175 | 0.5 |
| 15 | 7 | 0 | 3.0 | 1025 | 0.83 |
| 17 | 7 | 15 | 11.0 | 1025 | 0.83 |
| 20 | 7 | 15 | 11.0 | 1175 | 0.83 |
| 21 | 7 | 0 | 6.0 | 1025 | 1.66 |
| 23 | 7 | 0 | 6.0 | 1175 | 1.66 |

## 2.2 Experimental Facility Description

The tests were conducted in the Blowdown Loop of the LOFT Test Support Facility (LTSF) at the Idaho National Engineering Laboratory (INEL). This loop, which is normally used to conduct blowdown type tests, was modified for the quench tests. The modified loop configuration is shown in Figure 2. The main loop consisted of a pressure vessel, a coolant pump, a warmup heater vessel, and associated valves and piping. A high pressure nitrogen source was connected to the top end of the pressure vessel to provide a regulated pressure in the main loop to drive the primary coolant into the test section. The test section containing the heater rod was connected to a surge tank to maintain a fairly constant pressure in the test section during a test run. The surge tank and test section were initially pressurized to a nominal 7 MPa with nitrogen. The pressure in the test section was maintained relatively constant during a test run by allowing excess steam to be released through a relief valve on top of the surge tank.

The flow rate to the test section was controlled by the nitrogen pressure in the pressure vessel and an orifice located immediately upstream of the test section. The pressure in the primary loop was maintained high enough to keep the fluid upstream of valve FCV-2 subcooled at all times such that an accurate measurement of the flow rate to the test section could be made with the turbine meter FE-1.

The following orifice sizes were used for the various tests:

| Orifice Size (mm) | Run Numbers |
|---|---|
| 0.8 | 1, 3 |
| 1.6 | 6, 7, 8 |
| 3.454 | 10, 11, 11A, 11B, 12, 13, 14, 24 |
| 4.496 | 15, 17, 20 |
| 6.299 | 21, 23 |

The orifice sizes were all calculated assuming a discharge coefficient of 0.60. These orifice sizes produced very nearly the desired flow rates. Appendix C lists the actual discharge coefficients determined from the measured flow rate and pressures from each test run. The discharge coefficients ranged from 0.609 to 0.647. These data verify current literature stating that the standard orifice equation (explained in Appendix C) is valid for the case of subcooled fluid entering the orifice with flashing occurring immediately downstream of the orifice.

## 2.3 Test Section

2.3.1 Test Vessel. A 2.43 cm I.D. stainless steel test vessel was used for these tests. Figure 3 shows the configuration of the heater rod in the test section relative to the inlet and outlet flow nozzles. Centering pins at 4 axial levels were used to hold the heater rod in the test section as shown in Figure 4.

2.3.2 Heater Rod. A swaged electrical heater rod was used for Phase 1 testing. The swaged electrical heater contained a helical wound constantan heater wire surrounded by packed boron nitride and enclosed in a stainless steel sheath. The electric heater is illustrated in Figure 5 and a rod cross section is shown in Figure 6. Heater dimensions are as follows:

| | |
|---|---|
| Outside diameter: | 10.72 mm |
| Composite sheath wall thickness: | 0.89 mm |
| Overall sheath length: | 5.26 m |

The heaters were manufactured using a dual stainless steel composite sheath. The inner sheath was creased concavely, relative to the outside diameter, at four places along the total length and equally spaced, circumferentially, to accept a 0.635 mm diameter stainless steel sheathed thermocouple assembly. Four thermocouple

assemblies were laser-beam tack-welded into the creases at axial rod locations with all terminal ends exiting at the heater terminal end. The creases from the thermocouple junction to the grounded end of the inner sheath were filled with 0.635 mm welding wire placed in the crease and laser-beam tack-welded. The outersleeve was assembled over the creased sheath and the composite sheath assembly was redrawn. These four internal thermocouples were located at the cladding inner surface to measure the internal cladding temperature. Comparisons of these four measurements were used to evaluate the cooldown rates and quench behavior of the rod with and without the cladding outer surface thermocouples. The axial and azimuthal locations of the internal thermocouple junctions are given in Table 2.

TABLE 2. INTERNAL THERMOCOUPLE LOCATIONS

| TC Number | Location of TC Junction From Beginning of Heated Length (cm) | Azimuthal Location in a Clockwise Direction Looking Down From the Top End of the Rod (Note Fig. 4) |
|---|---|---|
| ITC1 | 36.45 | 0° |
| ITC2 | 72.39 | 90° |
| ITC3 | 72.39 | 270° |
| ITC4 | 113.41 | 180° |

The active component subassembly is electrically insulated from the heater sheath by the compacted boron nitride, with a mica moisture seal at the heater terminal end. The filament was brazed to the lead-in conductor and to the ground lead extension. A tab, approximately 2.54 cm square, was brazed to the top end of each lead-in conductor; the copper cables from the power supply system were bolted to the tabs. The grounding plug was welded to the ground lead extension and to the composite sheath. The ground lead extension was threaded to provide for termination of a Nickel plated AWG #10 copper grounding wire. The grounding wire provides a low-resistance path to ground for the heater current. The heater rod has an electrical

resistance of approximately 0.9 OHMS. The heater was designed to have a cosine axial power distribution with a peak-to-average power ratio of 1.58. The axial power distribution is shown in Figure 7.

2.3.3 External Thermocouples. Four external thermocouples were laser welded to the swaged heater rod with junctions and attachments similar to the thermocouples on LOFT fuel rods. The thermocouples were of Type K with a stainless steel sheath and an outer diameter of 1.02 mm. Dummy thermocouple extensions were attached to the rod from the 3 thermocouple junctions highest on the rod to the level of the lowest thermocouple junction (i.e., closest to the beginning or bottom of the heated length of the rod) the same as on LOFT fuel rods. Figure 8 shows a photograph of the attachment of the external thermocouples on the rod. The axial location and azimuthal placement of the external thermocouples are given in Table 3 and are shown in Figures 3 and 4.

TABLE 3. EXTERNAL THERMOCOUPLE LOCATIONS

| TC No. | Location Of TC Junction From Beginning Of Heated Length (cm) | Azimuthal Location In A Clock-Wise Direction Looking Down From The Top End Of The Rod |
|---|---|---|
| ETC1 | 5.1 | 315° |
| ETC2 | 36.5 | 45° |
| ECT3 | 72.4 | 135° |
| ETC4 | 113.4 | 225° |

## 2.4 Instrumentation and Data Processing

Instrumentation for this test was designed to evaluate heater rod quench behavior under high pressure reflood conditions. The instrumentation of the test section and the single swaged heater rod has been previously discussed. Process instrumentation in the Blowdown Loop was also recorded to ensure repeatable test conditions for tests on the rod with and without external thermocouples. While

measurements were recorded for all facility instruments, only those pertinent to evaluating cladding surface thermocouple effects on quench behavior are contained in this report. These instruments and their locations are listed in Table 4. A data uncertainty analysis is provided in Appendix A.

Fluid, piping and test section temperatures were obtained from type K, grounded junction thermocouples. One resistance temperature detector in the pressure vessel provided a reference fluid temperature. Pressure and differential pressure measurements were obtained with strain-gage transducers while turbine flow meters were used for flow rate measurements. The fluid density at a rod elevation of 36.45 mm was measured by a gamma densitometer through the attenuation of gamma rays from a $Ce^{137}$ source.

All data channels were filtered at 10 Hz and digitized with 16 bit resolution. The channels were sampled at a rate of 50 samples/sec except for FCV-2, the signal which opens the flow control valve to flood the test section and BF-TE-1, the test section inlet temperature. These two were sampled at 1250 samples/sec. The signal was converted to engineering units by a digital computer using a polynomial equation of the form:

$$\text{Meas.} = D_0 + D_1 V + D_2 V^2 + D_3 V^3$$

where V is the original transducer output and the $D_i$ Coefficients are constants that depend on calibration data. The measurement in engineering units is recorded on digital disc and then transferred to digital tape.

Data were processed through computer programs BITPIK[4], MODMAC[5], MACRAN[6], and QKPLOT. The first two programs reformat and sort the data. MACRAN is a program for the analysis of time series data. At this point, the time scales were adjusted to initialize the test to the opening of the FCV-2 valve. No other coefficient changes

TABLE 4

MEASUREMENTS LIST

| Measurement | Description | Range | Comments |
|---|---|---|---|
| Temperature | | | |
| BF-TE-5 | Fluid temperature pressure vessel | RTD 0-350°C | Figure 2 Reference temp. |
| TE-RL-1 | Recirculating line fluid temperature | Type K 0-350°C | Figure 2 |
| BF-TE-1 | Fluid temperature at test section inlet | Type K 0-350°C | Figure 2 |
| ITC-1 | Rod internal temperature 36.45 cm elevation 0° azimuthal angle | Type K 0-1093°C | Figures 3, 4 |
| ITC-2 | Rod internal temperature 72.39 cm elevation 90° azimuthal angle | Type K 0-1093°C | Figures 3, 4 Temperature at rod hot spot |
| ITC-3 | Rod internal temperature 72.39 cm elevation 270° azimuthal angle | Type K 0-1093°C | Figures 3, 4 |
| ITC-4 | Rod internal temperature 113.41 cm elevation 180° azimuthal angle | Type K 0-1093°C | Figures 3, 4 |
| ETC-1 | Cladding surface TC 5.08 cm elevation 315° azimuthal angle | Type K 0-1093°C | Figures 3, 4 |
| ETC-2 | Cladding surface TC 36.45 cm elevation 45° azimuthal angle | Type K 0-1093°C | Figures 3, 4 |
| ETC-3 | Cladding surface TC 72.39 cm elevation 135° azimuthal angle | Type K 0-1093°C | Figures 3, 4 |
| ETC-4 | Cladding surface TC 113.41 cm elevation 225° azimuthal angle | Type K 0-1093°C | Figures 3, 4 |
| VW-TC-1 | Vessel wall temperature 5.08 cm elevation | Type K 0-538°C | Figure 3 |

TABLE 4 (Cont'd)

| Measurement | Description | Range | Comments |
|---|---|---|---|
| Temperature (Cont'd) | | | |
| VW-TC-2 | Vesse' wall temperature 72.39 cm elevation | Type K 0-538°C | Figure 3 |
| VW-TC-3 | Vessel wall temperature 113.41 cm elevation | Type K 0-538°C | Figure 3 |
| Pressure | | | |
| PE-2A | Test section outlet pressure | 0-20.68 MPa | Figure 2 |
| PE-ST-1 | Surge tank pressure | 0-6.89 MPa | Figure 2 |
| PE-N-1 | Nitrogen pressure downstream of regulator | 0-20.68 MPa | Figure 2 |
| BF-PE-3 | Pressure vessel pressure | 0-20.68 Mpa | Figure 2 |
| Differential Pressure | | | |
| BF-PDE-16 | ΔP across test section | 0-69 KPa | Figure 2 |
| Density | | | |
| BF-DE-1B | Fluid density at 36.45 cm elevation on rod | 0-10 volts | density ($kg/m^3$) = 9049.7 LN (10/voltage) only B-beam used |
| Flow Rate | | | |
| BF-FE-1 | Test section inlet flow rate | 15-3155 ml/s | Figure 2 |
| Heater Rod Parameters | | | |
| BF-HRC-1 | Heater rod current | 0-300 amps | |
| BF-HRV-1 | Heater rod voltage | 0-500 volts | |
| HRC X HRV | Heater rod power | 0-150 Kw | |

were made. QKPLOT then overlays one measurement chann from several different runs for comparison. The temperatures were converted from degrees celsius to degrees Kelvin during plotting.

## 2.5 Experimental Procedure

The blowdown facility at LTSF was used for these tests to simulate as nearly as possible the thermal-hydraulic conditions in the LOFT core at the time the LOFT fuel rods quenched during the blowdown phase of the L2-2 and L2-3 tests. The LOFT fuel rods experienced critical heat flux (CHF) and then went into film boiling with a subsequent heat up to about 790 K for the L2-2 test and 910 K for the L2-3 test during the first 6 sec. following blowdown. At the time of quench (about 6 seconds into the transient) a large slug of high density fluid entered the core. Post-test calculations indicate this slug of fluid had a velocity of 1 to 2 m/sec, a core inlet quality of about 7 percent, and a pressure of about 7 MPa.

These conditions were simulated in the blowdown facility by bringing the electric rod to a high temperature in a fairly stagnant gas environment, simulating film boiling on the LOFT fuel rods, and then rapidly flooding the test section by opening valve FCV-2 (see Figure 2). The test section was flooded over a range of flooding rates from 0.4 to 6 m/sec and test section inlet qualities from 0 to 15 percent as shown in Table 1. A scenario of a typical test is as follows:

(1) Heat up the pressure vessel and main coolant loop to the specified initial temperature.

(2) Establish the specified test pressure in the surge tank and test section with a small amount of nitrogen flow from the surge tank through the test section and out the vent line near FCV-2 to remove any fluid leaking through FCV-2.

(3) Apply power to the heater tape attached to FCV-2 and test section inlet piping and bring the temperature to the specified value.

(4) Turn on the power to the heater rod and bring to the specified initial temperature.

(5) Allow the test vessel to heat up to about 600 K near the hot spot of the heater rod.

(6) Turn off the main coolant pump, open the nitrogen supply to the pressure vessel, close the small circulation line from FCV-2 to the primary pump inlet, and close the nitrogen vent line at the test section inlet.

(7) Open valve FCV-2 to initiate the test.

(8) When the thermocouple highest on the heater rod (ITC4) indicates a quench, close FCV-2 to stop the test.

# 3. RESULTS

The results of the tests include comparisons of cooldown rates and quench times between tests with and without cladding external thermocouples on the heater rod. In addition the effects of various test parameters on quench behavior such as flooding rate, initial rod temperature, and test section inlet quality are discussed. Also, the repeatability of test conditions and test results are discussed.

## 3.1 Cooldown Rates and Quench Times

Comparisons of the cooldown rates and quench behavior between the heater rod with and without external thermocouples for each test run are shown in Figures 9 through 26. The comparisons are for the internal thermocouple (ITC2) located at the hot spot of the rod. Comparisons of the other thermocouple at the hot spot (ITC3) showed essentially identical results, so only data from ITC2 are given in the report.

For the high pressure tests at 7 MPa, the rod with external thermocouples quenched in about half the time required for the rod without external thermocouples. Reasons for this difference include: (a) the rod with external thermocouples had a higher precursory cooldown rate than the bare rod and (b) the rod with external thermocouples quenched from a higher temperature than the bare rod. The quench temperature is defined as the temperature at which the rod begins an extremely rapid cooldown to the surrounding fluid temperature. The quench temperature can be easily determined from the curves for the bare rod. Quench temperatures are listed in Table 5 for the rod without external thermocouples. The quench temperature for the bare rod varied from about 712 to 795K. However, for the rod with external thermocouples, a quench temperature cannot be readily determined due to the gradually increasing cooldown rate at the time of quench. Once the bare rod reached its quench temperature, its

TABLE 5

QUENCH TEMPERATURE OF THE ROD
WITHOUT EXTERNAL THERMOCOUPLES

| Run No. | Quench Temp. (K) |
|---|---|
| 11 | 760 |
| 13 | 730 |
| 12 | 750 |
| 10 | 712 |
| 14 | 795 |
| 11A | 765 |
| 11B | 760 |
| 17 | 730 |
| 20 | 750 |
| 15 | 760 |
| 21 | 770 |
| 23 | 790 |
| 3 | 770 |
| 1 | 700 |
| 8 | 740 |
| 7 | 765 |
| 6 | 722 |
| 24 | 782 |

cooldown rate was larger than that of the rod with external thermocouples. This is probably due to the fact that there is less stored heat in the bare rod at the time of quench which could be transferred to the cladding surface, thus allowing the cladding to cool more readily.

The quench times for the swaged heater rod, either with or without external thermocouples, were longer than anticipated, particularly at these high flooding rates. Although the long periods of precursory cooling were not expected, the experimental results can be explained in terms of the high thermal diffusivity of the test rod which is not typical of a nuclear fuel rod. A fin effect would be expected on the swaged heater rod during precursory cooling where the external thermocouples may increase the heat transfer coefficient and increase the surface area for heat transfer. A similar fin effect would be expected on a nuclear rod but may not be noticeable depending on the length of time a nuclear rod could be in a precursory cooling mode. If a bare nuclear rod can quench from a very high temperature with minimal precursory cooling, then adding external thermocouples to the rod would not noticeably increase its ability to quench. However, the results of these tests indicate that if a bare nuclear rod does not readily quench from a high temperature and with minimal precursory cooling, then cladding external thermocouples could have a significant effect on the quench behavior of a nuclear rod. Therefore, the results of these tests cannot be extrapolated to a nuclear rod, but serve to indicate the possibility of a thermocouple effect on the quench behavior of a nuclear rod.

## 3.2 Effect of Test Parameters On Quench Behavior

3.2.1 Flooding Rate. Test runs 7, 11, 15, and 21 had similar test conditions except for flooding rate. The flooding rates for these runs were 0.4, 1.8, 3.0 and 6.0 m/sec respectively. All 4 runs had saturated liquid inlet conditions and an initial rod hot spot

temperature of 1025K. The quench behavior for these 4 runs can be compared in Figures 9, 18, 19, and 22. The quench times for the bare rod are plotted versus flooding rate in Figure 25. It can be seen that the quench time is reduced with increasing flooding rate but becomes asymptotic at about 4 m/sec. The reduced quench times result from an increased precursory cooldown rate for the higher flooding rates with the quench temperature being about the same for these 4 runs. Quench times for the rod with external thermocouples are not plotted in Figure 25 because of the difficulty in establishing a quench temperature; however, the same trend exists for the rod with external thermocouples, as compared to the rod without external thermocouples.

3.2.2 Test Section Inlet Quality. Test runs 11, 12, and 13 had the similar conditions except for the test section inlet quality. These runs had inlet qualities of 0, 5, and 15 percent respectively, the same test section inlet flow rate, and an initial rod hot spot temperature of 1025K. The quench behavior of these 3 runs can be compared in Figures 9, 10 and 11. The quench temperature is about the same for these runs but the precursory cooldown rate increases as the inlet quality increases, resulting in shorter quench times.

3.2.3 Effect of Initial Rod Temperature. Test runs 11 and 14 had the same test conditions except for the initial rod hot spot temperature. Run 11 had an initial rod temperature of 1025K while run 14 had an initial temperature of 1175K. Both runs had saturated liquid inlet conditions and a flooding rate of 1.8 m/sec. The quench behavior for these runs can be compared in Figures 9 and 13. The quench temperatures and precursory cooldown rates for these runs were virtually the same. Run 14 showed a longer quench time than run 11 because the rod started at a higher temperature.

Run 10 had the same test conditions as runs 11 and 14 except for the initial rod temperature of 775 K. Even though the initial rod temperature was at or below the quench temperature of runs 11 and 14,

the rod still experienced a significant period of precursory cooling. In comparison, the quench temperature for the bare rod, for this run, was 712 K; well below the quench temperature for the other runs.

Runs 17 and 20 were conducted with initial rod temperatures of 1025 and 1175 K respectively, but with an inlet quality of 15 percent (see Figures 16 and 17). The same trends were observed for these runs as for runs 11 and 14.

### 3.3 Repeatability of Test Results and Test Conditions

The test conditions for run 11 were conducted 4 times (runs 11, 11A, 11B, 24) in order to evaluate the repeatability of the test data from the start to finish of the test matrix and to determine the capability of repeating test conditions in the Blowdown Facility.

Figure 26 shows a comparison of the quench behavior of the bare rod for runs 11, 11A, 11B and 24. Runs 11, 11A and 11B show good agreement. Run 24 indicated a quench about 1.6 to 2 seconds earlier than the other runs. Run 24 had the same precursory cooldown rate as the other 3 runs but also had a quench temperature about 20K higher than the other runs. Due to the slow precursory cooldown rate, this difference in quench temperature resulted in the 2 second difference in quench time. Although it is possible that an oxide layer buildup on the rod over the time of the test program could have caused the higher quench temperature for Run 24, it cannot be concluded that this was the reason for the earlier quench because the quench temperature for Run 24 (782K) is well within the scatter of quench temperatures for the various test runs.

The test conditions for all 4 runs showed good repeatability. Figures 27 and 28 show comparisons of test section flow rate and pressure for runs 11, 11A, 11B, and 24.

Figure 29 shows a comparison of the quench behavior of the rod with external thermocouples for runs 11, 11A, 11B and 24. Runs 11A and 11B, which were conducted in succession, showed excellent agreement. However, a trend was apparent indicating that the rod quenched sooner as the testing progressed, the difference between the first and last runs being 1.6 seconds. A couple of explanations for this phenomenon include (a) an oxide layer buildup over the duration of the testing (b) the external thermocouples bowed away from the rod between the laser welds during the course of the testing as shown in Figure 30. It is not known if the thermocouples deformed during the first test or gradually over the duration of the testing. If the deformation had been gradual, the thermocouples could have increased the cooldown rate of the rod throughout the test program as they protruded farther into the fluid stream. It is not felt that the deformation of the external thermocouples alter the general behavior of the rod with external thermocouples since the first run with external thermocouples (Run No. 11) had the same behavior as the other runs, and since the external thermocouples would not have totally deformed until the rod was completely quenched in run no. 11.

The test conditions for these 4 runs also showed good repeatability. Figures 31 and 32 show comparisons of test section flow rate and pressure for these 4 runs.

Figure 33 shows a comparison of the quench behavior for these 4 runs for both the rod with and without external thermocouples. The magnitude of the thermocouple effect on quench time can be seen in this figure where the thermocouple effect is much larger than the variation between the repeat runs with or without external thermocouples. It is important to note that the heater rod was clean and free of any oxide layer prior to the start of the test matrix either with or without external thermocouples. Since the test sequence was the same in both cases, any change in the surface condition of the rod would have been about the same for the tests with

and without external thermocouples for any given test run. Comparisons of the test section flow rates and pressures for these runs are shown in Figures 34 and 35. It can be seen that good repeatability existed in the test conditions for these 8 test runs.

## 3.4 Low Pressure Test Results

Tests 1 and 3 were conducted at ambient pressure with flooding rates of 4 and 11 cm/sec. The inlet fluid was 67°C subcooled for these runs. Figure 36 shows a comparison of the quench behavior of the rod with and without external thermocouples for a flooding rate of 4 cm/sec. The bare rod started to cool slightly sooner and had a slightly greater cooldown rate than the rod with external thermocouples. This is probably due to the fact that the test for the bare rod had a slightly higher flooding rate over the first 60 seconds of the transient as shown in Figure 37. Nevertheless, the rod with external thermocouples quench from a higher temperature. The combination of these two compensating effects resulted in quench times about the same for the two runs.

For test no. 3 with a flooding rate of 11 cm/sec, the rod with external thermocouples quenched about 3 seconds earlier than the rod without external thermocouples as shown in Figure 38. The bare rod had a faster cooldown rate early in the precursory cooling mode even though this test had a slightly lower flooding rate as shown in Figure 39. However, the rod with external thermocouples quenched from a higher temperature causing it to quench earlier than the bare rod.

## 4. CONCLUSIONS

1. Cladding surface thermocouples significantly increase the cooldown rate and reduce the quench time of a swaged electrical heater rod at high pressure (7 MPa) over a large range of flooding rates.

2. Due to the high thermal diffusivity of the swaged electrical heater rod, the precursory cooling times of this rod were much longer than those expected for a nuclear fuel rod under the same flooding conditions. Therefore, the magnitude of the thermocouple effect on this rod should not be extrapolated to a nuclear fuel rod. The results of these tests indicate that external thermocouples enhance the cooling of the swaged heater rod over a large range of flooding conditions. The same effect is expected to occur on a nuclear fuel rod; however, the relative magnitude of the effect may be much smaller (possibly even negligible) depending on how fast a bare nuclear rod quenches at the same flooding conditions; i.e., a thermocouple effect would be less significant on a rod which has a lower thermal diffusivity than the swaged heater rod, such as a nuclear fuel rod.

   The second phase of testing on a 9-rod bundle with a cartridge heater will provide information more typical of the effect of external thermocouples on the quench behavior of a nuclear fuel rod. Also the possibility of a bare fuel rod to quench from very high temperatures with little or no precursory cooling will be observed.

3. The Blowdown Loop at LTSF has been successfully used to conduct separate effects tests to evaluate the effect of cladding surface thermocouples on quench behavior. Well controlled test conditions and repeatable test data have been obtained.

4. The Blowdown Loop and method of testing used in the Phase 1 single rod tests are satisfactory for the Phase 2 9-rod bundle tests.

## 5. REFERENCES

1. L. J. Ball, et al., Semiscale Program Description, TREE-NUREG-1210, May 1978.

2. F. F. Cadek, et al., PWR FLECHT (Full Length Emergency Cooling Heat Transfer) Final Report, WCAP-7665, April 1971.

3. L. J. Ott and K. W. Childs, Surface Heat Flux Perturbation in BDHT Fuel Pin Simulators, NUREG/CR-0610, ORNL/NUREG-54, April 1979.

4. E. B. Henry, Baseline Program Document, BLPD-BITPIK-0, August 1977.

5. E. B. Henry, MODMAC IBM 360/75 Computer Program CPDOMODMAC-I, May 1978.

6. Applications Manual, MAC/RAN III Time Series Data Analysis System, University Software Systems, Agbabian Associates, Copyright 1974.

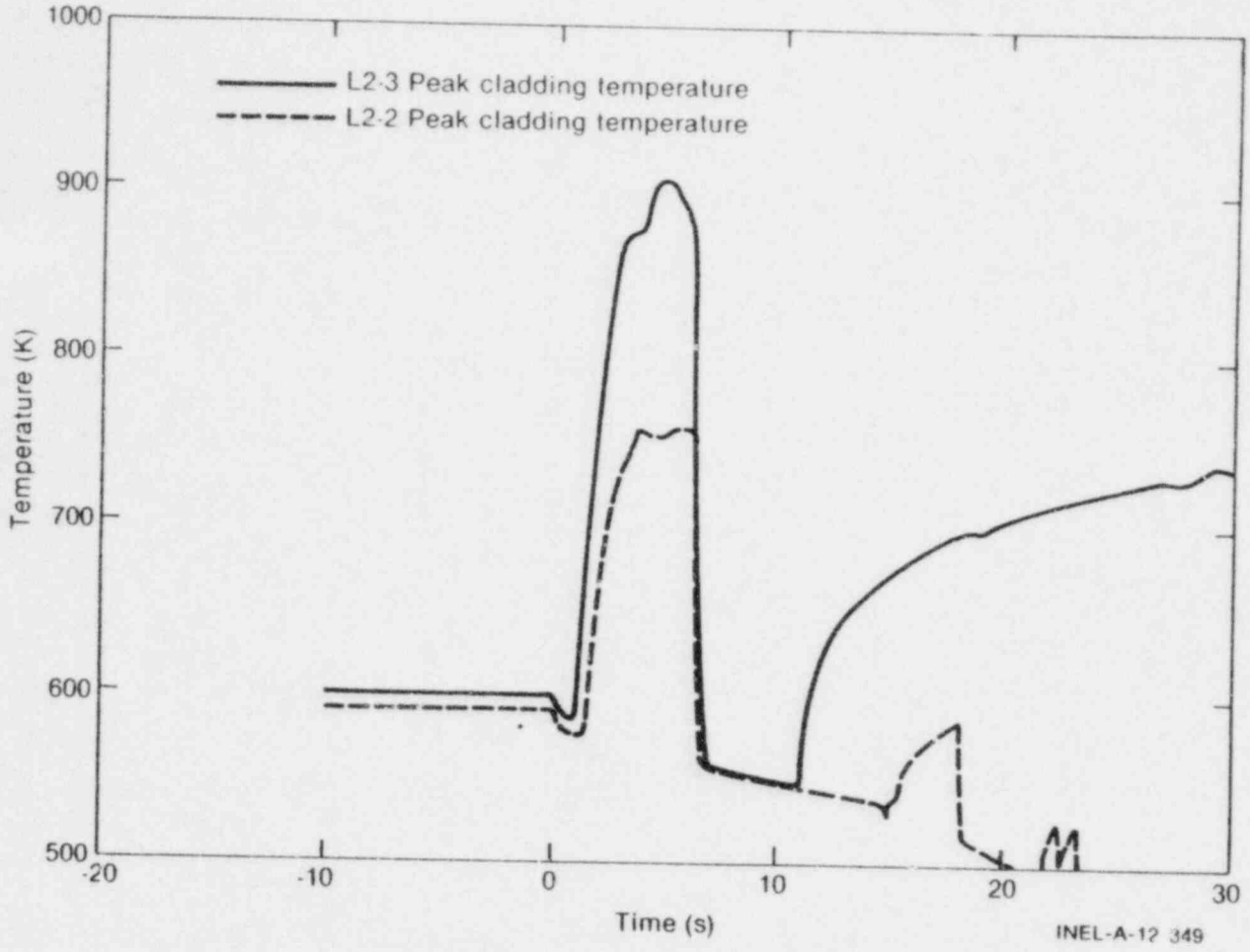


Figure 1. LOFT Cladding Temperature Response for the L2-2 and L2-3 Loss-of-Coolant Experiments

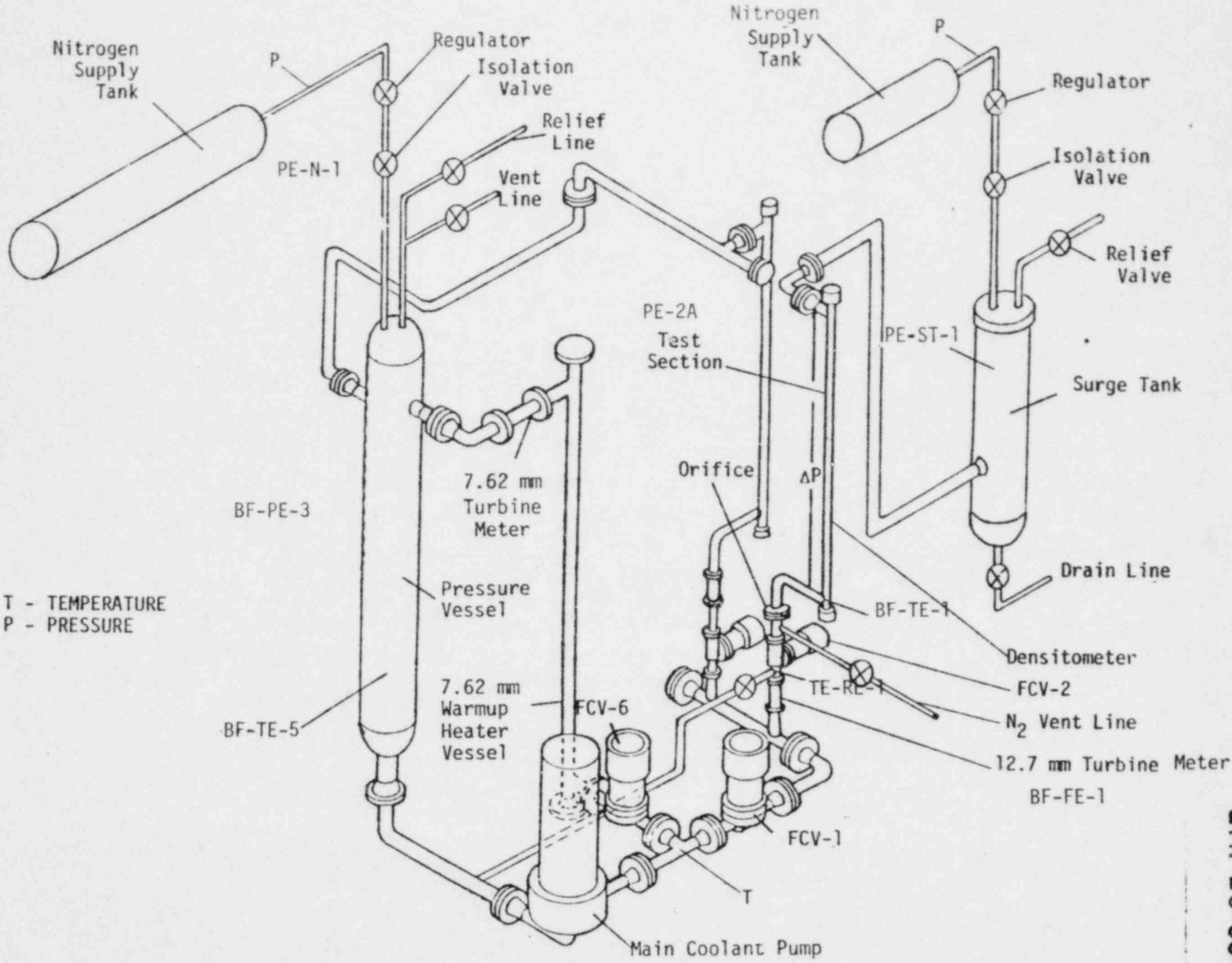


Figure 2. Loop Configuration for Quench Tests

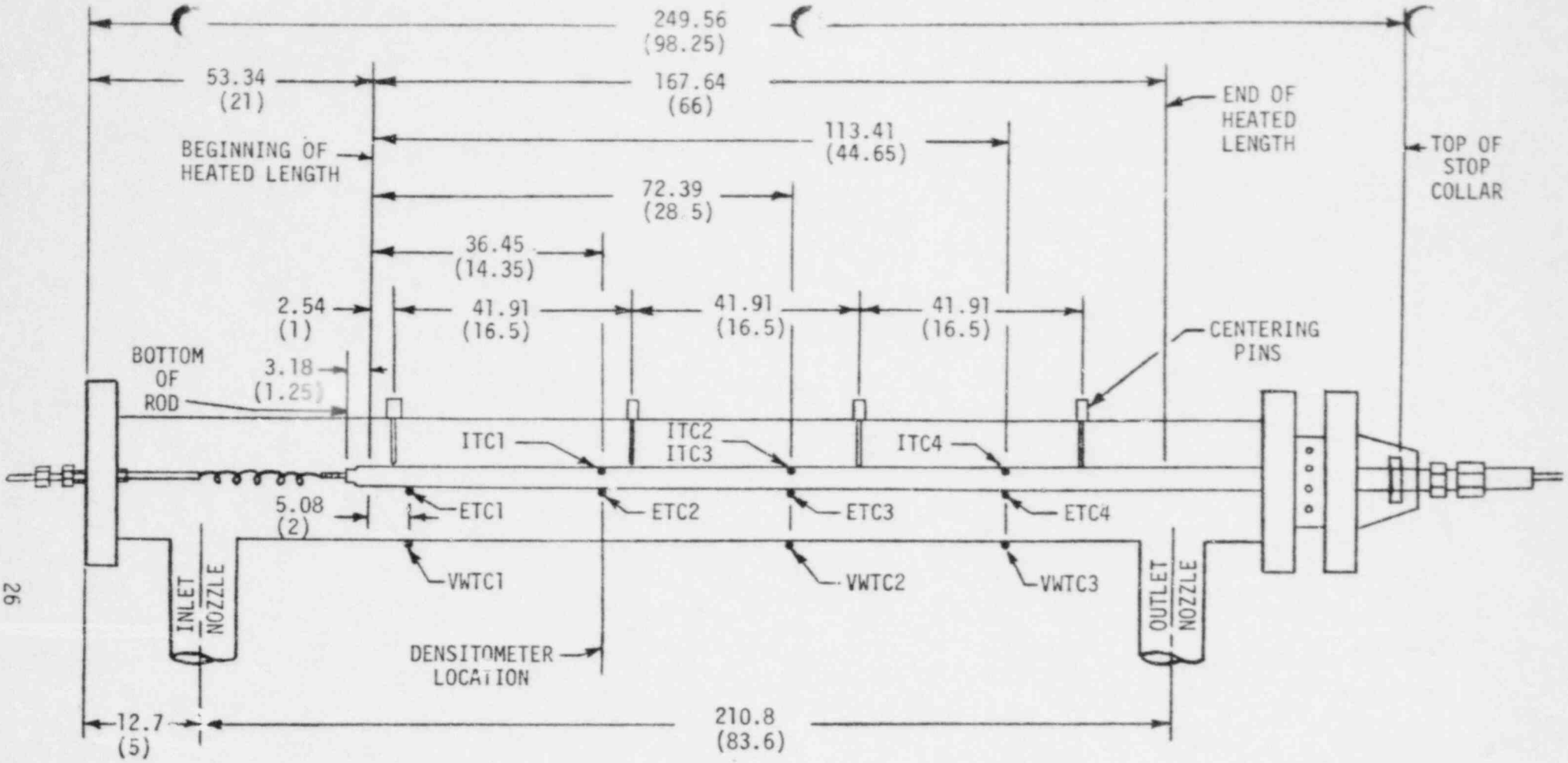


ITC - INTERNAL THERMOCOUPLE

ETC - EXTERNAL THERMOCOUPLE

VWTC - VESSEL WALL THERMOCOUPLE

DIMENSIONS IN CM (INCHES)

Figure 3. Configuration of Heater Rod in Test Vessel.

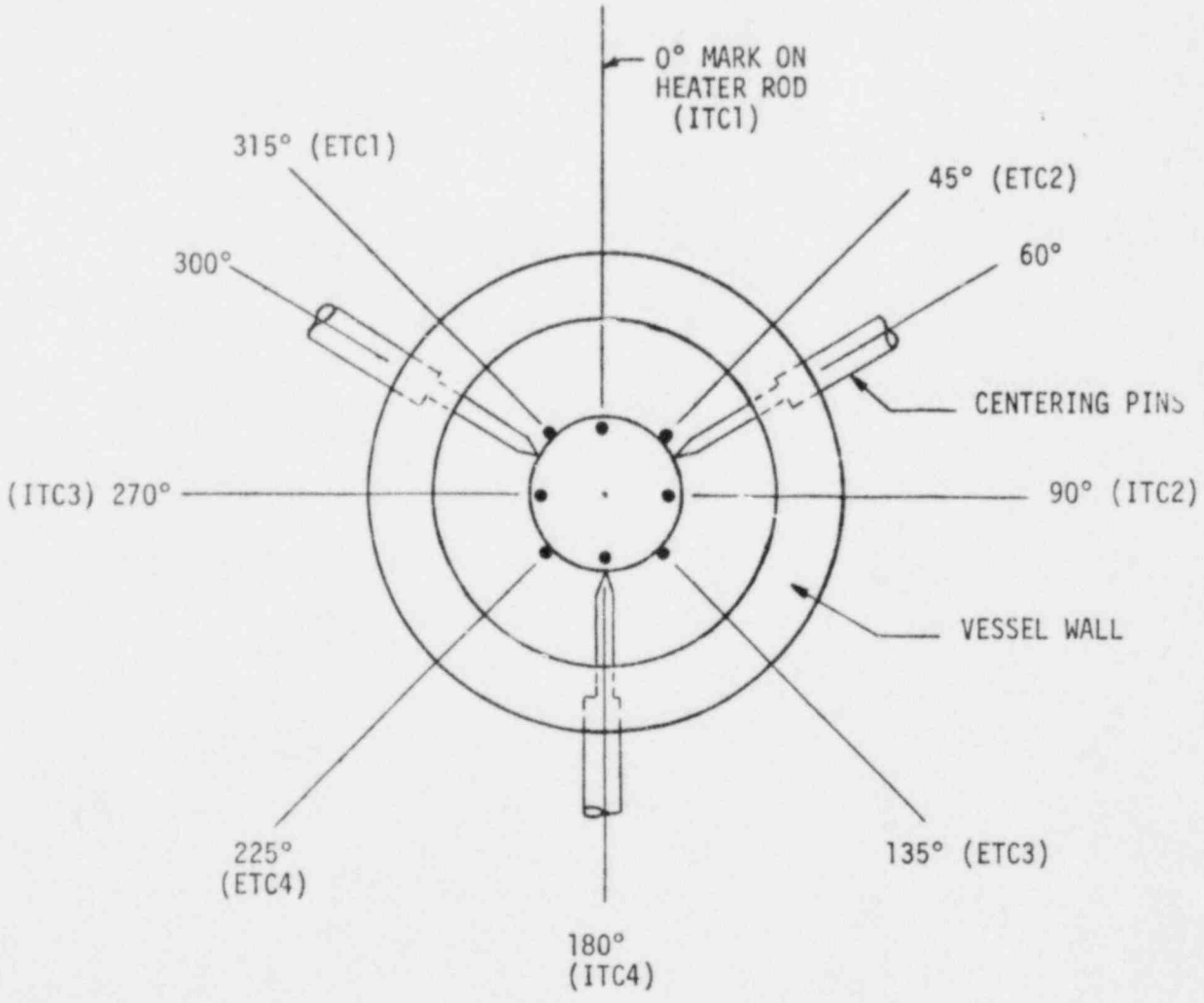


ITC - INTERNAL THERMOCOUPLE

ETC - EXTERNAL THERMOCOUPLE

VIEW FROM TOP OF HEATER ROD

Figure 4. Azimuthal Locations of Thermocouples and Centering Pins.

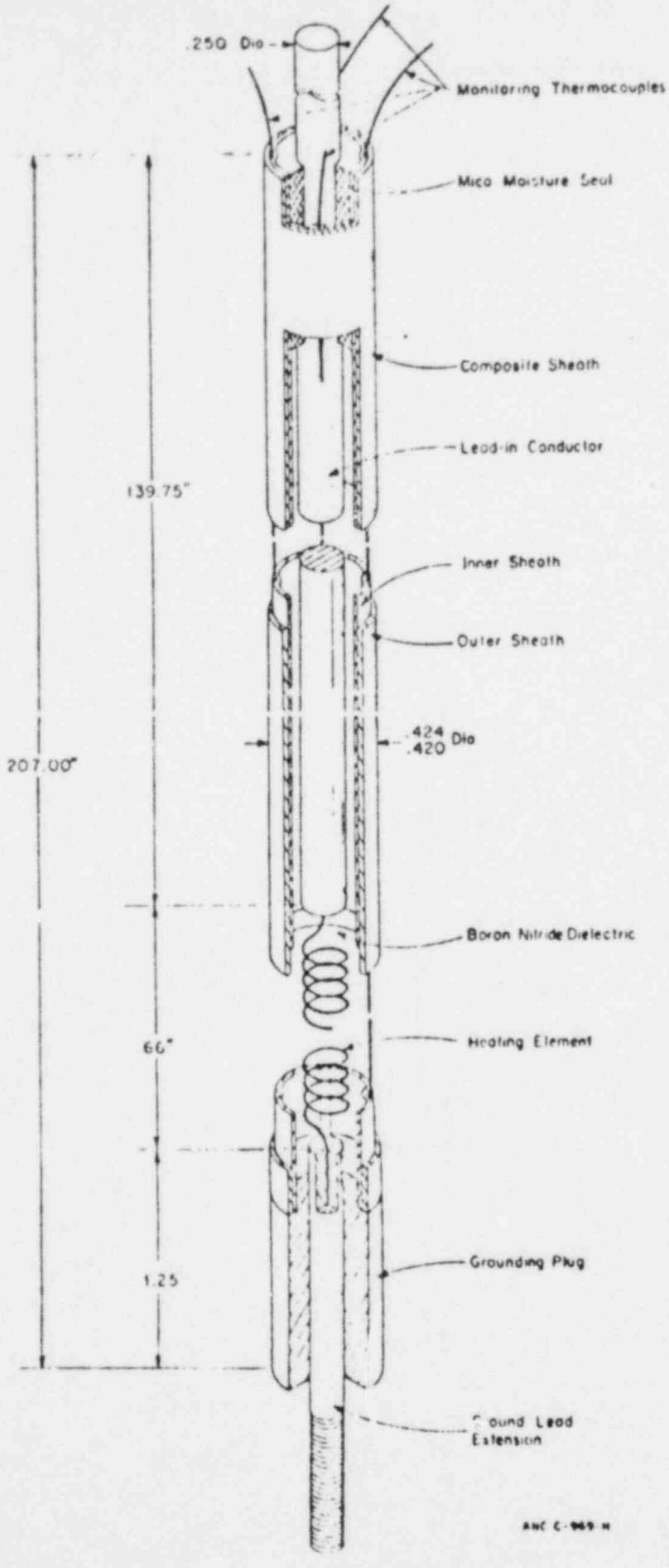


Figure 5. Diagram of the Swaged Electrical Heater

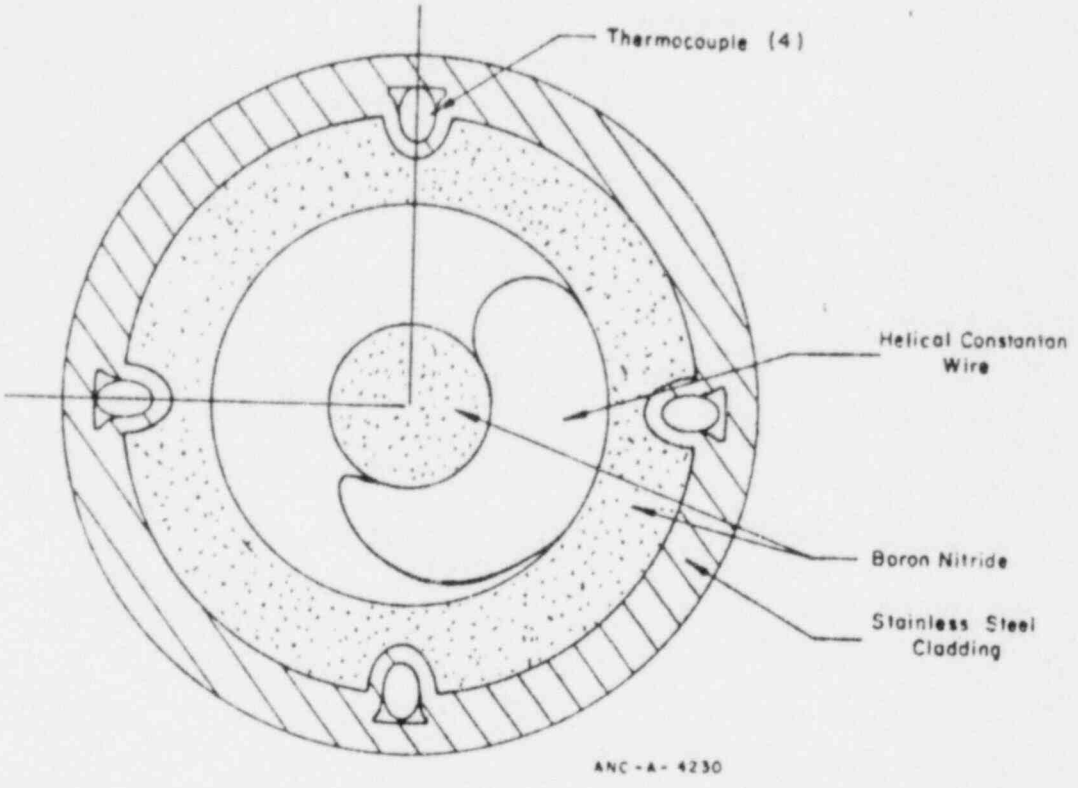


Figure 6. Swaged Electrical Heater Rod Cross Section

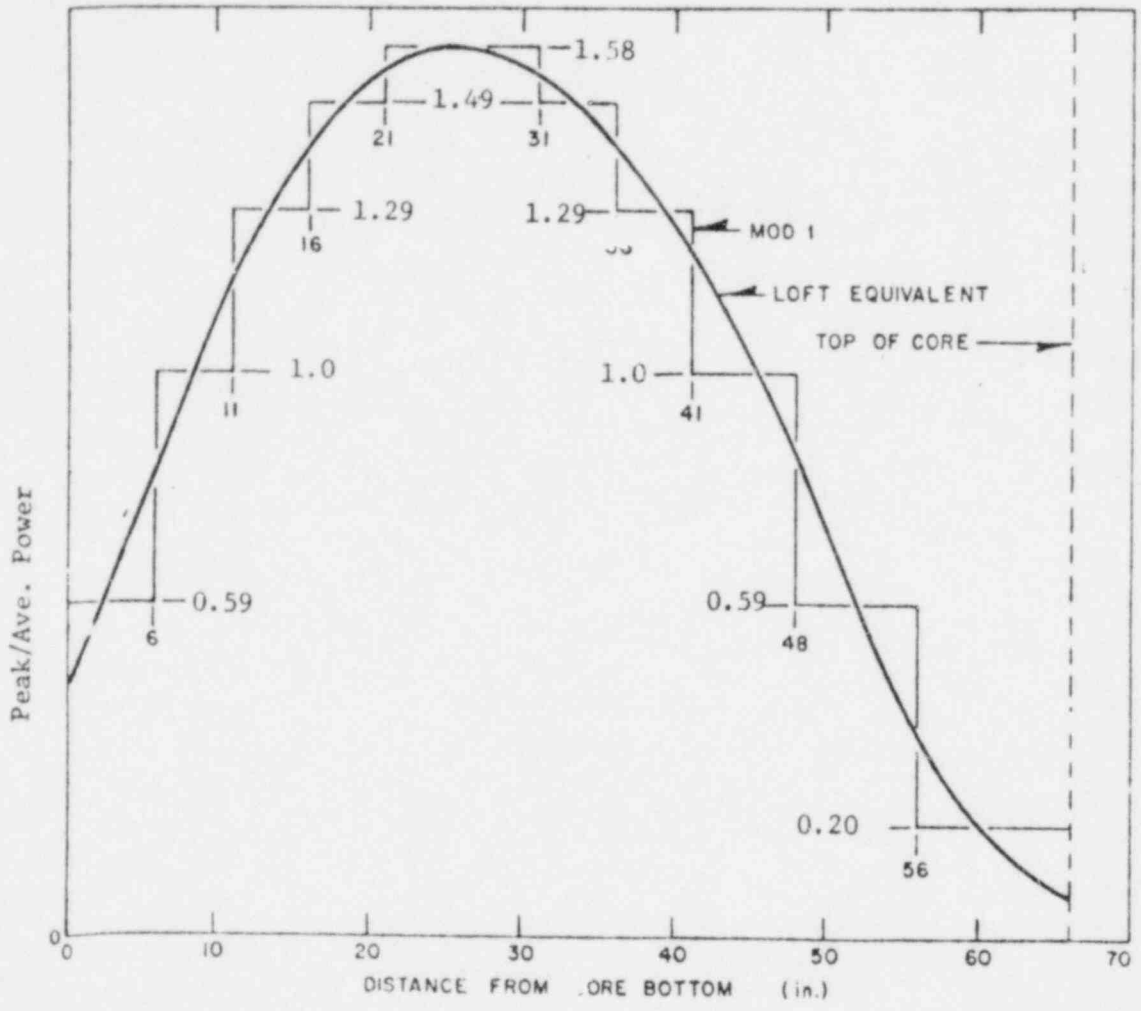


Figure 7. Axial Power Distribution

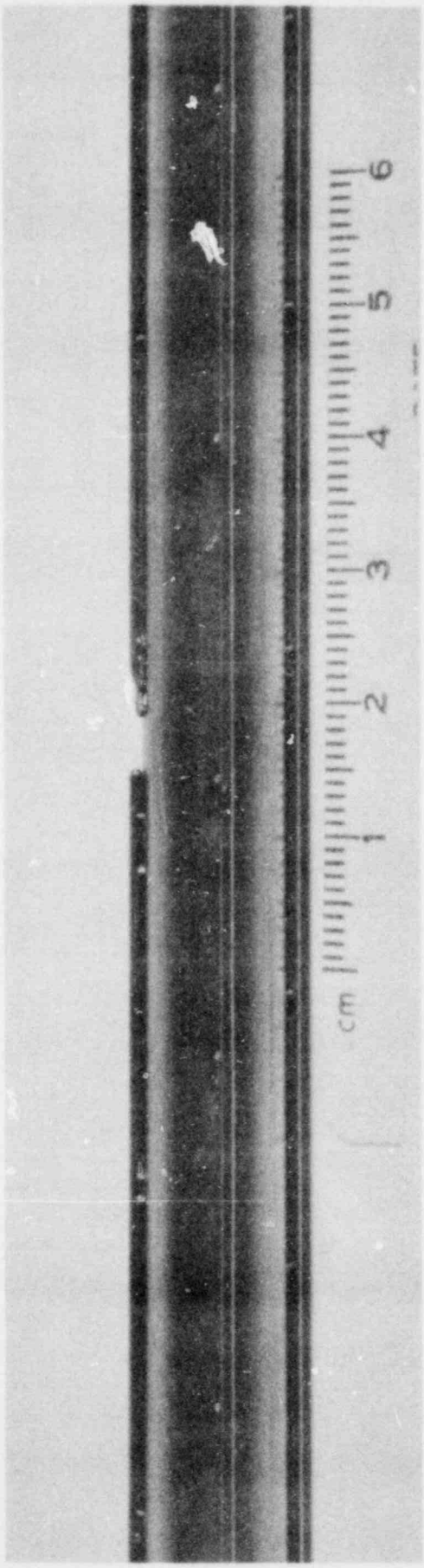


Figure 8. External Thermocouple Attachment

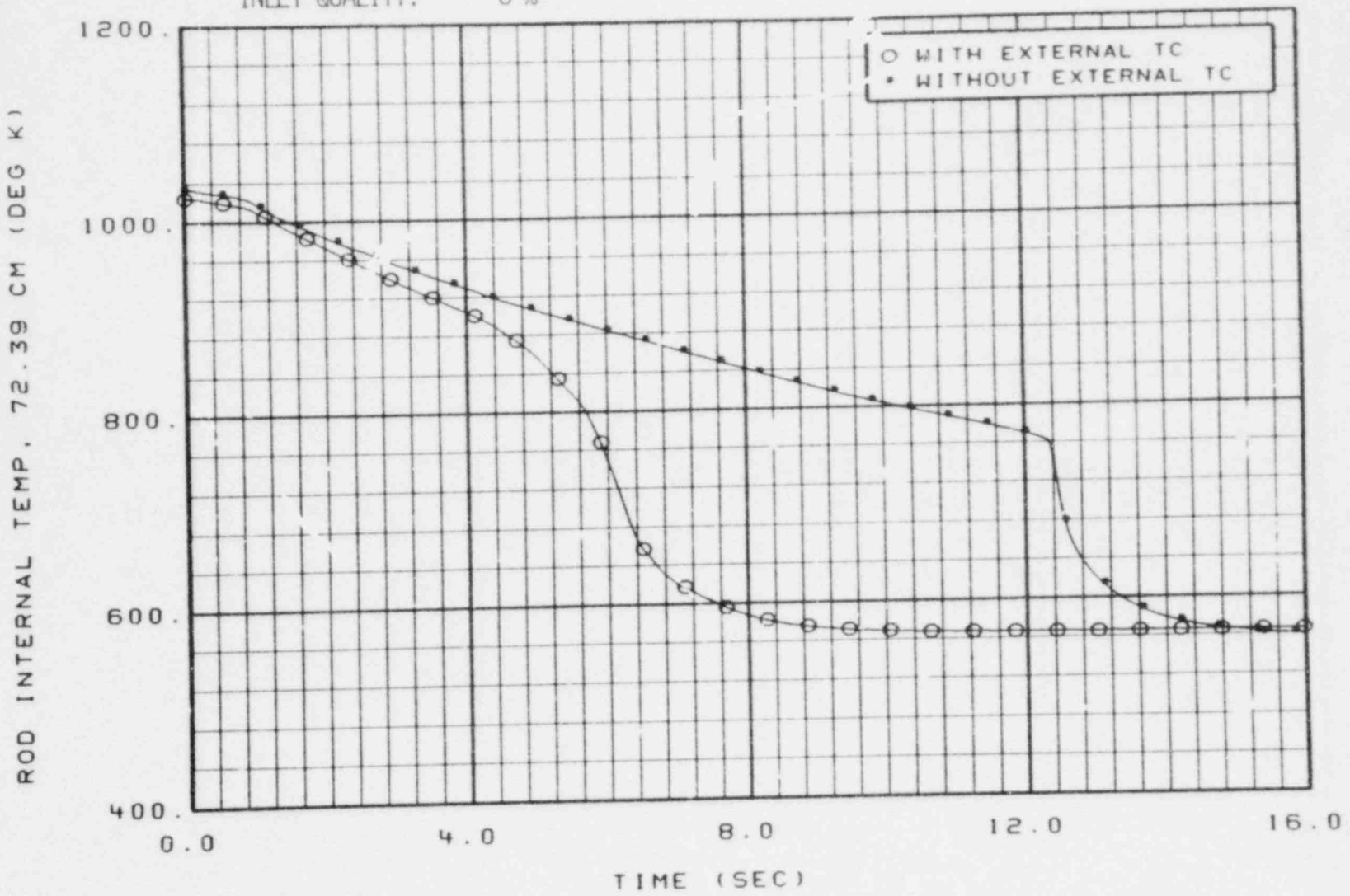


FIGURE 9. INTERNAL THERMOCOUPLE (2) COMPARISON FOR RUN 11

QKPLT MOD-5 VER 119 03/28/79 JAG115F TAU 11/09/79 17.11.05. GRAPH 2

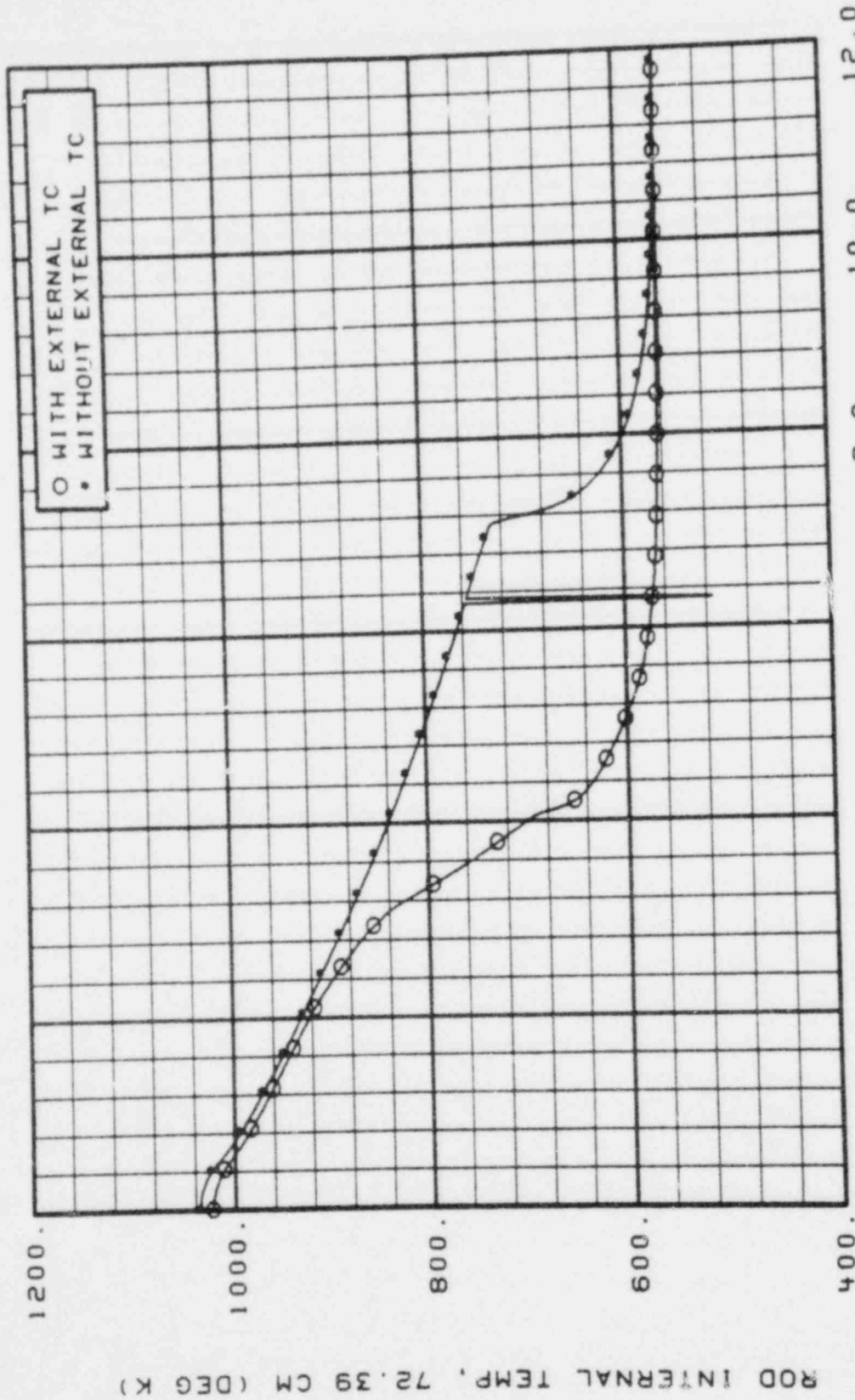


PRESSURE: 7 MPA
FLOODING RATE: 7.5 M/SEC
INLET QUALITY: 15%

FIGURE 10, INTERNAL THERMOCOUPLE (2) COMPARISON FOR RUN 13

QXPLT MOD-5 VER 119 03/28/79 JA0132H TAU 11/02/79 12.22.39. GRAPH 2

PRESSURE: 7 MPa
FLOODING RATE: 3.5 M/SEC
INLET QUALITY: 5%

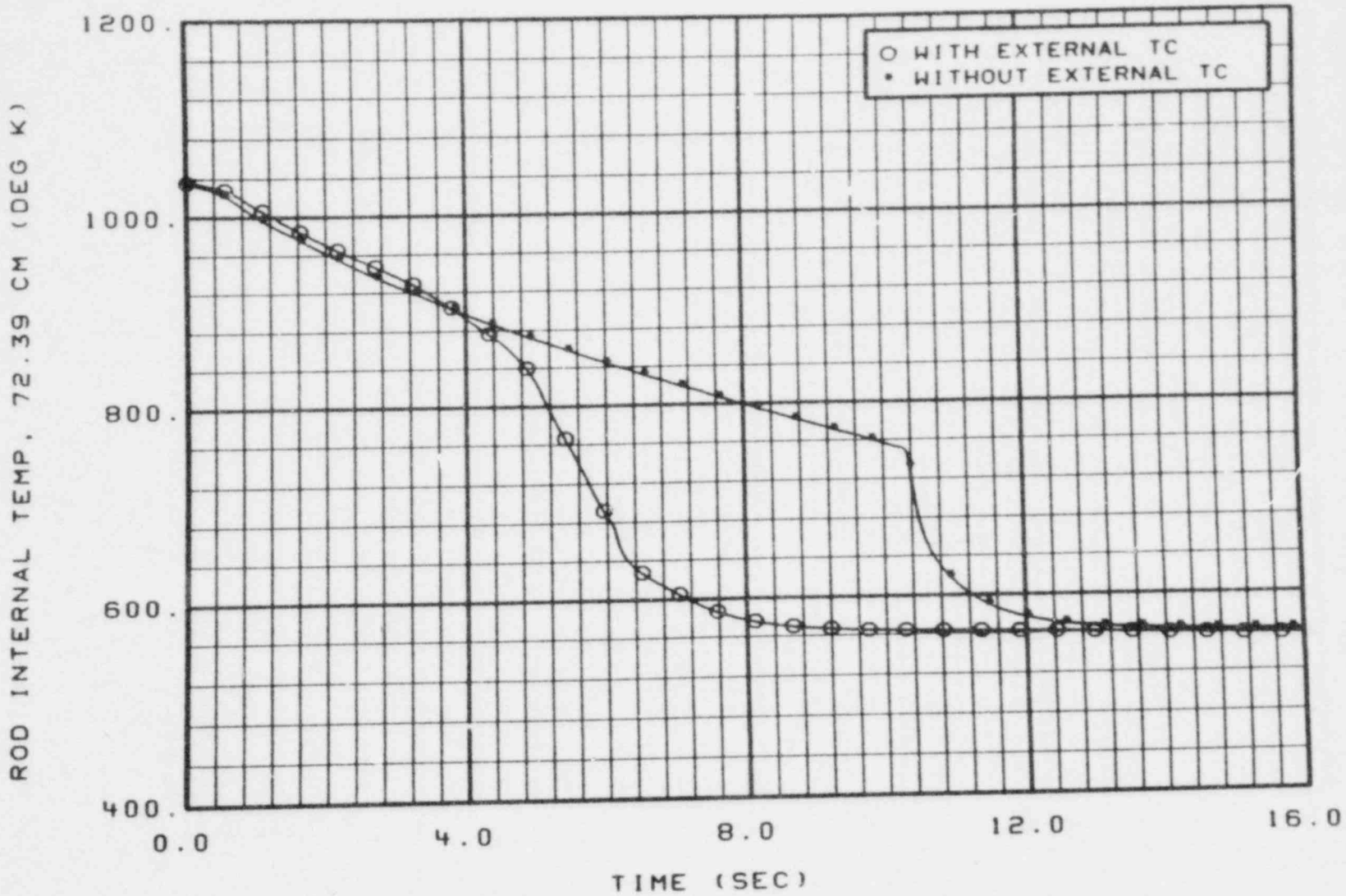


FIGURE 11. INTERNAL THERMOCOUPLE (2) COMPARISON FOR RUN 12

QKPLT MOD-5 VER 119 03/28/79 JA01212 TAU 11/02/79 12.02.29. GRAPH 2

PRESSURE: 7 MPa
FLOODING RATE: 1.8 M/SEC
INLET QUALITY: 0%

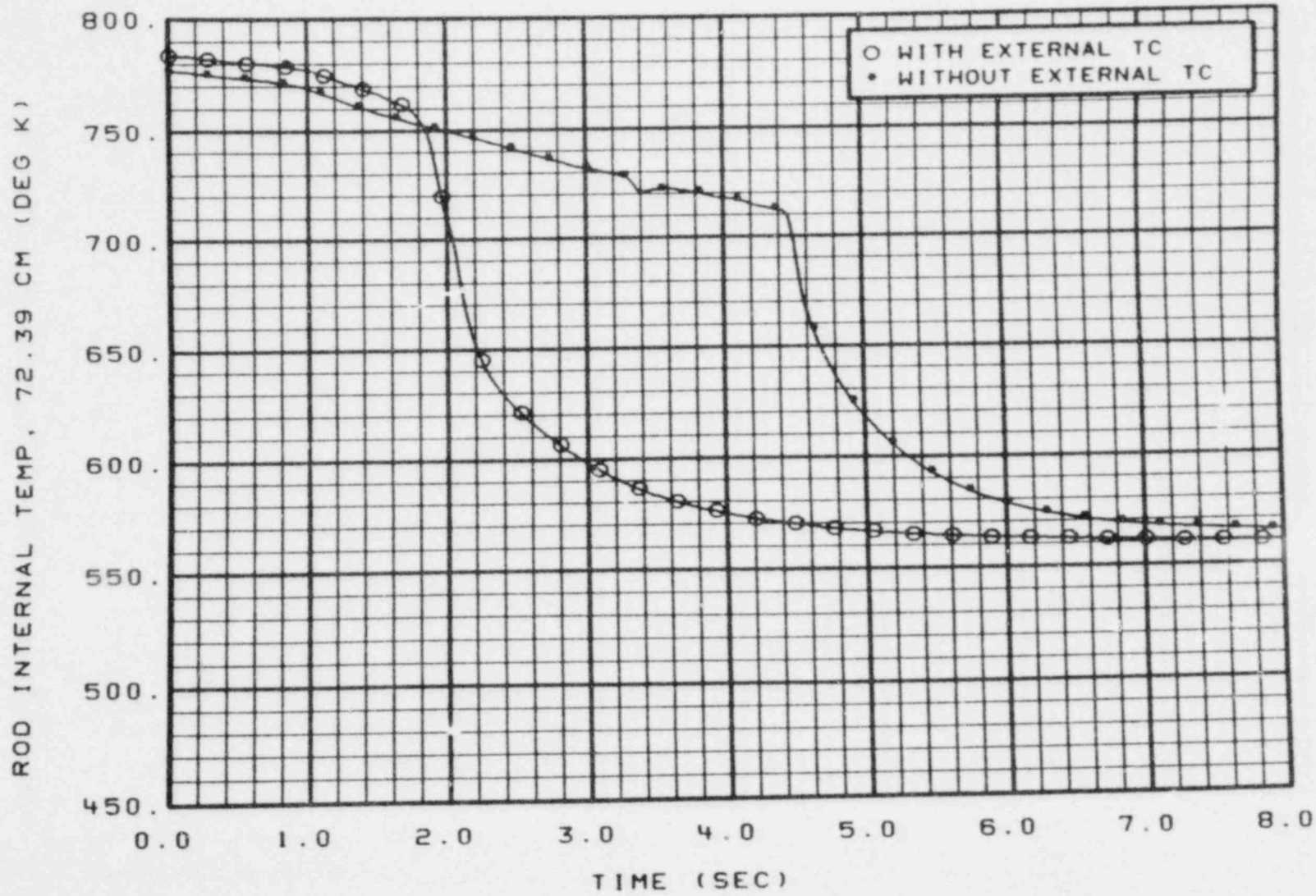


FIGURE 12. INTERNAL THERMOCOUPLE (2) COMPARISON FOR RUN 10

QKPLT MOD-5 VER 119 03/28/79 JA0102Z TAU 11/02/79 12.33.13. GRAPH 2

PRESSURE: 7 MPa
FLOODING RATE: 1.8 M/SEC
INLET QUALITY: 0%

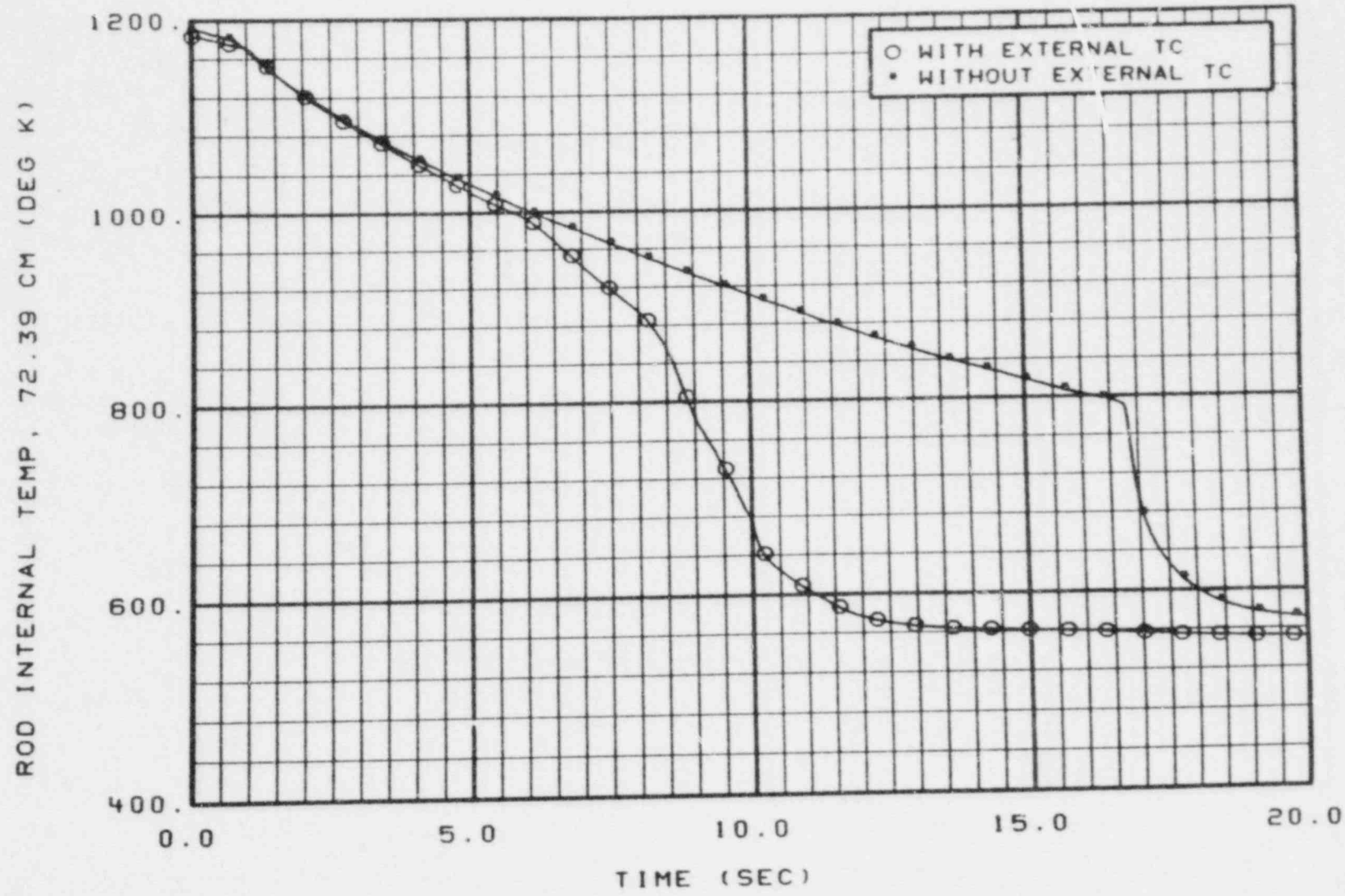


FIGURE 13. INTERNAL THERMOCOUPLE (2) COMPARISON FOR RUN 14

QKPLT MOD-5 VER 119 03/28/79 JA0141X TAU 11/02/79 12.01.10. GRAPH 2

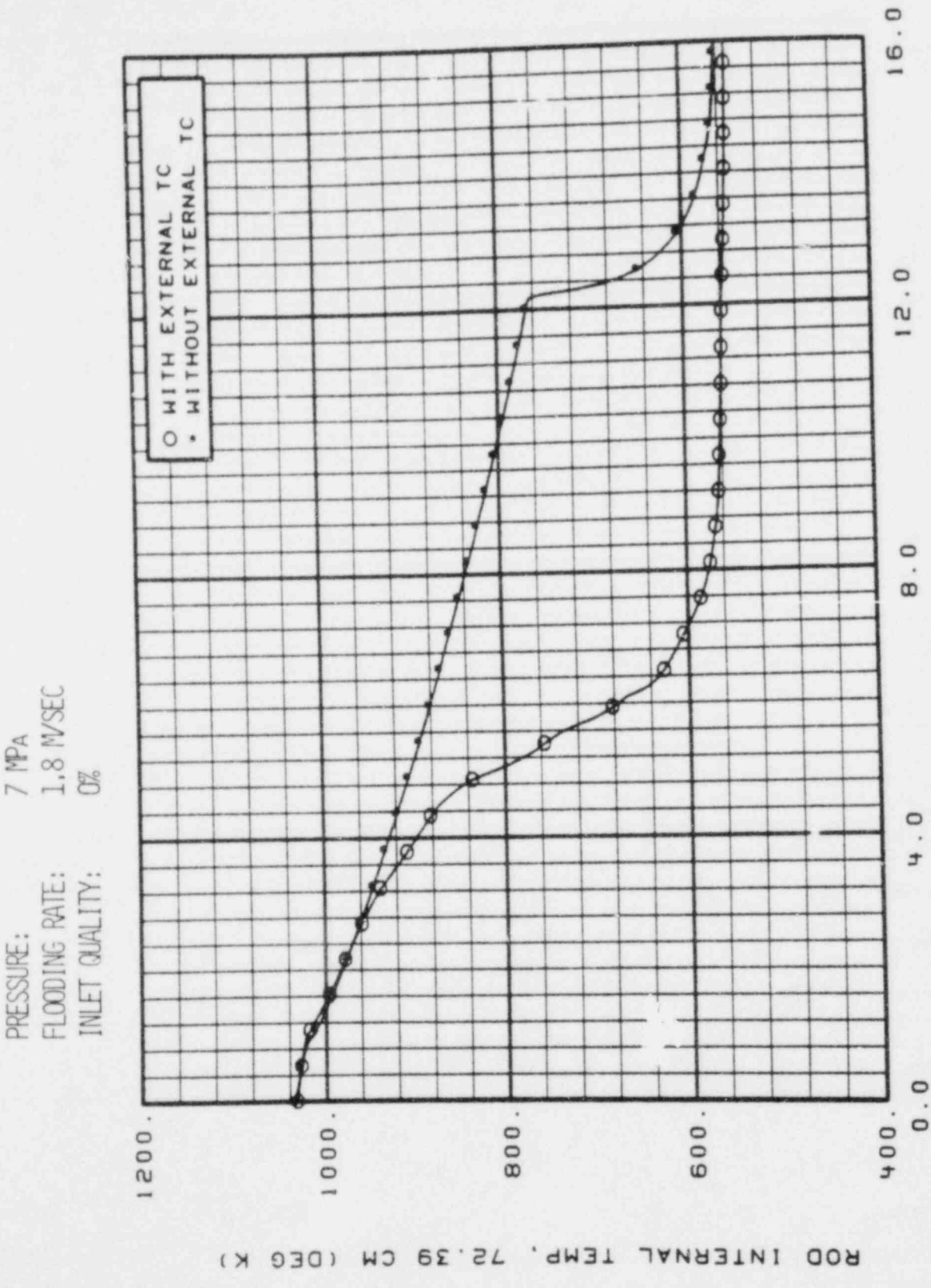


FIGURE 14. INTERNAL THERMOCOUPLE (2) COMPARISON FOR RUN 11A

PRESSURE: 7 MPA
FLOODING RATE: 1.8 M/SEC
INLET QUALITY: 0%

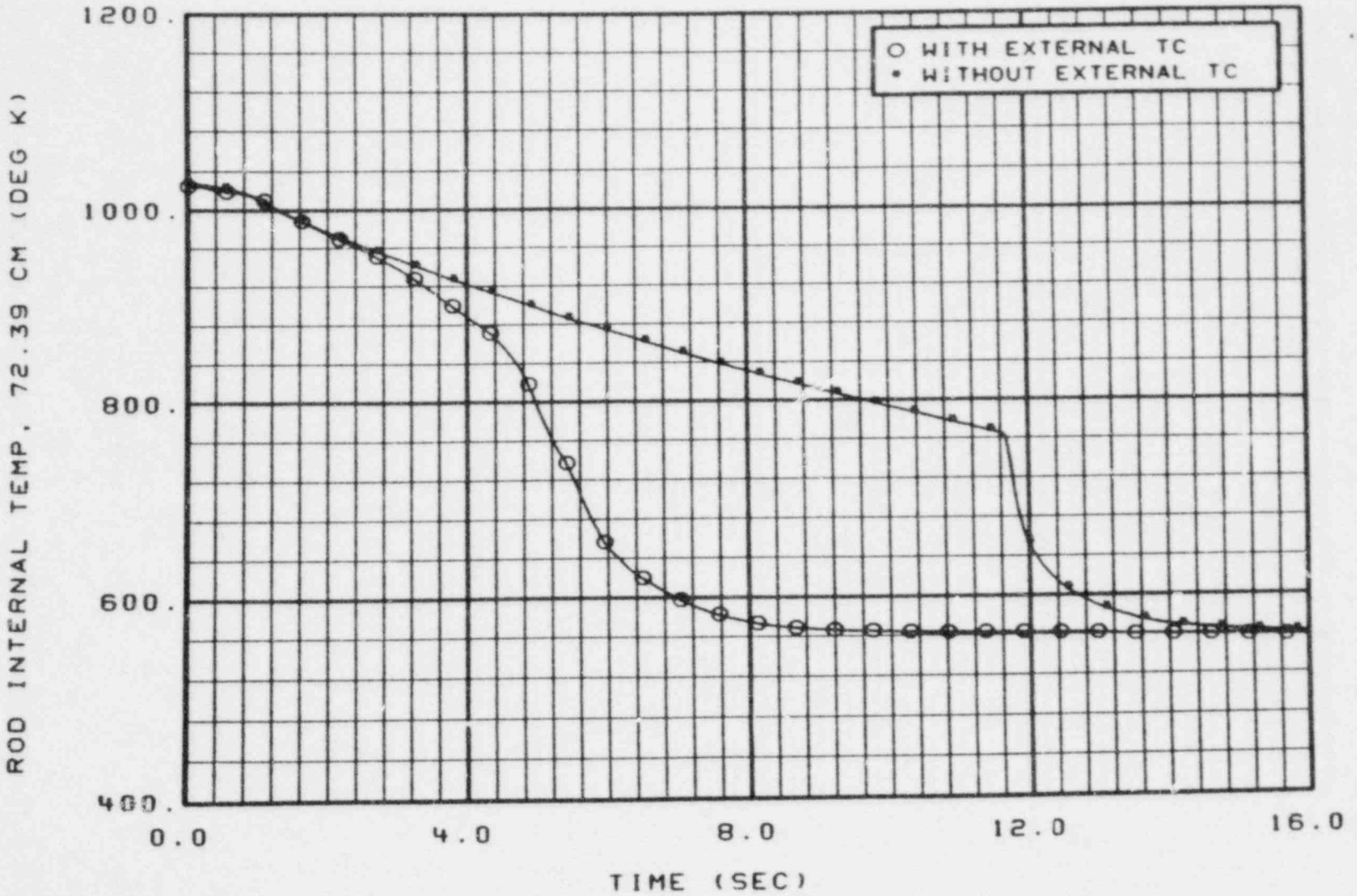


FIGURE 15. INTERNAL THERMOCOUPLE (2) COMPARISON FOR RUN 11B

QKPLT MOD-5 VER 119 03/28/79 JA00520 TAU 11/02/79 12.32.11. GRAPH 2

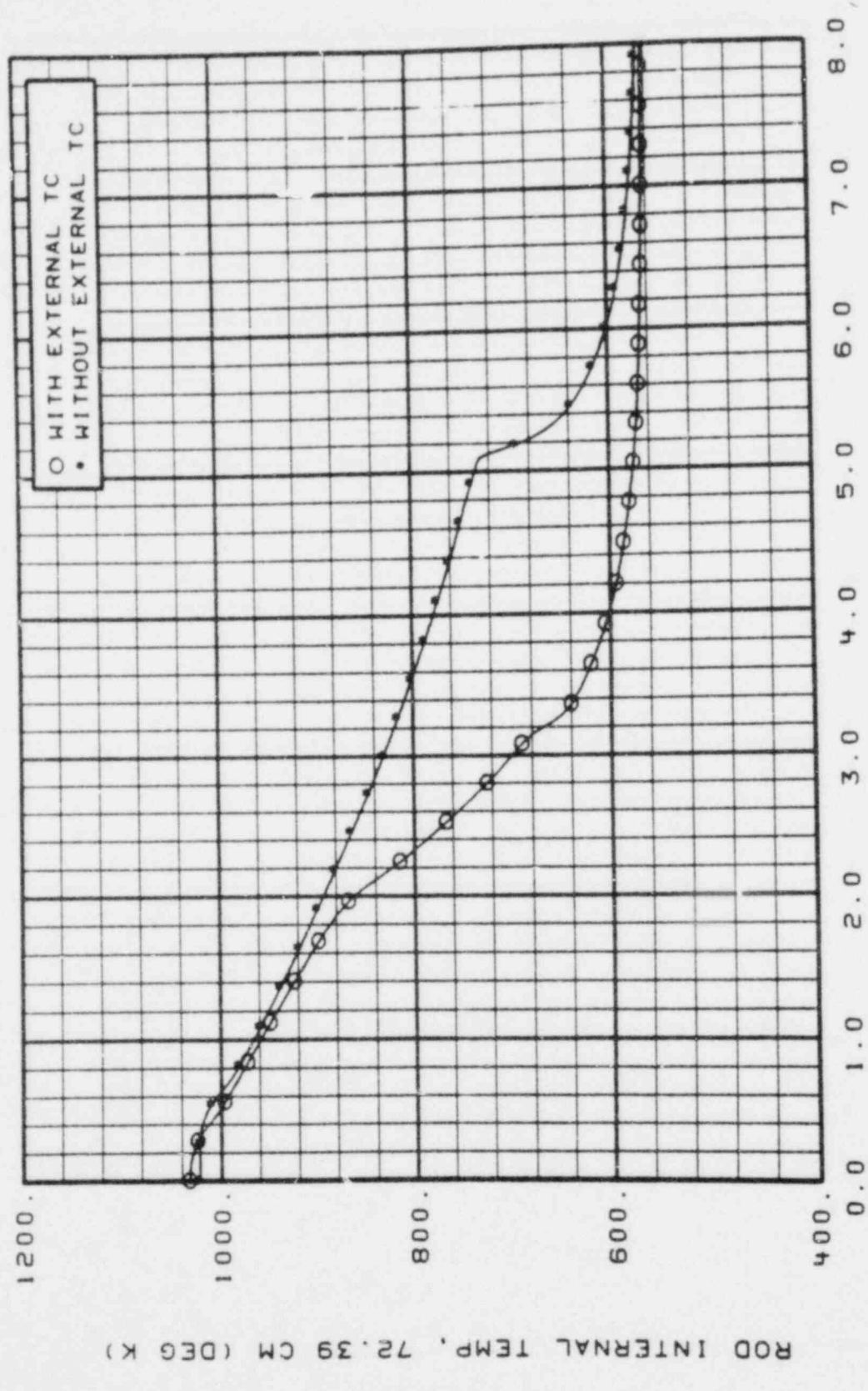


FIGURE 16. INTERNAL THERMOCOUPLE (2) COMPARISON FOR RUN 17

PRESSURE: 7 MPA
FLOODING RATE: 11 M/SEC
INLET QUALITY: 15%

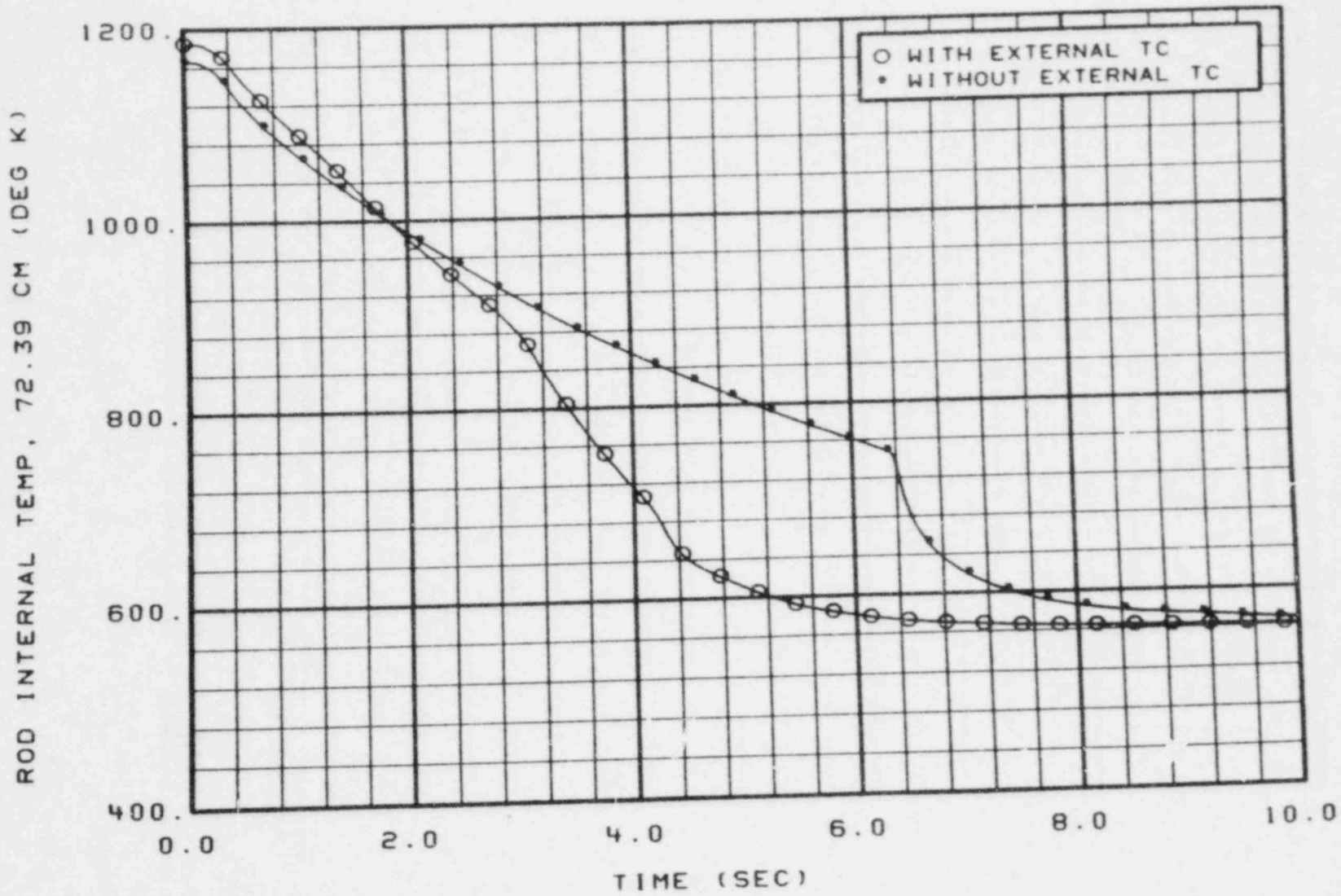


FIGURE 17. INTERNAL THERMOCOUPLE (2) COMPARISON FOR RUN 20

QKPLT MOD-5 VER 119 03/28/79 JA020:3 TAU 11/02/79 12.03.06. GRAPH 2

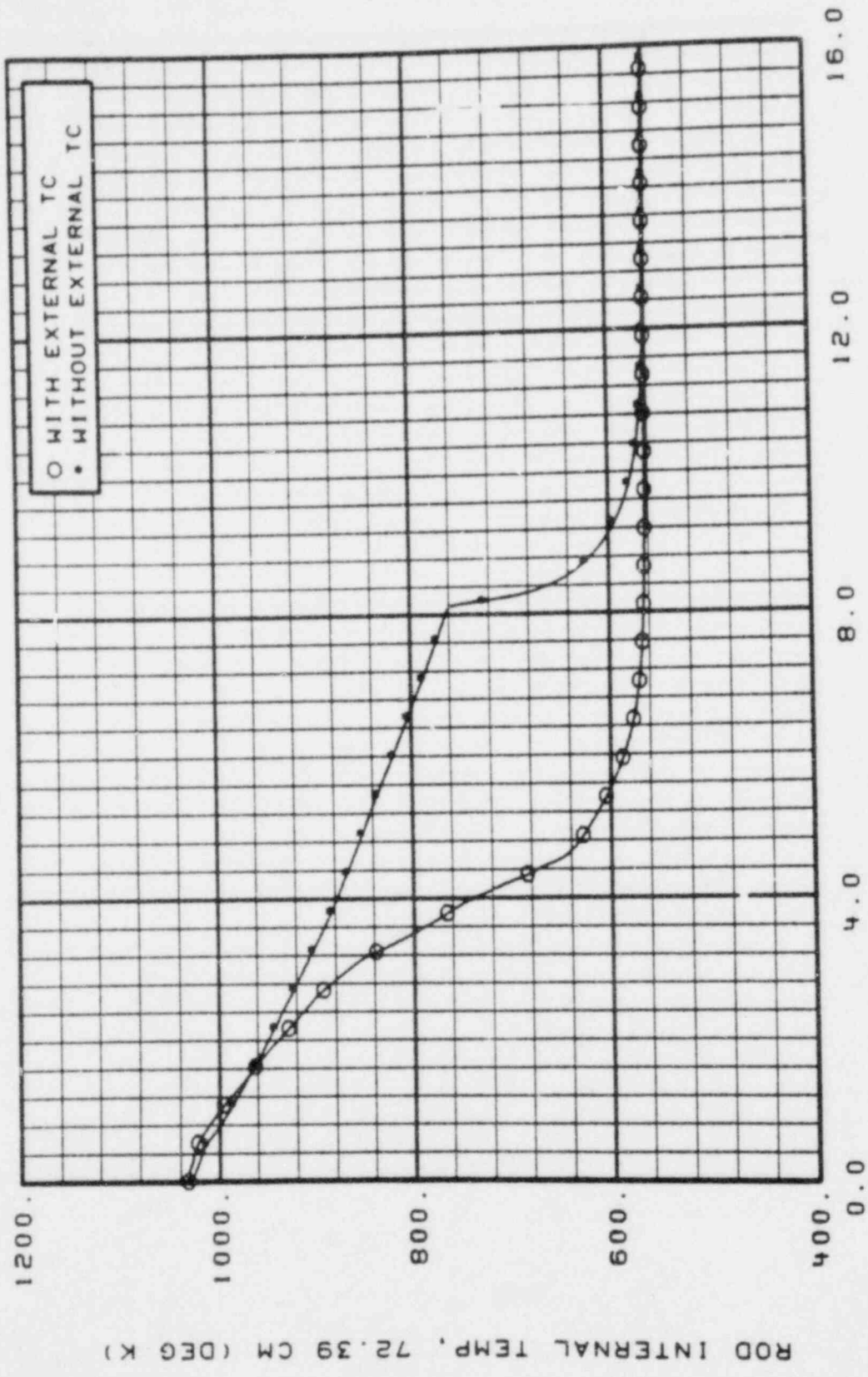


FIGURE 18, INTERNAL THERMOCOUPLE (2) COMPARISON FOR RUN 15

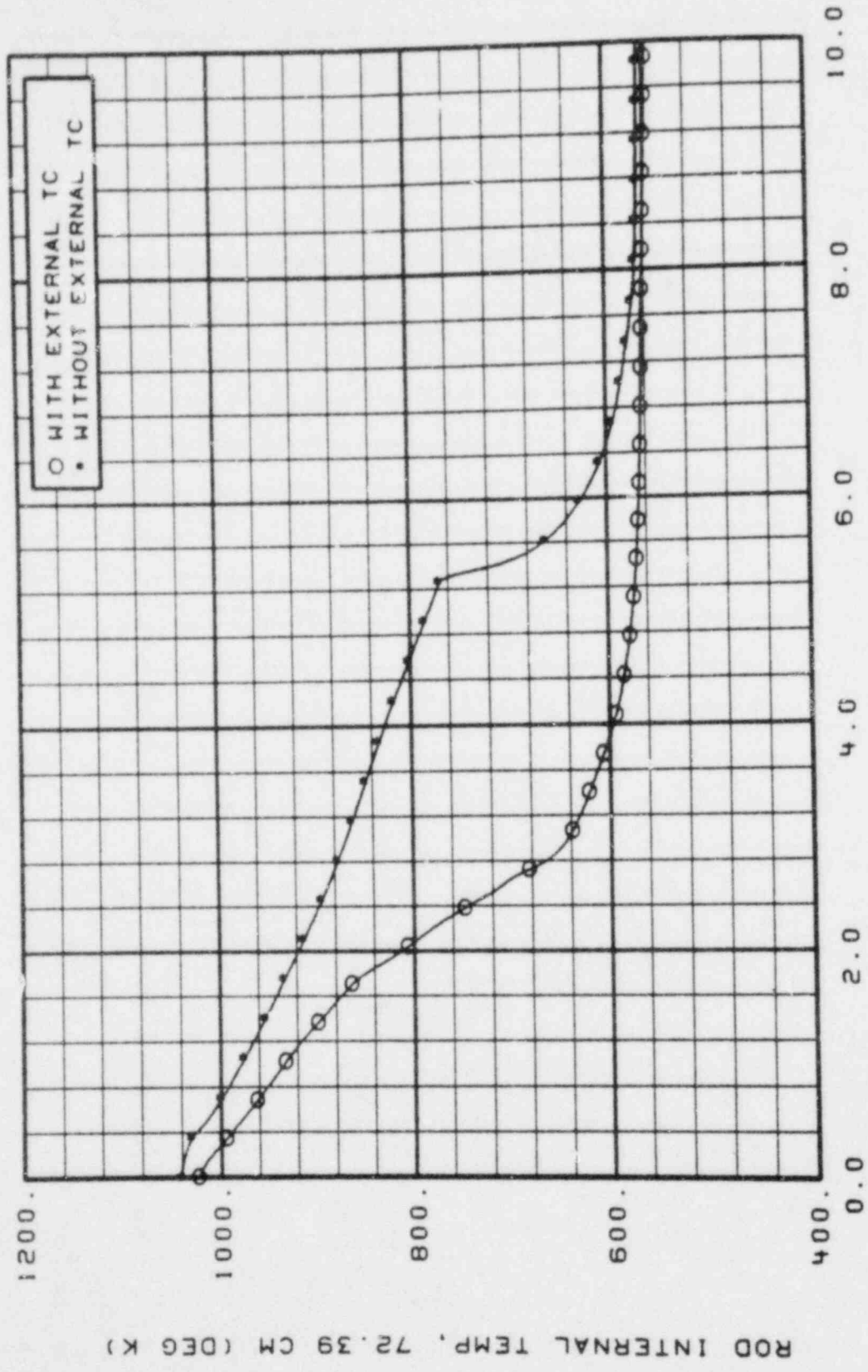


FIGURE 19. INTERNAL THERMOCOUPLE (2) COMPARISON FOR RUN 21

QXPLT MOD-5 VER 119 03/28/79 JAG2118 TAU 11/02/79 12.03.32. GRAPH 2

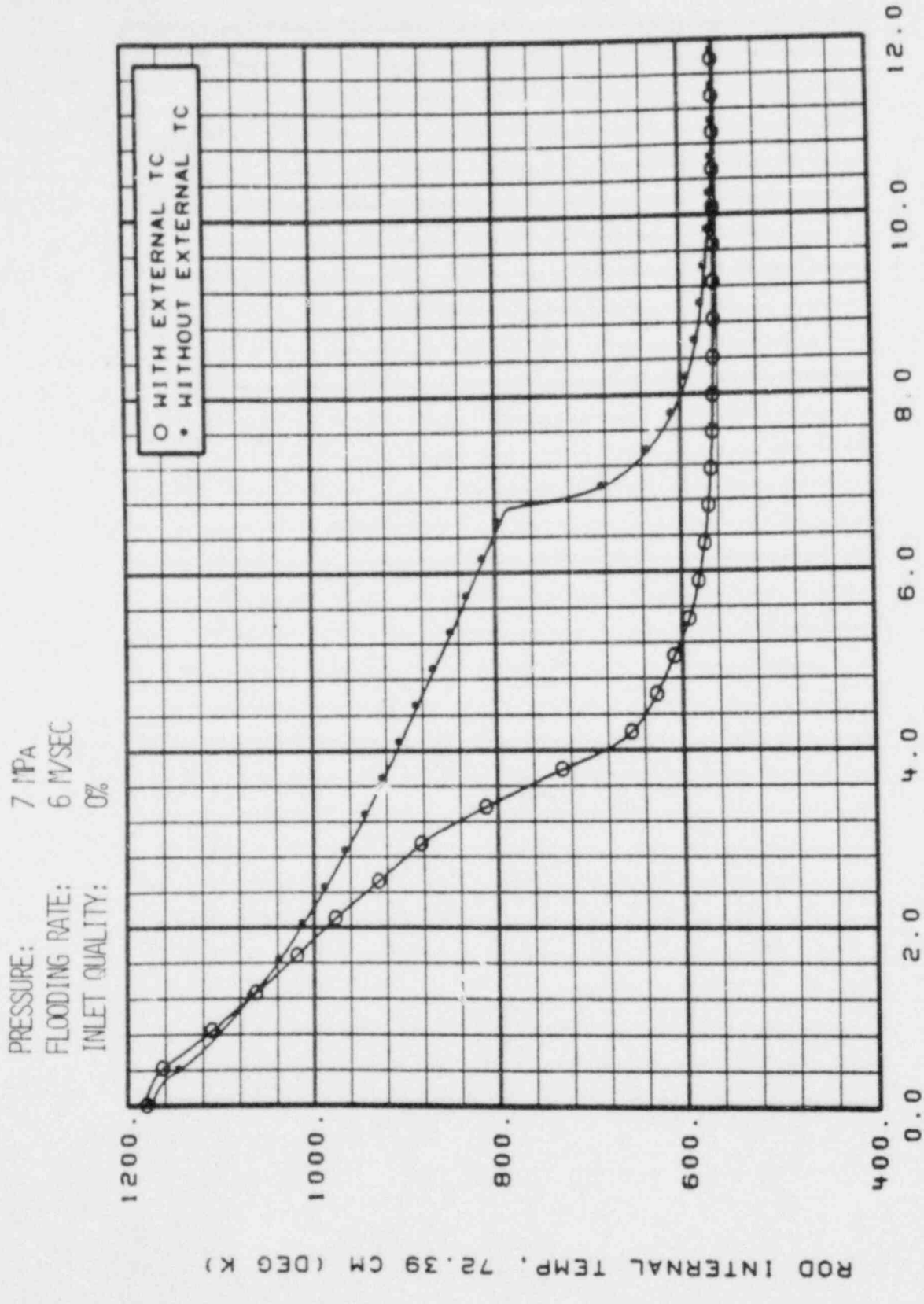


FIGURE 20. INTERNAL THERMOCOUPLE (2) COMPARISON FOR RUN 23

PRESSURE: 7 MPA
FLOODING RATE: 1.3 M/SEC
INLET QUALITY: 11%

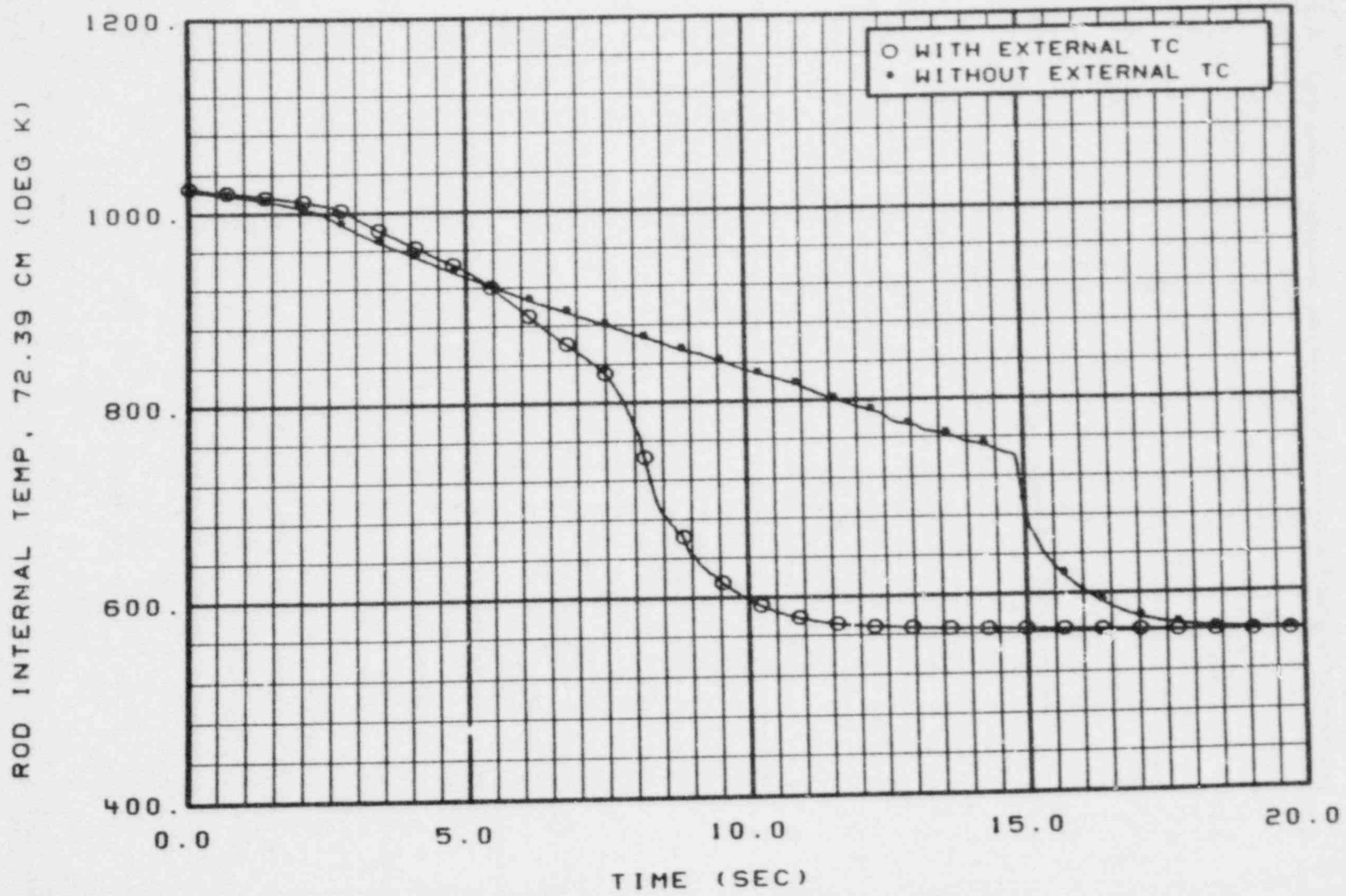


FIGURE 21. INTERNAL THERMOCOUPLE (2) COMPARISON FOR RUN 8

QKPLT MOD-5 VER 119 03/28/79 JA0088V TAU 11/02/79 14.45.21. GRAPH 2

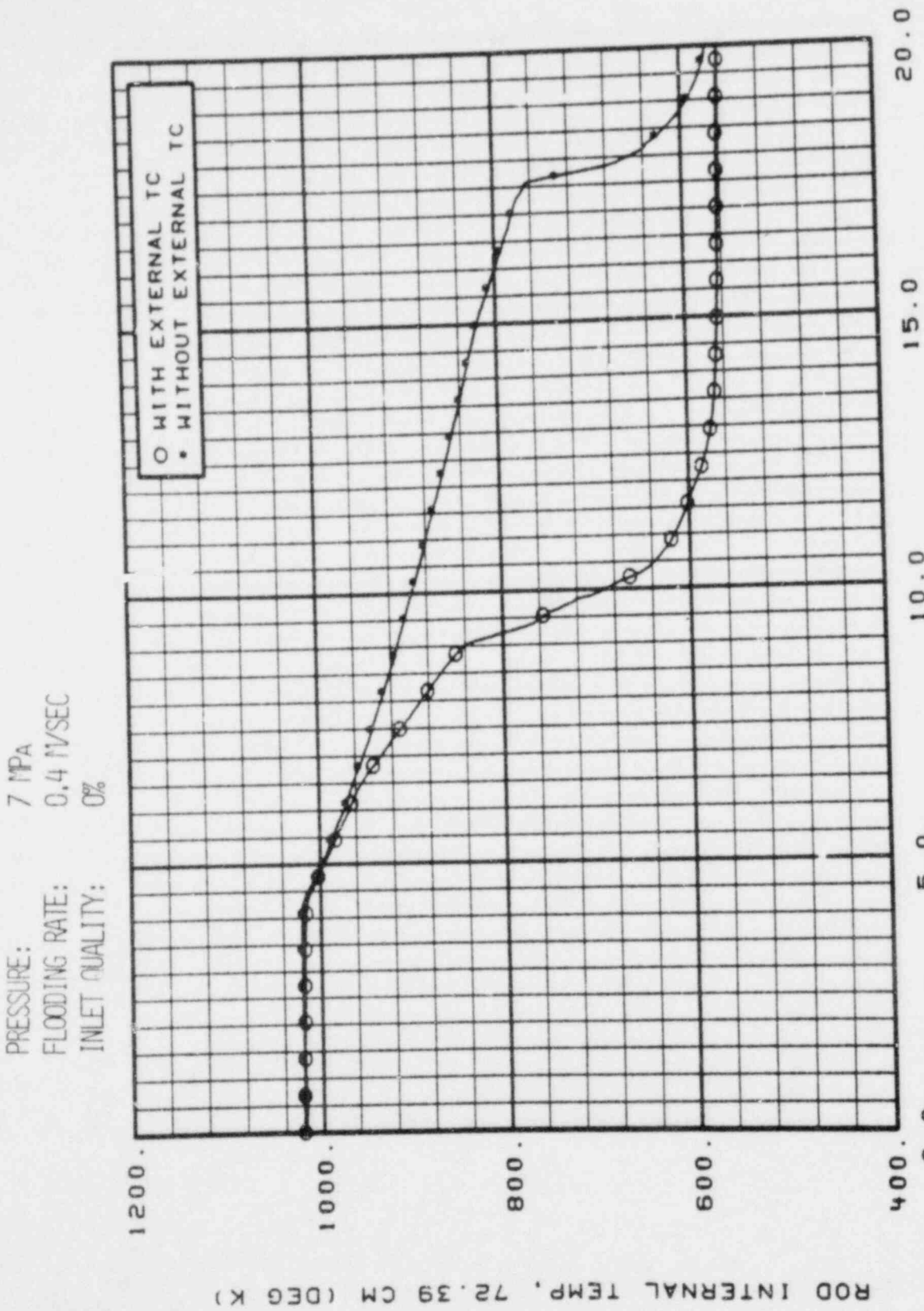


FIGURE 22. INTERNAL THERMOCOUPLE (2) COMPARISON FOR RUN 7

PRESSURE: 7 MPa
FLOODING RATE: 0.4 M/SEC
INLET QUALITY: 0%

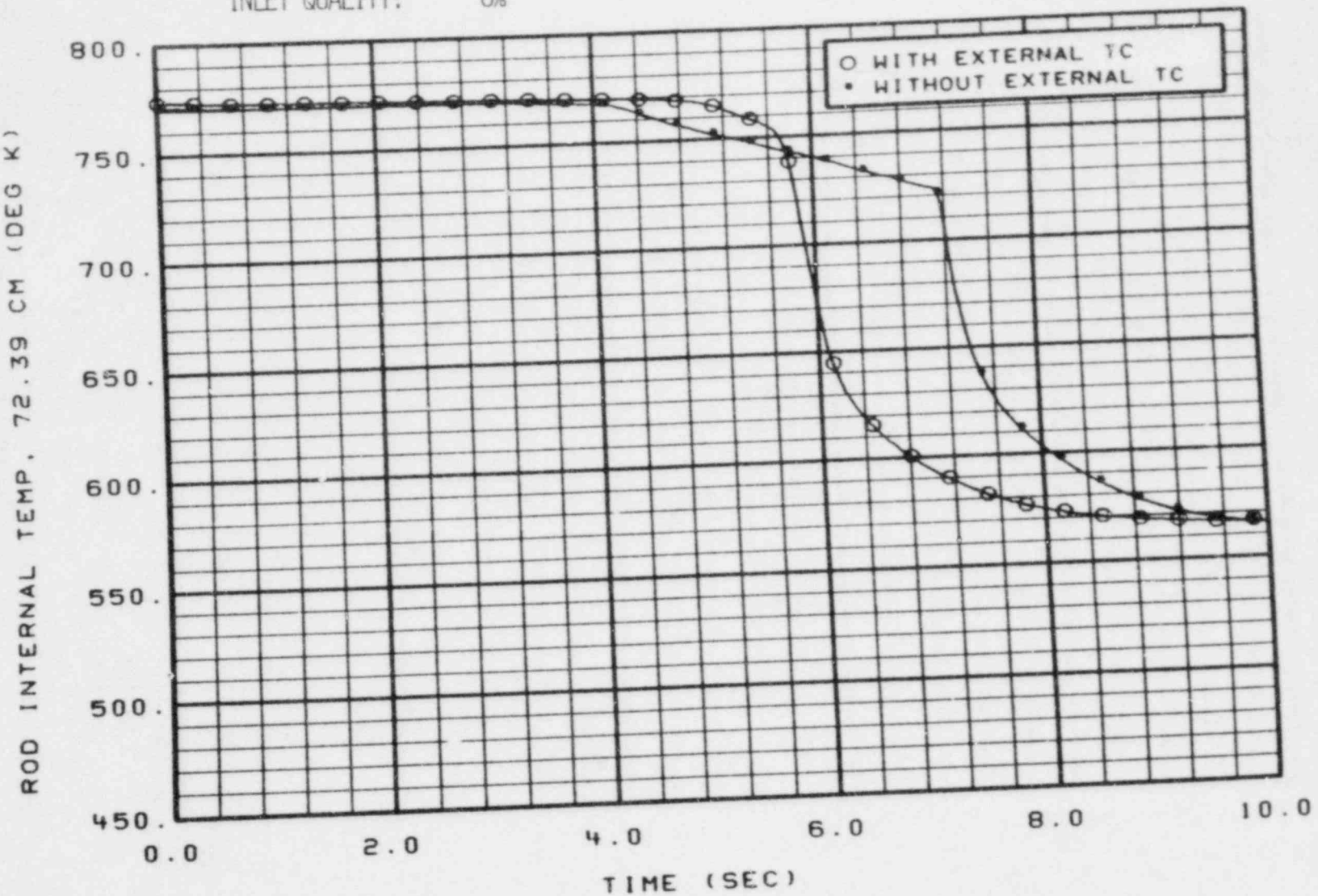


FIGURE 23. INTERNAL THERMOCOUPLE (2) COMPARISON FOR RUN 6

QKPLT MOD-5 VER 119 03/28/79 JAG0680 TAU 11/02/79 14.48.54. GRAPH 2

PRESSURE: 7 MPA
FLOODING RATE: 1.8 M/SEC
INLET QUALITY: 0%

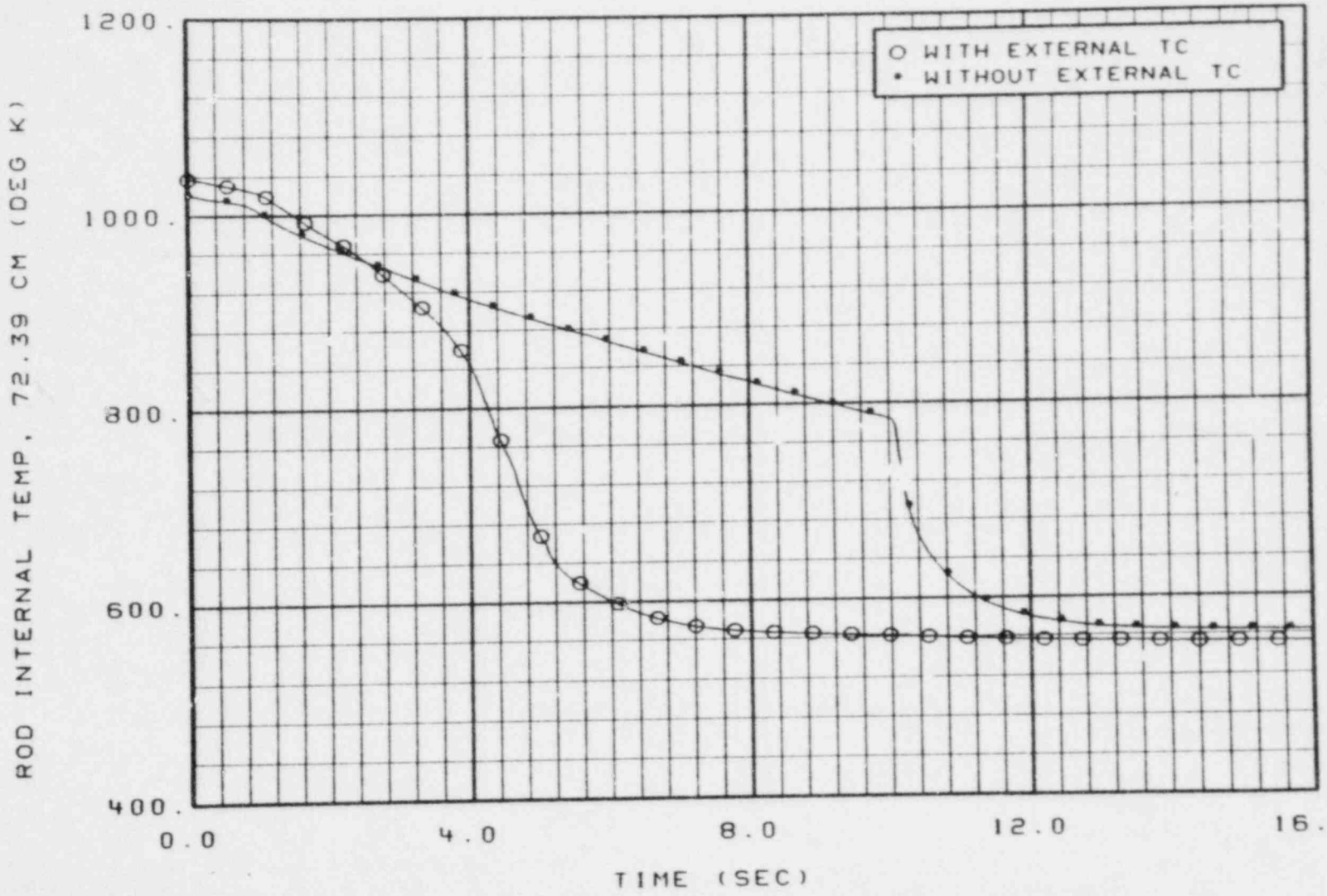


FIGURE 24, INTERNAL THERMOCOUPLE (2) COMPARISON FOR RUN 24

QKPLT MOD-5 VER 119 03/28/79 JAG245E TAU 11/09/79 17.10.31. GRAPH 2

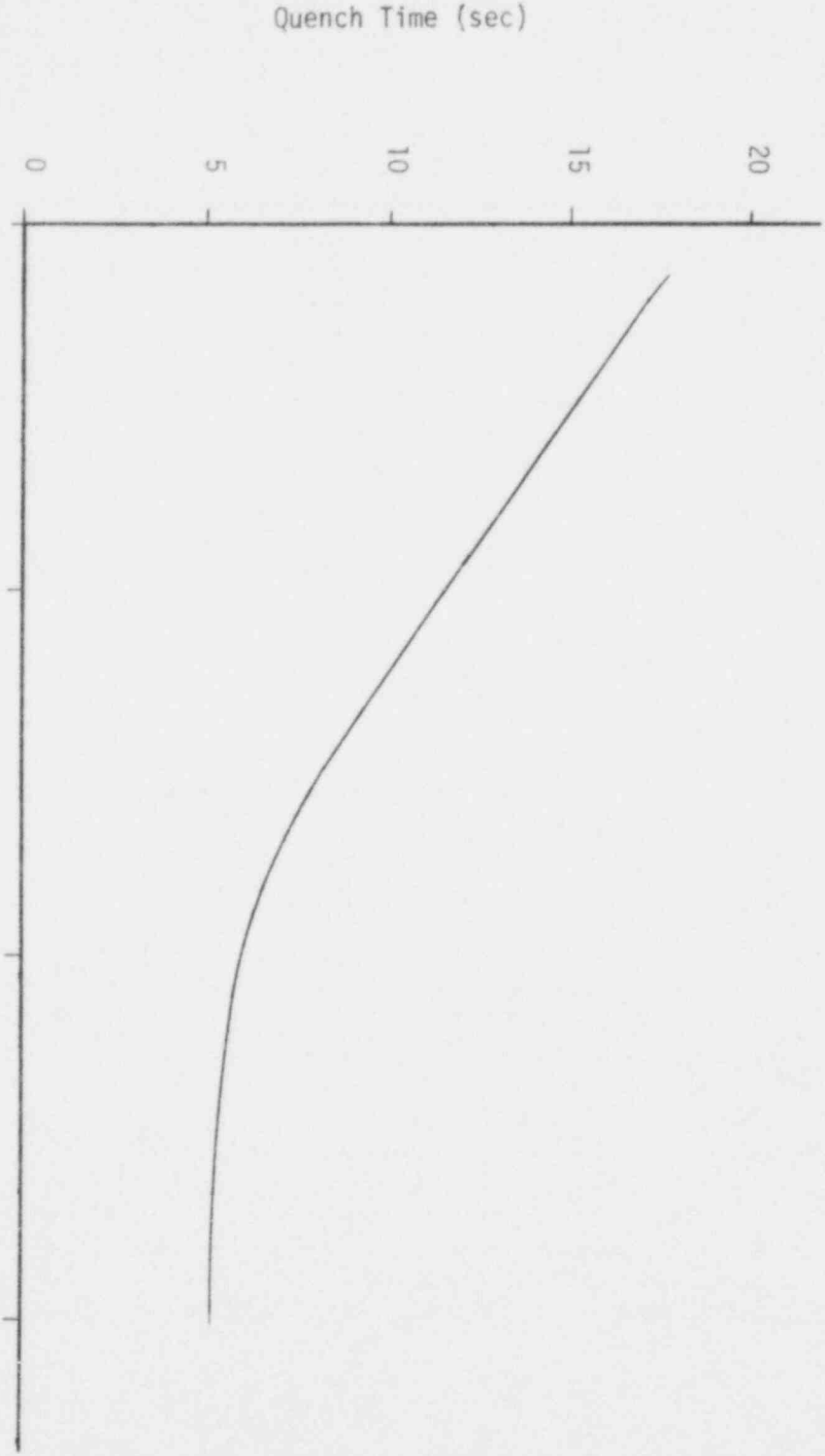


Figure 25. Quench Time vs. Flooding Rate for Rod Without External Thermocouples

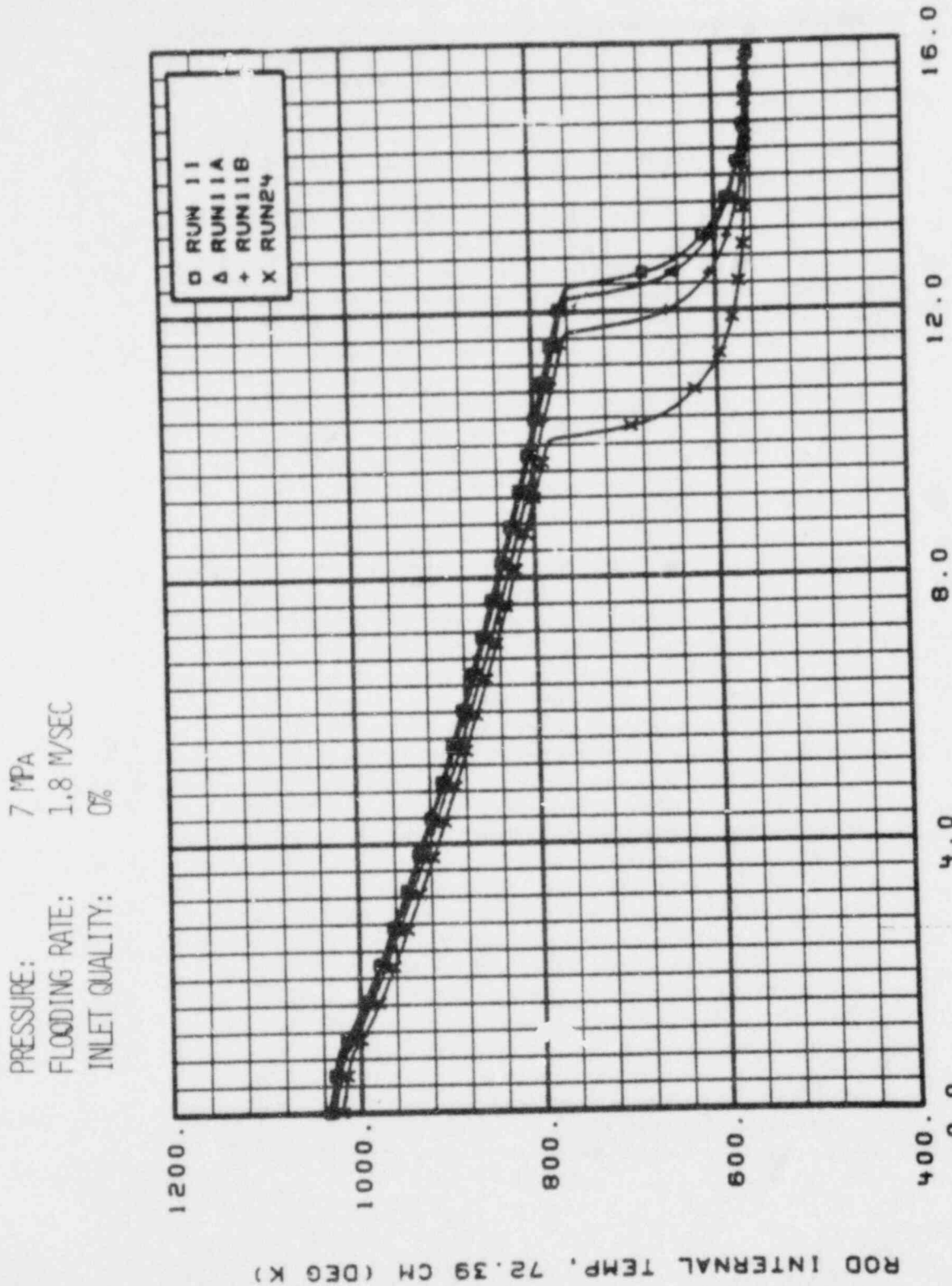


FIGURE 26, REPEATABILITY COMPARISON FOR ITC(2) WITHOUT EXTERNAL TC

PRESSURE: 7 MPa
FLOODING RATE: 1.8 M/SEC
INLET QUALITY: 0%

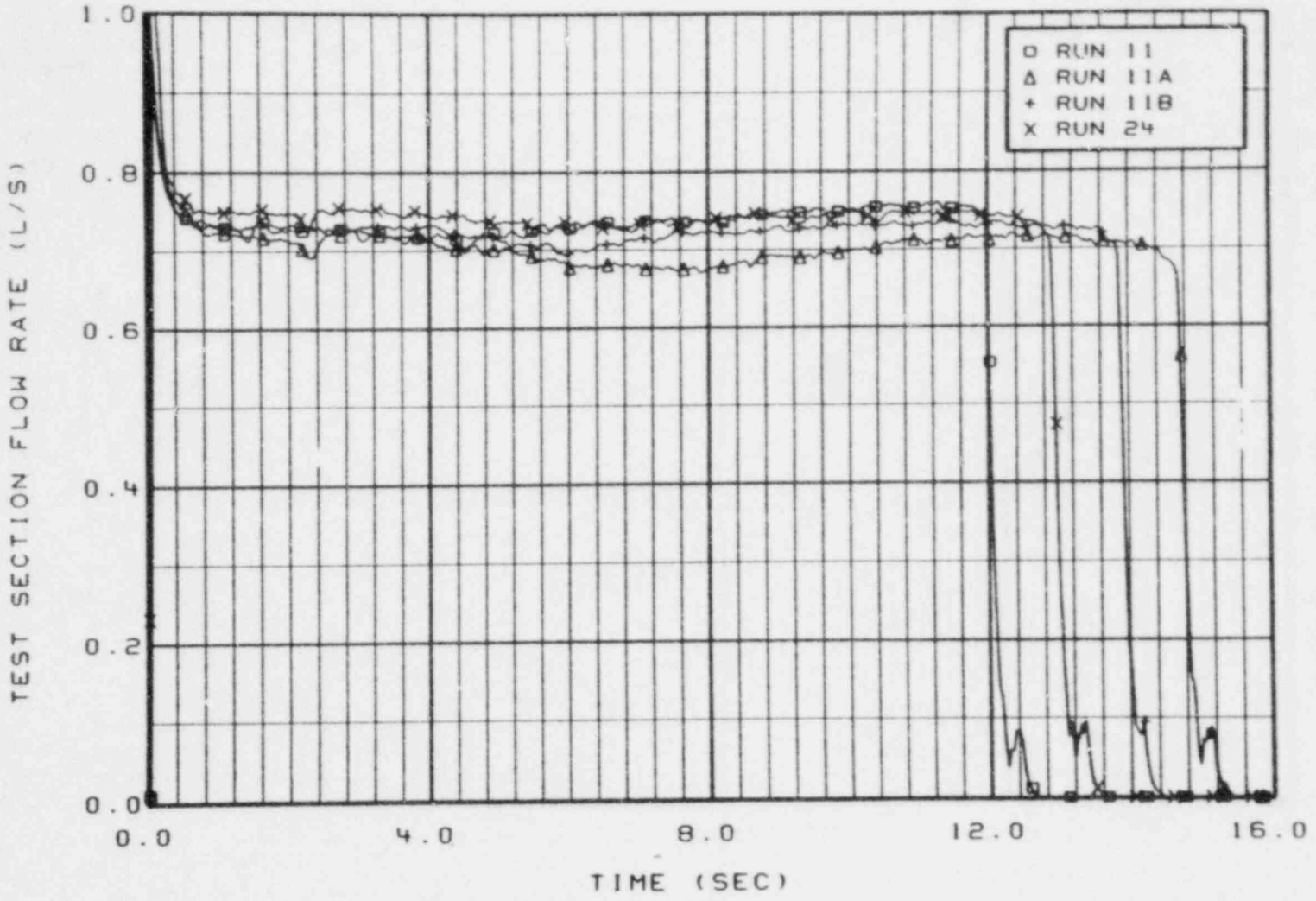


FIGURE 27, FLOW RATE COMPARISON WITHOUT EXTERNAL TC

QKPLT MOD-5 VER 119 03/28/79 JAGRINL TAU 11/28/79 15.34.33. GRAPH - 1

PRESSURE: 7 MPA
FLOODING RATE: 1.8 M/SEC
INLET QUALITY: 0%

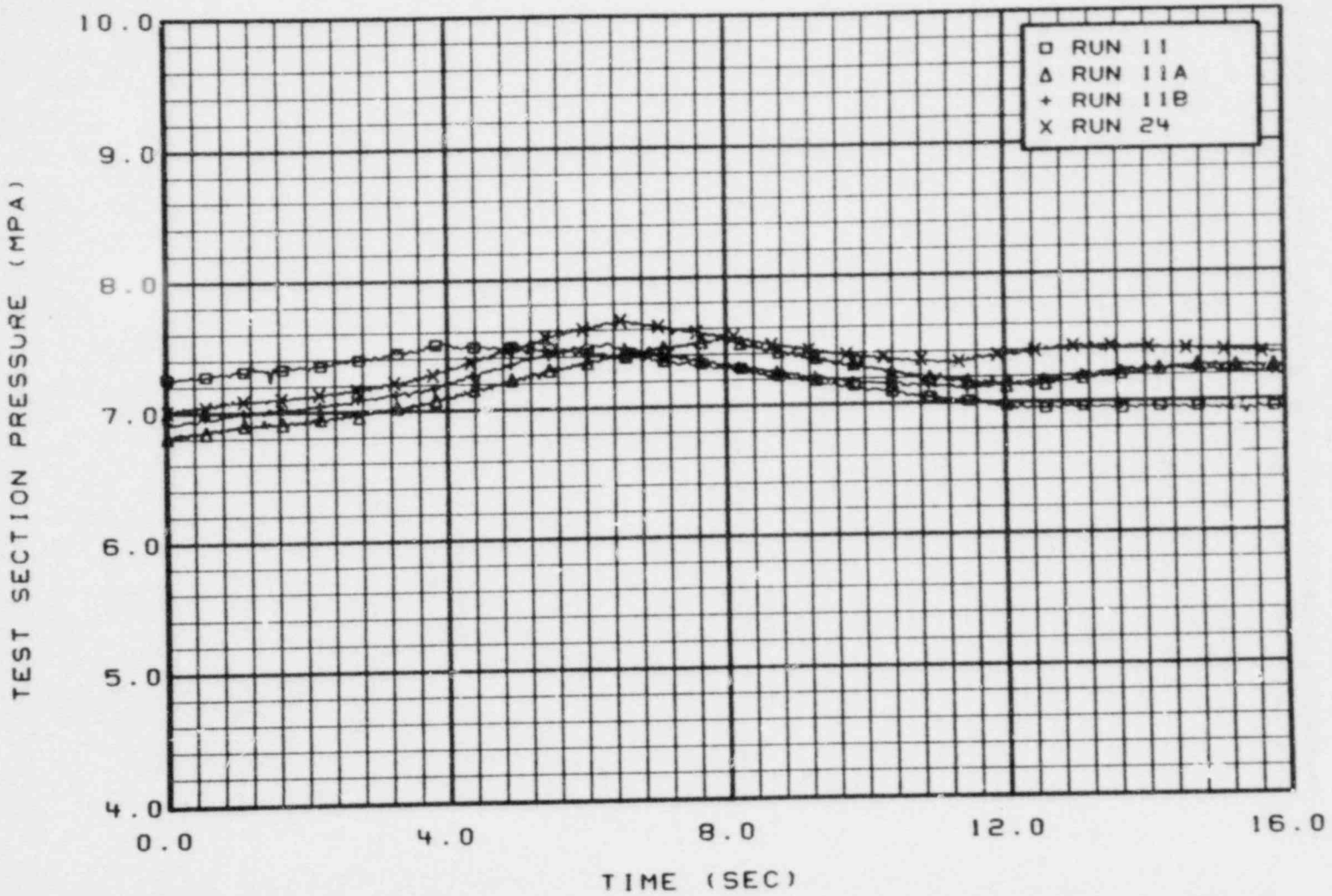


FIGURE 28. PRESSURE COMPARISON WITHOUT EXTERNAL TC

QKPLT MOD-5 VER 119 03/28/79 JAGR332 TAU 11/29/79 08.46.12. GRAPH 2

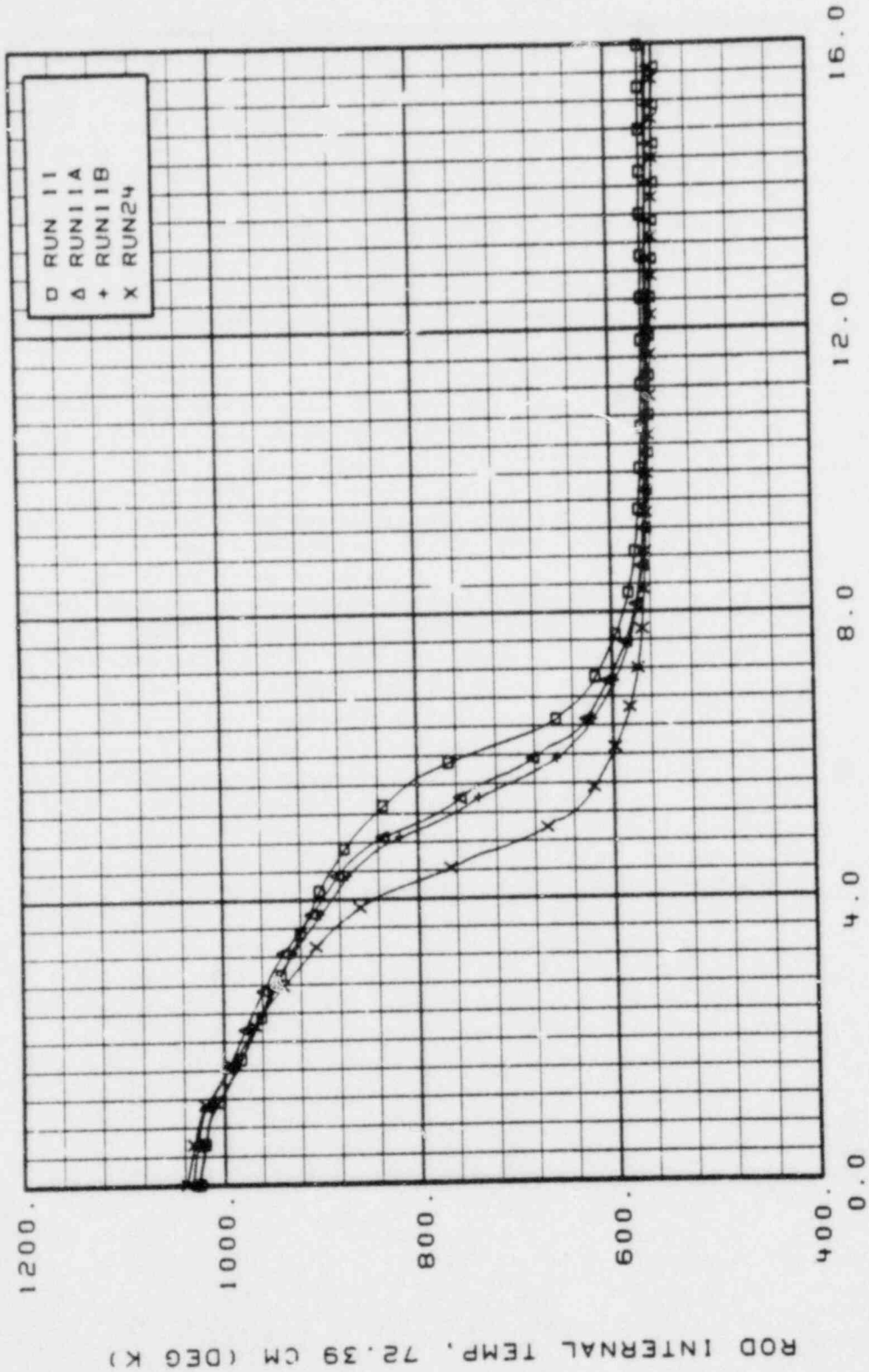


FIGURE 29, REPEATABILITY COMPARISON FOR ITC(2) WITH EXTERNAL TC

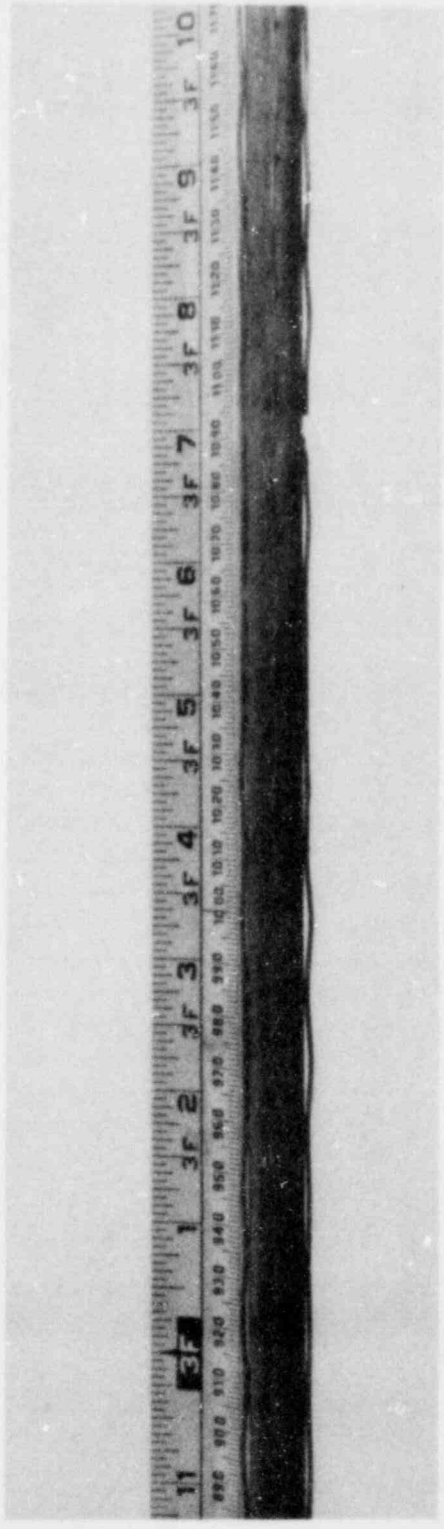

Figure 30. External Thermocouple Deformation

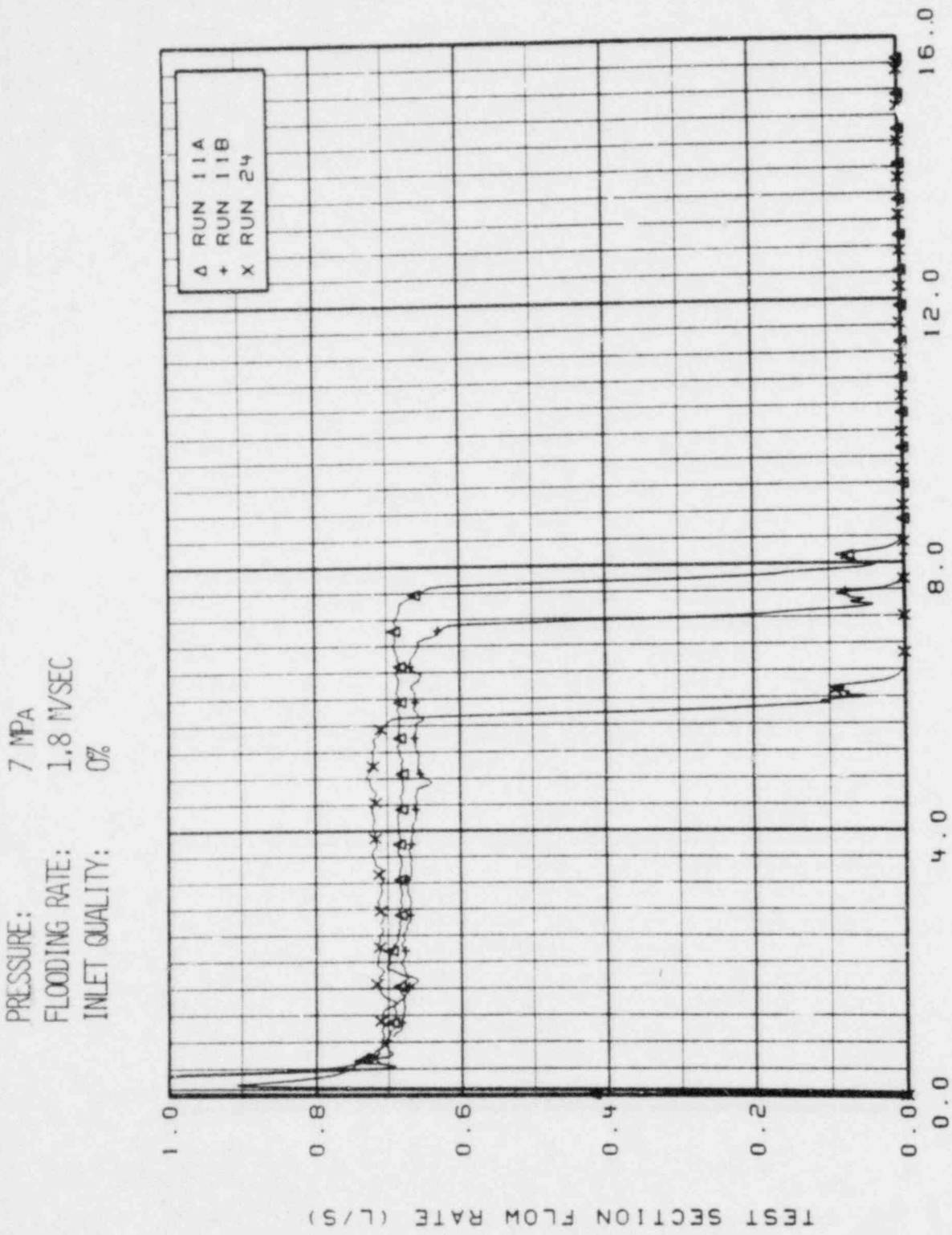


FIGURE 31. FLOW RATE COMPARISON WITH EXTERNAL TC

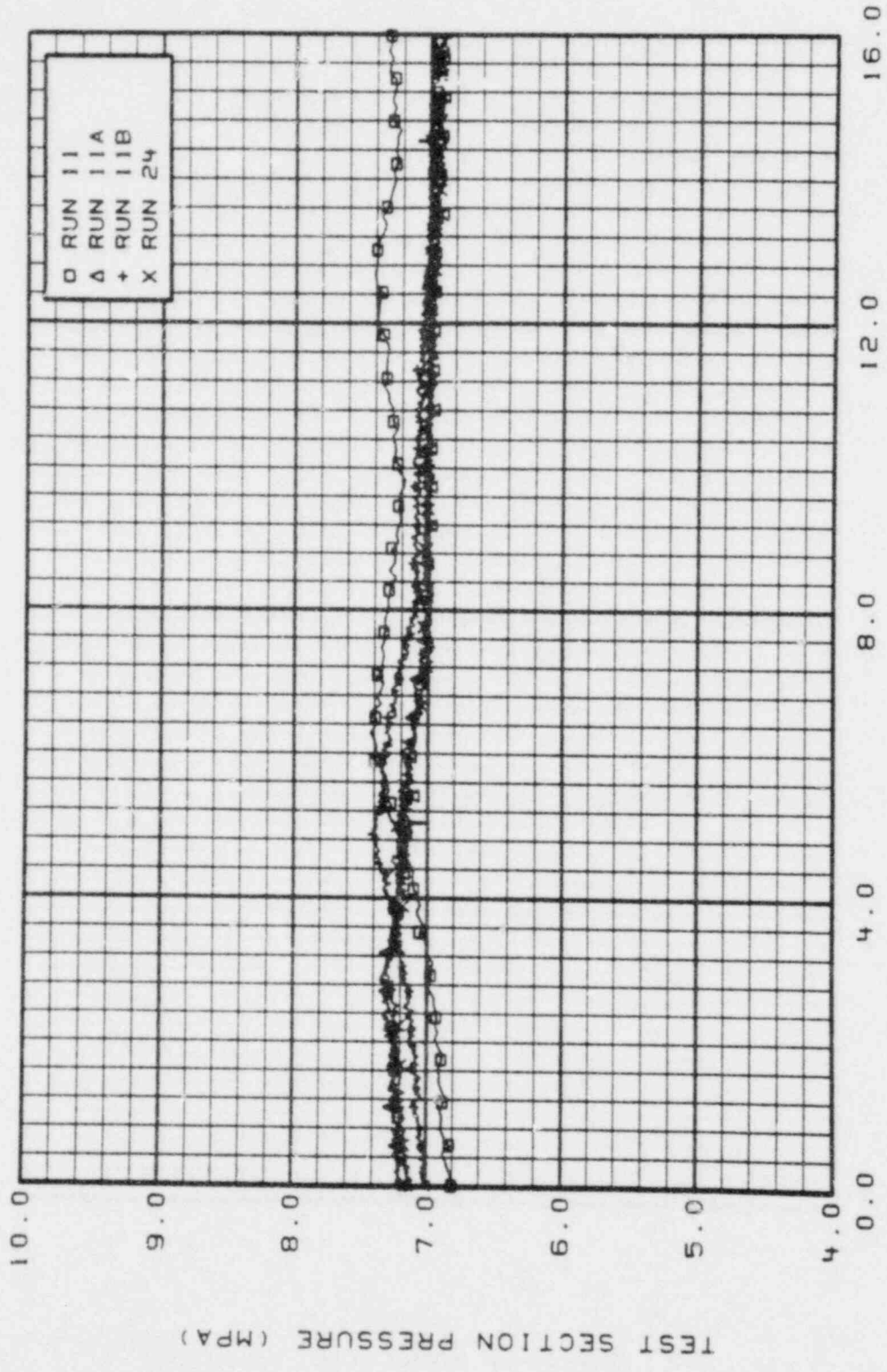


FIGURE 32, PRESSURE COMPARISON WITH EXTERNAL TC

PRESSURE: 7 MPA
FLOODING RATE: 1.8 M/SEC
INLET QUALITY: 0%

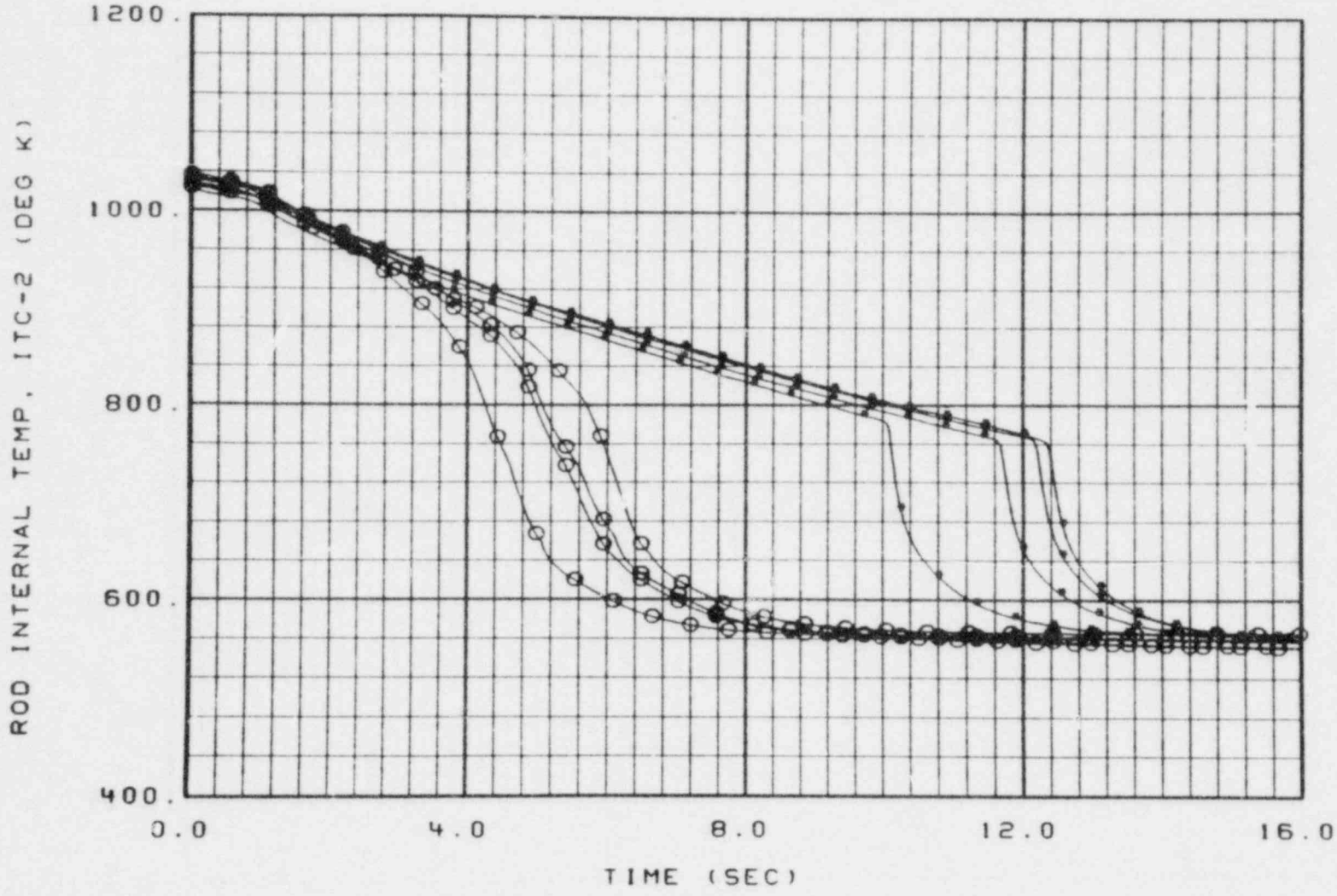


FIGURE 33. REPEATABILITY COMPARISON, O WITH ETC, * WITHOUT ETC

QKPLT MOD-5 VER 119 03/28/79 JA0R52R TAU 11/30/79 09.18.04. ORAPH 1

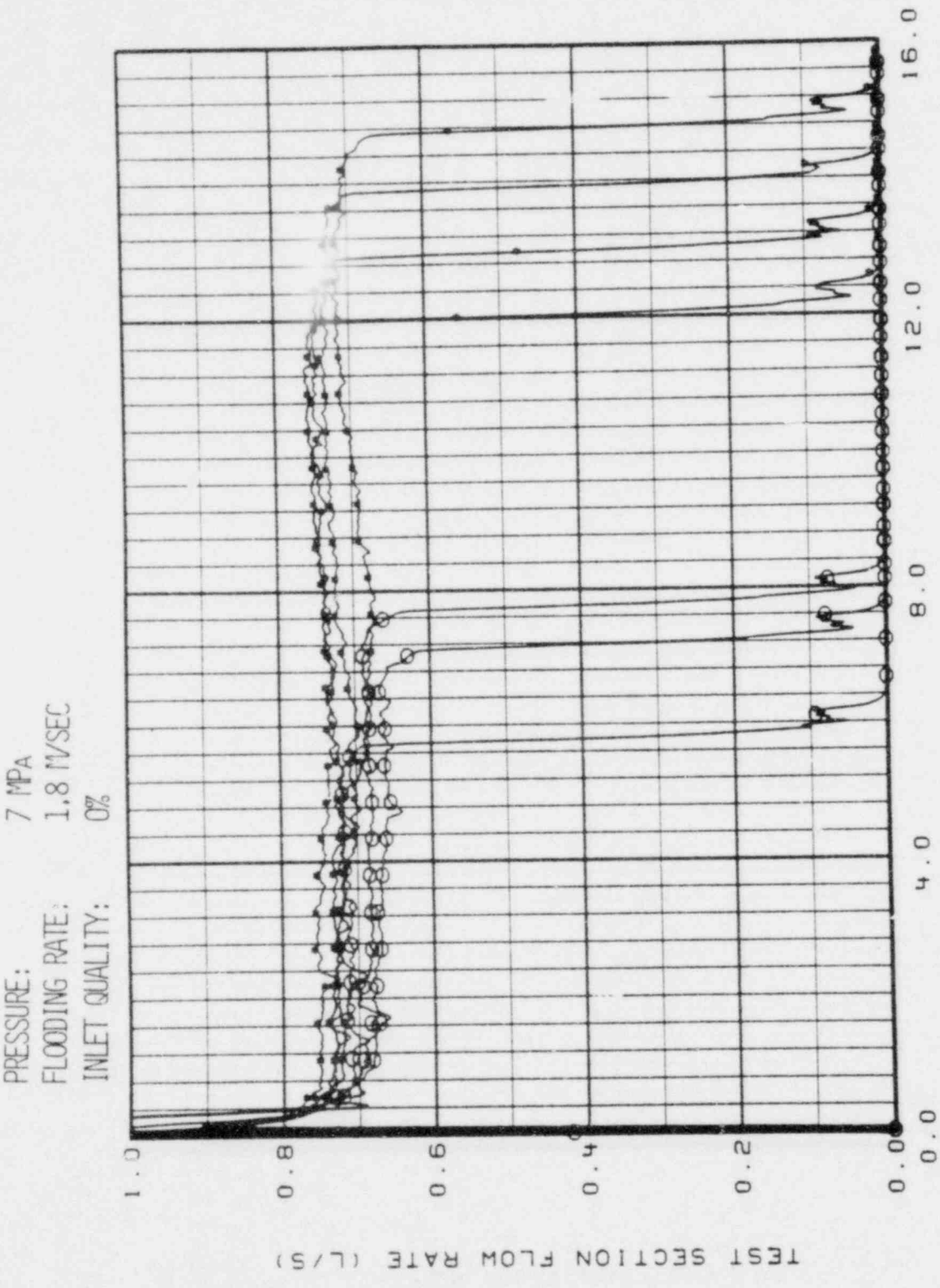


FIGURE 34. REPEATABILITY COMPARISON, O WITH ETC, • WITHOUT ETC

QKPLT MOD-5 VER 119 03/28/79 JAGR2NT TAU 11/28/79 15.34.03. GRAPH 1

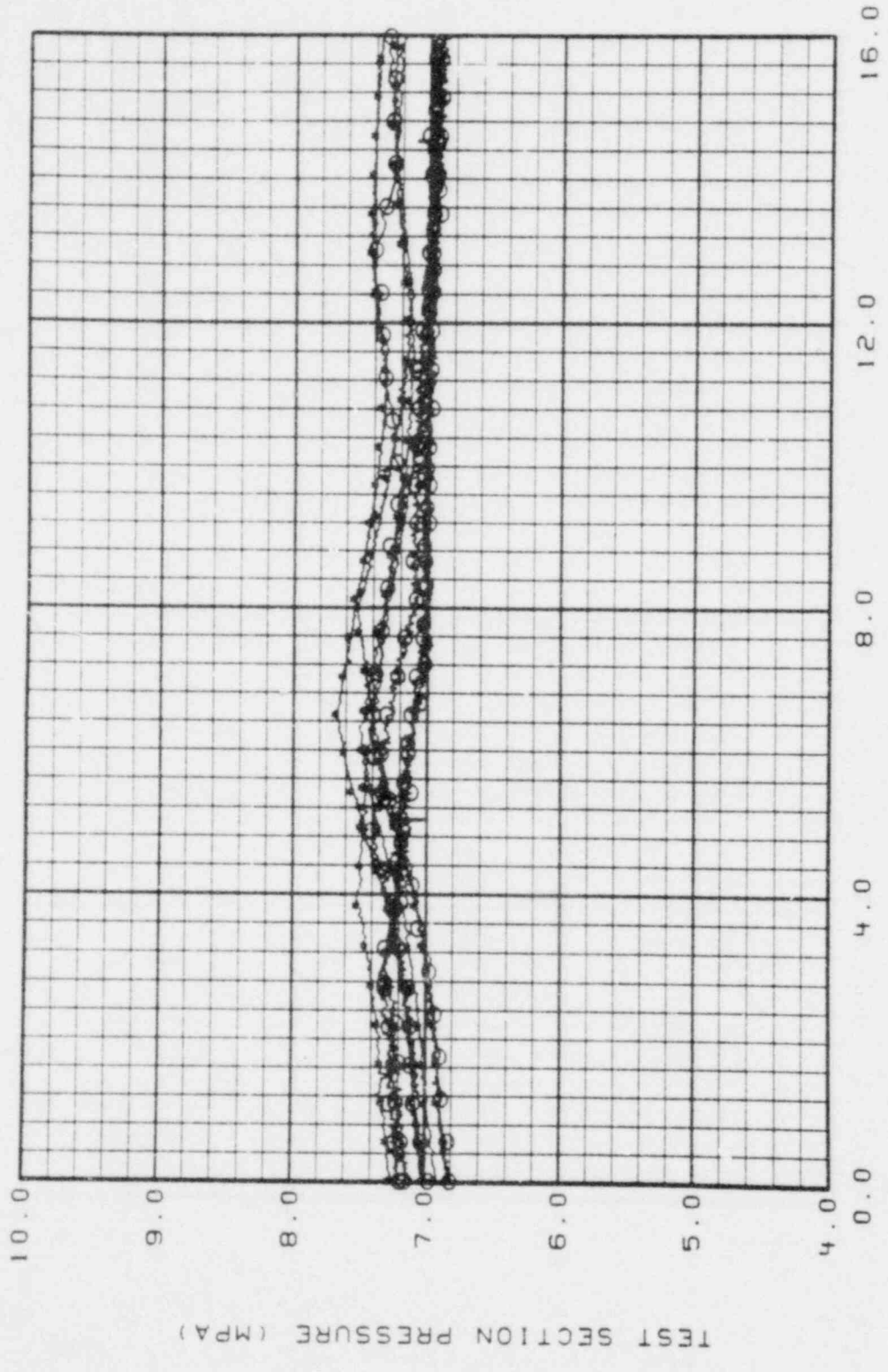


FIGURE 35, PRESSURE REPEATABILITY, O WITH ETC, * WITHOUT ETC

PRESSURE: 0.1 MPA
FLOODING RATE: 0.04 M/SEC
INLET SUBCOOLING: 67°C

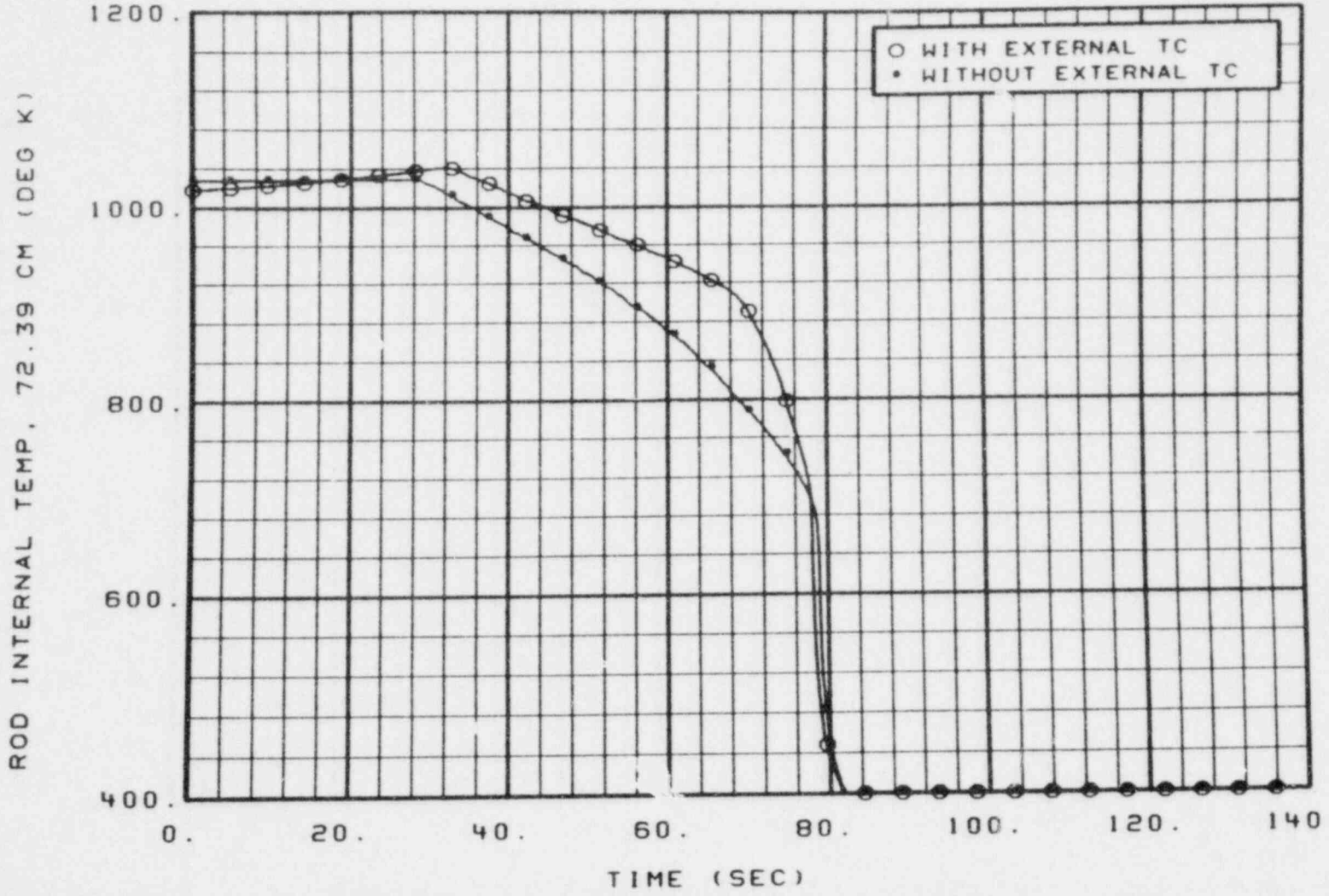


FIGURE 36. INTERNAL THERMOCOUPLE (2) COMPARISON FOR RUN 1

QKPLT MOD-5 VER 119 03/28/79 JAG0130 TAU 11/02/78 12.35.43. GRAPH 2

PRESSURE: 0.1 MPA
FLOODING RATE: 0.04 M/SEC
INLET SUBCOOLING: 67°C

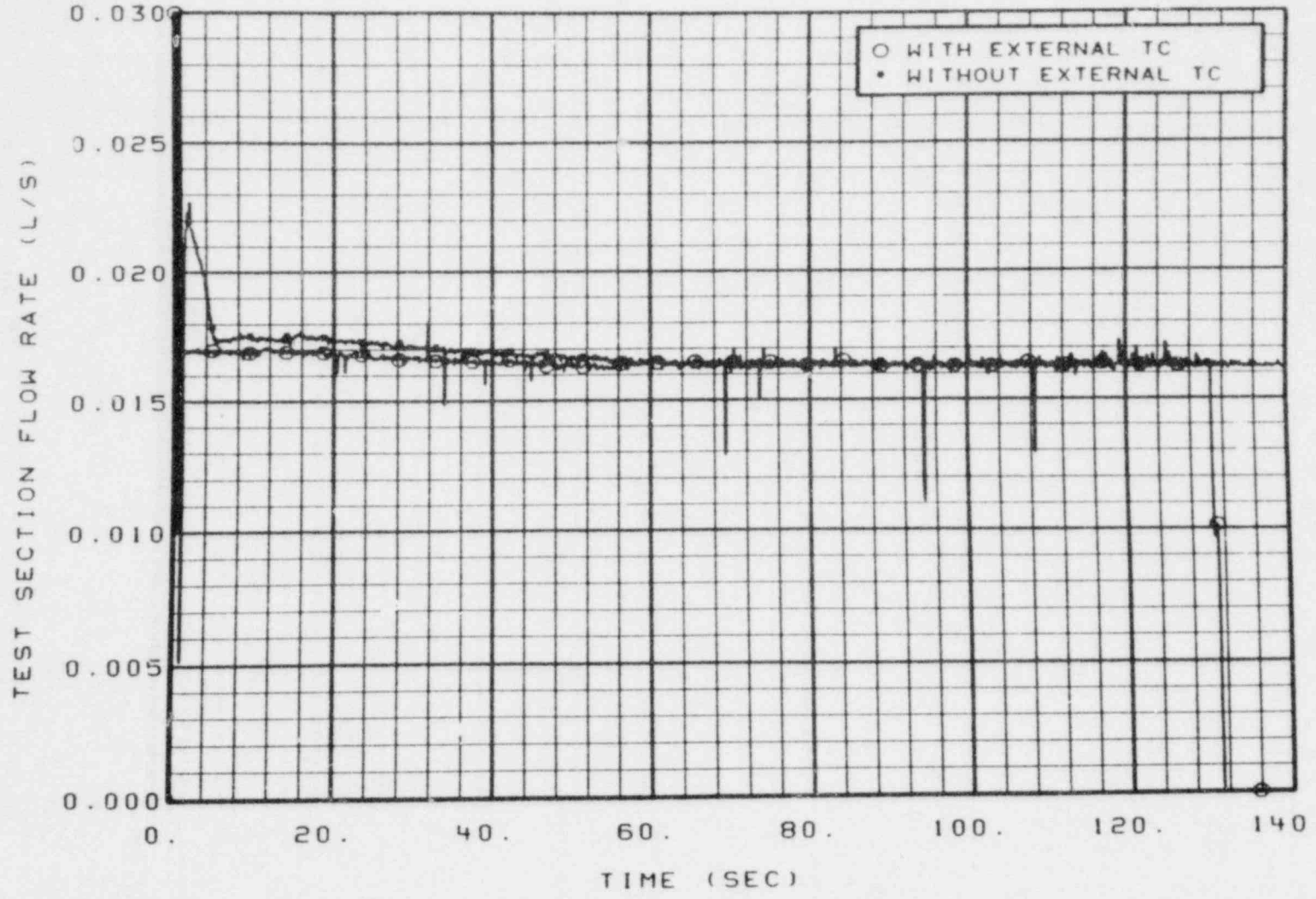


FIGURE 37. TEST SECTION FLOW RATE COMPARISON FOR RUN 1

QKPLT MOD-5 VER 119 03/28/79 JAG0130 TAU 11/02/79 12.35.43. GRAPH 5

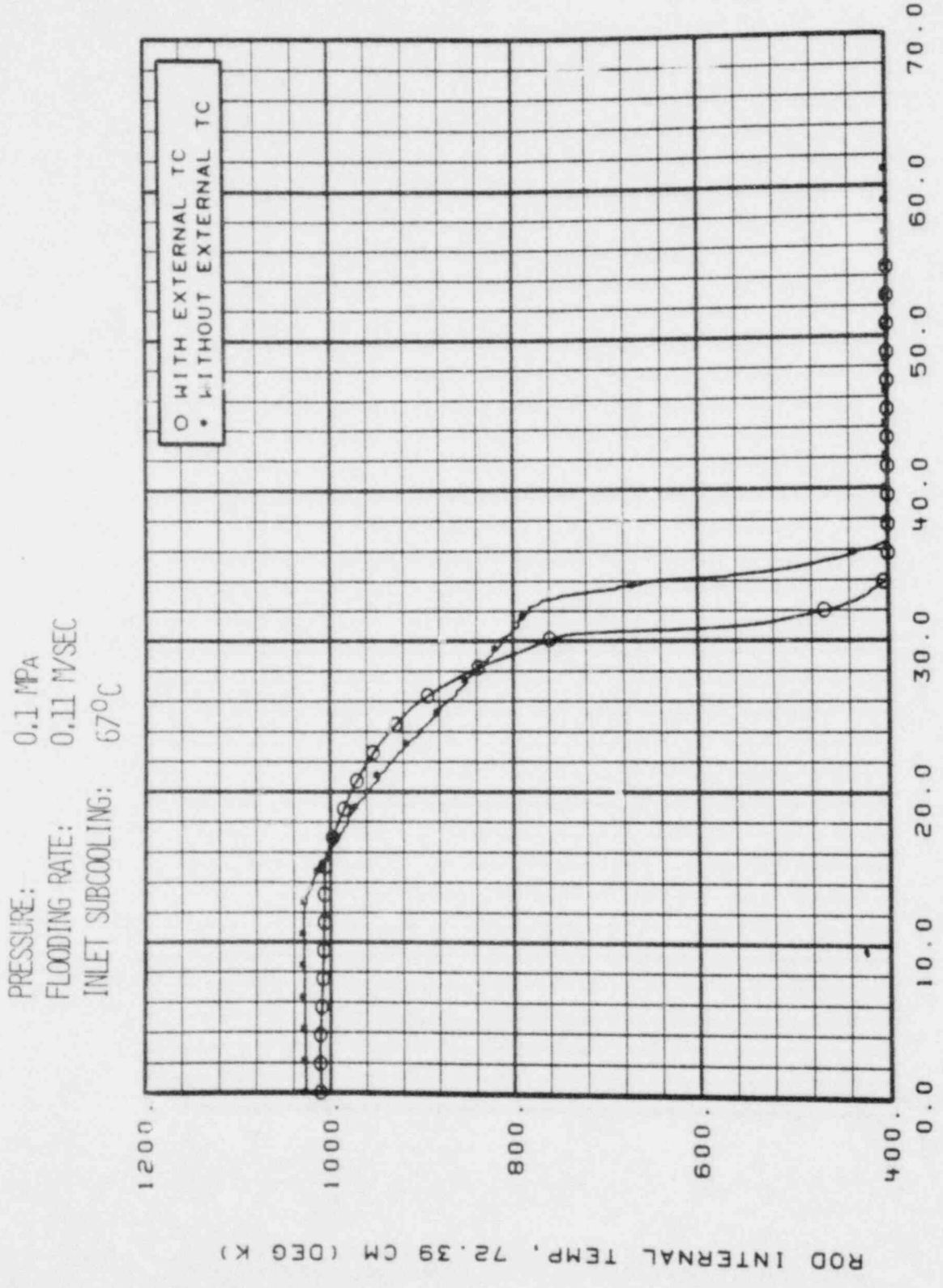


FIGURE 38. INTERNAL THERMOCOUPLE (2) COMPARISON FOR RUN 3

PRESSURE: 0.1 MPA
FLOODING RATE: 0.11 M/SEC
INLET SUBCOOLING: 67°C

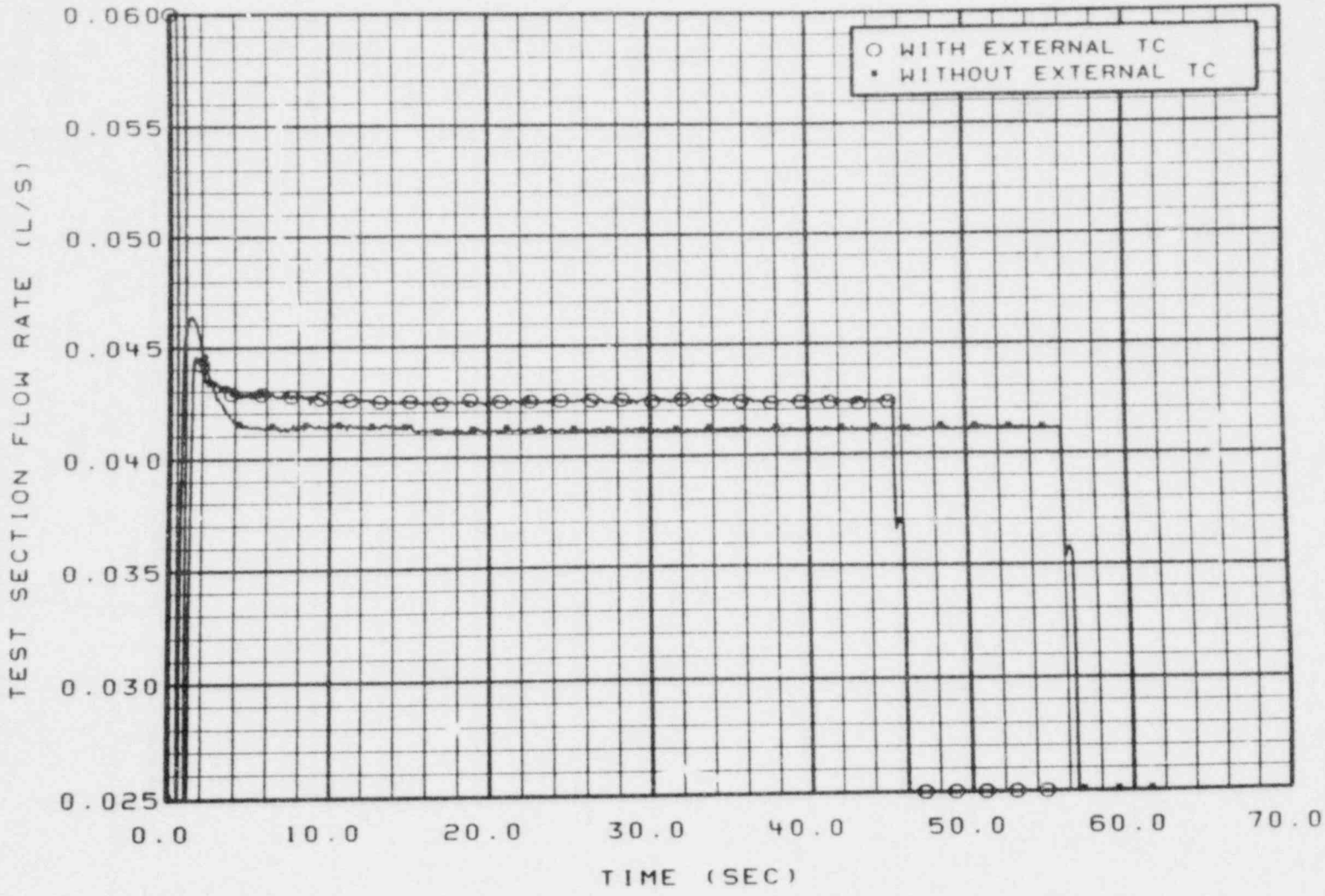


FIGURE 39. TEST SECTION FLOW RATE COMPARISON FOR RUN 3

QKPLT MOD-5 VER 119 03/28/79 JA0033C TAU 11/02/79 12.39.15. GRAPH 5

# APPENDIX A

## MEASUREMENT UNCERTAINTY ANALYSIS

This appendix describes the measurement uncertainty in the data taken during experimental testing to evaluate the effect of cladding surface thermocouples on quench behavior. The uncertainty limits stated are given for a two sigma or 95% confidence level. For convenience, each measurement has been divided into a measurement channel consisting of transducer and signal conditioning, and a data acquisition system (DAS) channel consisting of acquisition electronics and recording equipment. Accuracy uncertainties are combined with the standard Root Sum Square (RSS) technique for percent of range (% Rg) and percent of reading (% Rd) errors. These two components should then be summed. Methods used to quantify uncertainty limits are provided in References A1 through A3. Instrumentation calibration, calibration histories, and voltage insertion calibration data on the data acquisition system were also used, where applicable.

### Data Acquisition System

The data acquisition system consists of instrument cables, filters, an analog input subsystem and the MODCOMP II/45 Computer System. The cables used are shielded, twisted pair cables and the two pole Butterworth filters are set at 10 Hz. The analog input subsystem (Neff System 620 Signal Processor) amplifies and converts analog voltage signals to 16-bit digital word signals. The computer system formats and stores the data on a digital disc. The data is then transferred to magnetic tape for later use.

An automatic precision voltage calibration system, traceable to NBS Standards, is used to update the system calibration daily. This calibration error is assumed to be less than the daily drift, measured at less than 0.05% of range. Stability of the bridge circuit power supply is better than 0.02% of range. Crosstalk contributes an uncertainity of 0.09% of range. The total error attributed to the data acquisition system is 0.10% of range.

## Temperature Measurements

Two kinds of transducers were used for the temperature measurements. The majority were type K, grounded junction thermocouples, with the reference junction held at 150$^{o}$F. The largest thermocouple uncertainties result from standard accuracy tolerances of the transducers caused by impurities in the thermocouple and connecting lead materials; in this case, in the chromel and alumel wire. In addition the thermocouple millivolt output is not linear with temperature. Instead, a third order polynomial is fit to the standard calibration curve (ISA R.P. 1.6). Nevertheless, the deviation is small, over the range of interest, in comparison to the standard accuracy tolerances. The reference junction of the thermocouple has a long-term stability of 0.1 K and a short-term stability of approximately 0.05 K.

One resistance thermometer detector (RTD) was used as a reference temperature. The RTD consisted of a sheathed, precision wire coil used as a wheatstone bridge network. Associated uncertainties are 0.5%, 0.12%, and 0.1% of reading for accuracy tolerance, calibration and reference bridge stability, respectively. Percent of reading measurements assume reading in degrees Celsius.

Radiation heat transfer effects are assumed to be negligible for the given test configuration, as compared to the other temperature measurement uncertainties. Two other uncertainties not considered are mounting effects and fluid interaction. Mounting effects will introduce a greater anticipated measurement uncertainty in metal cladding thermocouples while fluid interaction is most significant for the heater rod LOFT cladding surface thermocouples (ETC1-4) when a two-phase mixture floods the test section. Table A-1 summarizes the uncertainty analysis conducted for the temperature measurements.

TABLE A-1. SUMMARY OF EXPERIMENTAL TEMPERATURE UNCERTAINTIES

| | Type K TC | RTD |
|---|---|---|
| Accuracy tolerances | 4.0% RD @ 38°C<br>1.3% Rd @ 149°C<br>0.75% RD @ 277 - 1260°C | 0.5% Rd |
| Deviation from calibration equation | 1.4% Rd @ 38°C<br>0.43% Rd @ 204°C<br>0.09% Rd @ 538°C | 0.12% Rd |
| Reference junction/ bridge stability (maximum) | 0.2% Rd | 0.1% Rd |
| Measurement Channel Subtotal (RSS) | 4.2% Rd, worst case<br>0.89% Rd @ 285°C = 2.5°C | 0.52% Rd |
| DAS | 0.10% Rg | 0.10% Rg |
| Total | 4.2% Rd + 0.10% Rg<br>0.89% Rd + 0.10% Rg*<br>@ 285°C | 0.52% Rd + 0.10% Rg |

* Although temperature measurements have low range requirements for heatup, temperatures from approximately 285 to 900°C occur during the test transient. Therefore, a maximum of 3.4°C uncertainty should be applied when evaluating temperature test data.

## Volumetric Flow Measurement

The operation of a turbine flowmeter is based on the reluctance principle which states that when a ferrous object approaches the pole face of a magnet, the flux path reluctance between the coil and magnet changes. If a reluctance detector is placed near the rotating blades of a flowmeter, then a sinusodial voltage output is produced as the blade moves toward the detector, increasing the coil voltage, and away from the detector, decreasing the voltage. The volumetric flow is directly proportional to the turbine rotation rate which is then in turn directly proportional to the number of peaks in the sinusodial voltage pattern.

During single phase flow operation, the accuracy of the flow meter is greatly enhanced over two-phase flow because of the precision in calibration. During testing, only liquid flowed through BF-FE-1. Uncertainties include temperature and pressure sensitivity, response limitations, electronics and measurement principles. Mechanical inertia of the turbine represents the limiting factor in instrument response. The uncertainty limits due to measurement principles is based on the comparison between flow experiments and analysis.

Reference A2 and calibration data for BF-FE-1 provided the basis for this analysis. Table A-2 summarizes the uncertainty analysis conducted for the flow rate measurement.

## Pressure Measurements

Sources of error in pressure cells include nonlinearity, hysteresis, drift in the calibration coefficient, thermal effects, inaccuracy of the excitation voltage, and zero setting. Nonlinearity,

TABLE A-2. SUMMARY OF FLOW RATE UNCERTAINTIES (BF-FE-1)

| | | | |
|---|---|---|---|
| Calibration | 0.5% Rg | | |
| Pressure Sensitivity | 0.05% Rg | | |
| Temperature Sensitivity | Negligible | | |
| Response Limitations | 0.35% Rg | | |
| Electronics | 0.56% Rg | | 0.2% Rd |
| Measurement Principle | 0.1% Rg | | |
| Measurement Channel Subtotal (RSS) | 0.84% Rg | + | 0.2% Rd |
| DAS | 0.10% Rg | | |
| Total | 0.84% Rg | + | 0.2% Rd |

hysteresis, and zero offset were estimated from the calibration data. Coefficient drifts were assumed to be 1.5% Rd while thermal effects were based on testing information presented in Reference A2. Table A-3 summarizes the uncertainty analysis conducted for the pressure measurements.

TABLE A-3. SUMMARY OF EXPERIMENTAL PRESSURE UNCERTAINTIES

| | BF-PE-3 | PE-2A | PE-N-1 | PE-ST-1 |
|---|---|---|---|---|
| Nonlinearity | 0.61% Rg | 0.5% Rg | 0.5% Rg | 0.57% Rg |
| Hysteresis | 0.07% Rg | 0.5% Rg | 0.5% Rg | 0.10% Rg |
| Coefficient Drift | 1.5% Rd | 1.5% Rd | 1.5% Rd | 1.5% Rd |
| Thermal Effects | 0.06% Rg | 0.06% Rg | 0.07% Rg | 0.17% Rg |
| Excitation Voltage | 0.05% Rg | 0.05% Rd | 0.05% Rd | 0.05% Rd |
| Zero Offset | 2.0% Rg | 0.06% Rg | 0.02% Rg | 0.17% Rg |
| Measurement Channel Subtotal (RSS) | 2.1% Rg + 1.5% Rd | 0.71% Rg + 1.5% Rd | 0.71% Rg + 1.5% Rd | 0.63% Rg + 1.5% Rd |
| DAS | 0.1% Rg | 0.1% Rg | 0.1% Rg | 0.1% Rg |
| Total | 2.1% Rg + 1.5% Rd | 0.72% Rg + 1.5% Rd | 0.72% Rg + 1.5% Rd | 0.64% Rg + 1.5% Rd |

## Differential Pressure Measurement

The differential pressure cell utilizes a strain gage where the gages are bonded to a diaphragm which separates the high and low sides of a $\Delta P$ sensing element. The excitation voltage is 10 VDC with a transducer response of 35 msec.

Sources of error discussed for pressure cell uncertainty are applicable to differential pressures as well. In addition, other errors may be introduced. For instance, differential pressure cells may have nonsymmetric calibration for the low and high side, called toggle. Also, sense lines may have gas bubbles, leakage, or they may not be completely filled. Toggle was found to be minimal and therefore, is not included in the uncertainty. However, uncertainties in filling sense lines contributes a significant error. Table A-4 summarizes the uncertainty analysis conducted for the differential pressure measurements.

TABLE A-4. SUMMARY OF DIFFERENTIAL PRESSURE MEASUREMENT UNCERTAINTY (BF-DE-1B)

| | | | |
|---|---|---|---|
| Nonlinearity | 0.6% Rg | | |
| Hysteresis | 0.08% Rg | | |
| Pressure Sensitivity | 0.8% Rg | | |
| Coefficient Drift | | | 1.0% Rd |
| Thermal Effects | 0.2% Rg | | 0.2% Rd |
| Excitation Voltage | | | 0.05% Rd |
| Sense Lines | | | 5.5% Rd |
| Zero Offset | 0.4% Rg | | |
| Measurement Channel Subtotal (RSS) | 1.10% Rg | + | 5.6% Rd |
| DAS | 0.10% Rg | | |
| Total | 1.10% Rg | + | 5.6% Rd |

## Gamma Densitometer

The gamma densitometer used is similar to the unit described in Reference A1. Using only the B-Beam, the fluid density is calculated via the attenuation of gamma rays from a $Ce^{137}$ source radiating through a 2.54 cm pipe with a 1.072 cm diameter heater rod mounted inside. Except for thermal effects, the uncertainties for this instrument are assumed to be similar to those in Reference A1. The densitometer voltage data was recorded uncalibrated as BF-DE-1B and was later converted to engineering units as follows:

$$\rho = \frac{1}{c} \ln \left(\frac{D}{V - V_{off}}\right)$$

where

$$c = \frac{1}{(\rho_l - \rho_g)} \ln \left(\frac{V_g - V_{off}}{V_l - V_{off}}\right)$$

$$D = (V_l - V_{off})\, e^{c\rho_l} = (V_g - V_{off})\, e^{c\rho_g}$$

$\rho$ = density

$\rho_l$ = known density of liquid phase

$\rho_g$ = known density of gas phase

$V_{off}$ = offset voltage

$V_l$ = signal voltage for full liquid phase

$V_g$ = signal voltage for full gas phase

$V$ = measured signal voltage

The first densitometer calibration occurred on July 31, 1979 and yielded a calibration equation of

$$\rho\ (kg/m^3) = 9887.7 \ln \frac{10.01}{V}$$

The densitometer was later calibrated to

$$\rho\ (kg/m^3) = 9049.7 \ln \frac{10.01}{V}$$

on August 21, 1979 (between runs 1 and 8 with cladding surface thermocouples), after noticing the test data indicated a cold water density over 1100 $kg/m^3$. Nothing was found to be incorrect with the first calibration and the assumption was made that either the heater rod or densitometer had shifted because of large temperature gradients on the rod during testing. A maximum thermal effects uncertainty was assigned to be the percentage difference in density during run 1 using the two calibration equations. Table A-5 below summarizes the uncertainty analysis conducted for the gamma densitometer.

TABLE A-5. SUMMARY OF GAMMA DENSITOMETER UNCERTAINTY

| | | | |
|---|---|---|---|
| Statistical Error | 0.6% Rg | | |
| Non-Mono Energetic Gamma | 0.5% Rg | | |
| Stability | 0.1% Rg | | |
| Calibration | 1.0% Rg | | 0.3% Rd |
| Linearity | 0.2% Rg | | |
| Noise | 0.4% Rg | | |
| Thermal Effects | 11.0% Rg | | |
| Measurement Channel Subtotal (RSS) | 11.1% Rg | + | 0.3% Rd |
| DAS | 0.1% Rg | | |
| Total | 11.1% Rg | + | 0.3% Rd |

## References

A1. G. L. Biladeau, et al, LOFT Experimental Measurements Uncertainty Analysis, LTR 141-39, September 15, 1975.

A2. R. P. Evans, et al., PBF-TFBP Experimental Measurements Test-Independent Uncertainty Analysis, TREE-1334, NUREG CR 0837, to be published.

A3. H. S. Crapo, One-Sixth Model BWR Jet Pump Test, Section VI, Error Analysis, LTR 20-105, October 1979.

# APPENDIX B

## EFFECT OF HEATER ROD POWER ON COOLDOWN RATES

# APPENDIX B

## EFFECT OF HEATER ROD POWER ON COOLDOWN RATES

The purpose of this study was to determine the effect of rod power fluctuations on test repeatability. Once the heater rod obtained the desired temperature for a given test run, the power was controlled to maintain that temperature. The power was controlled either manually or automatically. Either mode of operation resulted in small power fluctuations such that at the initiation of any repeat test, the power could vary several percent.

A typical power level on the rod for an initial temperature of 1025 K was about 1.9 Kw. The problem was bounded by comparing the cooldown rate of a rod powered at 1.9 kw throughout the transient to a rod with no applied power. The cooldown rates were generated from HEAT-1, a one-dimensional heat conduction code. Comparisons were considered over a wide range of surface heat transfer coefficients possible during precursory cooling and quench. The results showed an insignificant increase in the quench time for the powered rod as compared to an unpowered rod under the same boundary conditions. Fluctuations in rod power can then be concluded to have a negligible effect on test repeatability.

### Model and Study Description

Using HEAT-1, the swaged heater rod was modeled radially in four regions representing the different annular sections: a boron nitride center, helical constantan wire, boron nitride annulus and stainless

steel cladding. Nineteen mesh points were used, six in the first section, five in each of the next two sections and three in the cladding. The mesh points in each material were equally spaced. For each material the thermal conductivity, specific heat capacity, density, phase change temperature and latent heat of fusion were input from standard tables. The radial nodalization of the heater rod is shown schematically in Figure B1.

To vary initial and boundary conditions, the initial rod temperature, fluid temperature, surface heat transfer coefficient and rod power are input to the program. Uniform initial rod temperatures of 1023 K (750$^{o}$C) and 773 K (500$^{o}$C) were considered with the fluid temperature held constant at 558 K (285$^{o}$C).

The surface heat transfer coefficient was varied as a function of time, as given in Table B1, to simulate typical values during a rod quench. These values were calculated from temperature measurements on the nuclear fuel rods in the L2-2 experiment. Constant surface heat transfer coefficients of $1.356 \times 10^{-1}$, $6.780 \times 10^{-2}$, $4.068 \times 10^{-2}$, and $1.356 \times 10^{-2}$ cal/sec cm$^{2}$ K, representative of precursory cooling were also studied.

## Results and Conclusions

For identical boundary conditions, an increase in rod power decreases the cooldown rate. For lower surface heat transfer coefficients the effect is larger; however, over the range of boundary conditions studied the difference in cooldown rates between a rod powered at 1.9 kw and an unpowered rod is insignificant. Consequently, fluctuations in rod power would be less noticeable and their effect on test repeatability negligible.

Figure B1 -- Type

RADIAL NODALIZATION OF SWAGED HEATER RODS

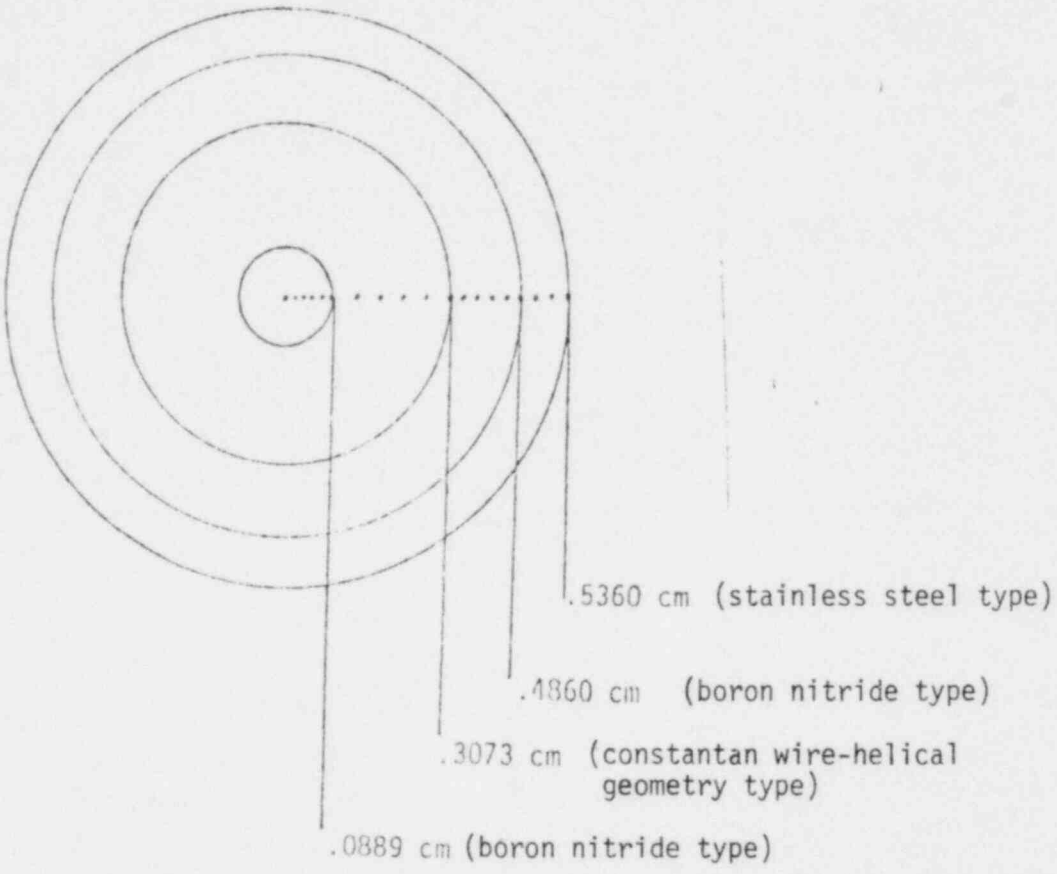

TABLE B1

HEAT TRANSFER COEFFICIENT AS A FUNCTION OF TIME AT HOT SPOT IN L2-2

| Time (sec) | Heat Transfer Coefficient (cal/sec $cm^2$ K) |
|---|---|
| 0 | $3.404 \times 10^{-2}$ |
| 0.25 | $6.346 \times 10^{-2}$ |
| 0.50 | $1.246 \times 10^{-1}$ |
| 0.75 | $2.038 \times 10^{-1}$ |
| 1.00 | $3.623 \times 10^{-1}$ |
| 1.25 | $5.661 \times 10^{-1}$ |
| 1.50 | $8.379 \times 10^{-1}$ |
| 1.75 | 1.132 |
| 2.00 | 1.356 |

For time greater than 2 seconds, surface heat transfer coefficient = 1.356 cal/sec $cm^2$ K

Figure B2 compares the cooldown rates from 500°C for a rod with the L2-2 heat transfer coefficient history and a constant surface heat transfer coefficient of $1.356 \times 10^{-1}$ cal/sec $cm^2$ K, both with and without power. Likewise, Figures B3 and B4 show cooldown rates from 750°C for heat transfer coefficients ranging from $1.356 \times 10^{-1}$ to $1.356 \times 10^{-2}$ cal/sec $cm^2$ K.

Figure B2

# ELECTRIC HEATER ROD COOLDOWN RATES

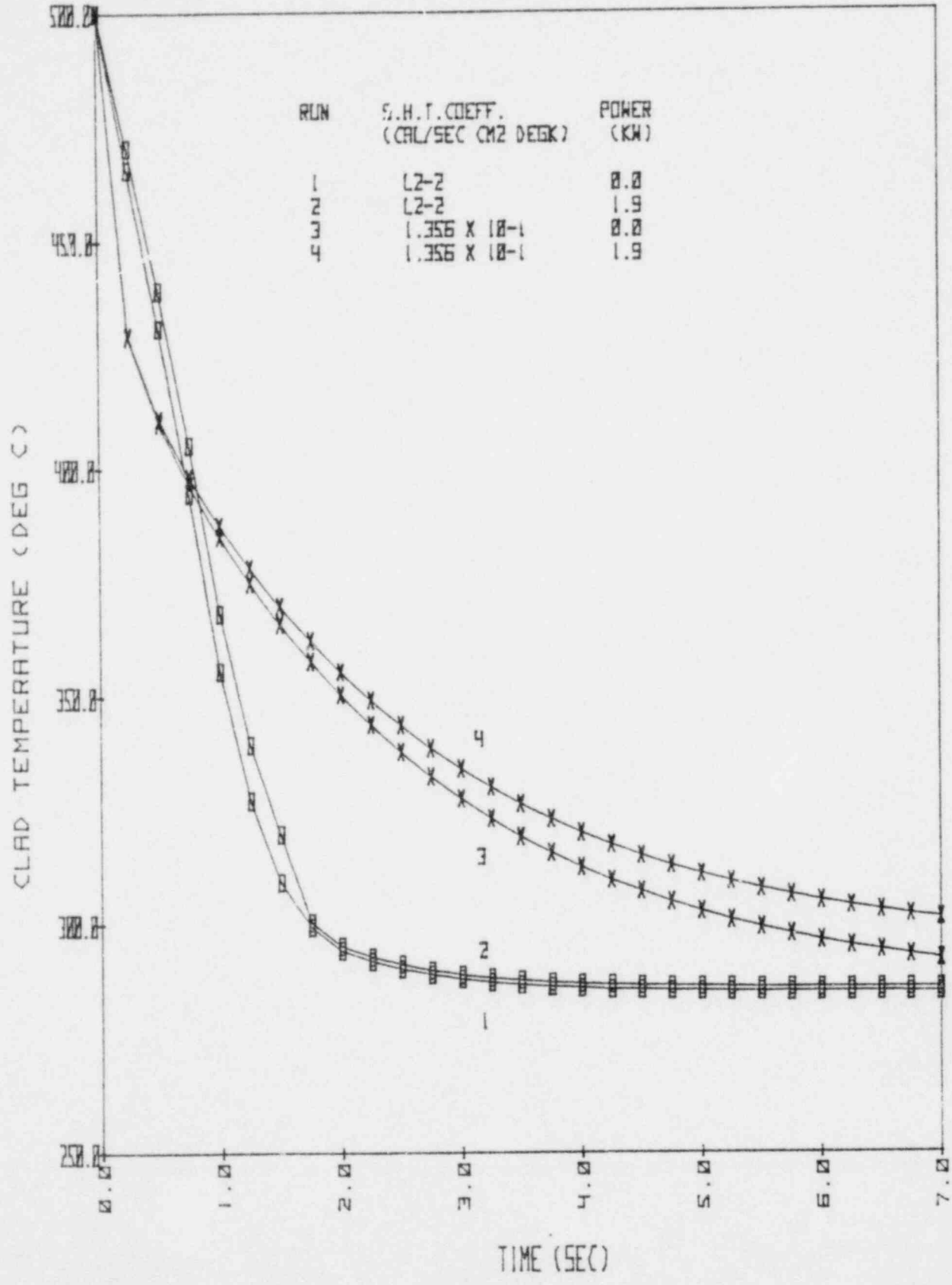


COMPUTED PARAMETER HEATI DATA, OCTOBER, 1979.

FIGURE B3

# ELECTRIC HEATER ROD COOLDOWN RATES

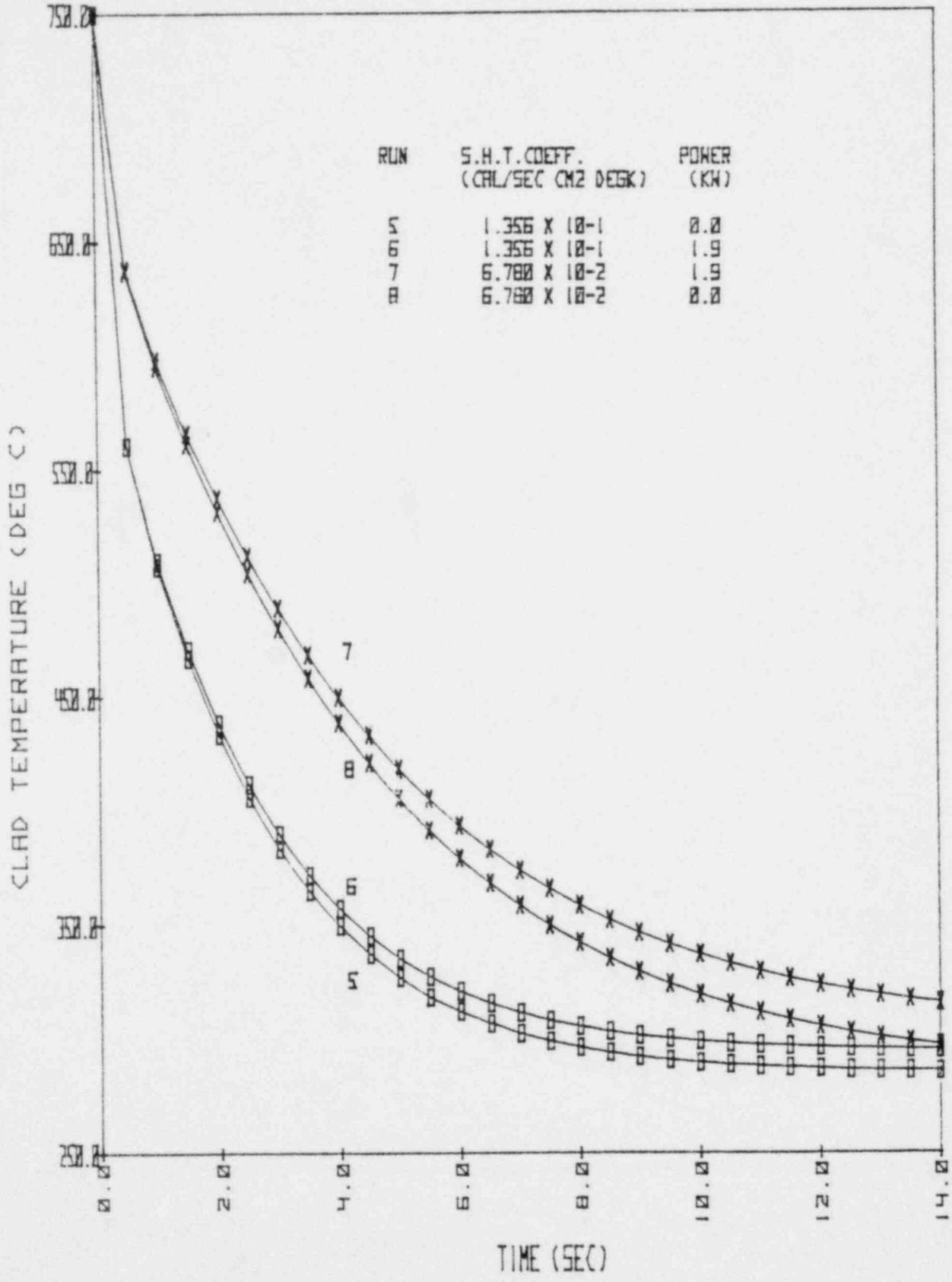


COMPUTED PARAMETER HEAT1 DATA, OCTOBER, 1979.

FIGURE B4

# ELECTRIC HEATER ROD COOLDOWN RATES

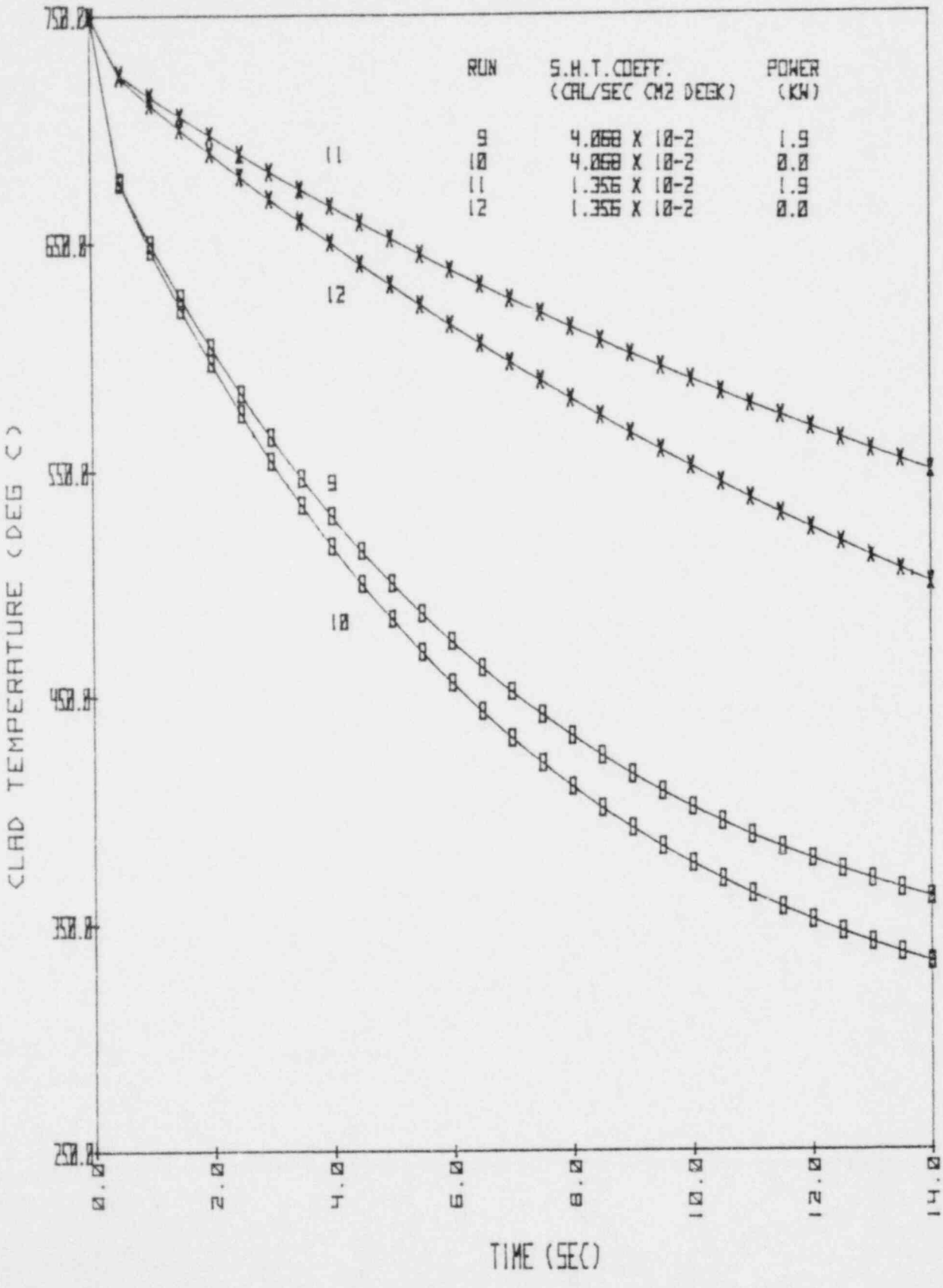


COMPUTED PARAMETER HEAT1 DATA, OCTOBER, 1979.

# APPENDIX C

## ORIFICE DISCHARGE COEFFICIENTS

# APPENDIX C

## ORIFICE DISCHARGE COEFFICIENTS

The orifice sizes for the LTSF tests were calculated using the standard orifice Equation below to provide the test section flooding rates specified in Table 1.

$$Q = C_d A_o \sqrt{\frac{2 g_c \Delta P}{\rho}}$$

where

$Q$ = volumetric flow rate

$C_d$ = discharge coefficient

$A_o$ = orifice area

$g_c$ = gravitational constant

$\Delta P$ = pressure drop across orifice

$\rho$ = upstream fluid density

A discharge coefficient of 0.6 was assumed to properly size the orifices. Following the tests, the actual orifice discharge coefficients were evaluated from the measured flow rates and pressures of each test run. Flange taps or pipe taps were not used to measure the actual pressure drop across the orifice. Instead, to compute the

orifice pressure drop, a calculation was made of the difference between the upstream pressure, which was determined from the PE-4A measurement (located a short distance upstream of the orifice), and the downstream pressure, which was determined from the test section pressure PE-2A. For the orifice to pipe diameter ratios used, the pressure recovery downstream of the orifice is very small. Therefore, the test section pressure can be reasonably assumed to be very close to the vena contracta pressure immediately downstream of the orifice. The difference between the measured pressures of PE-4A and PE-2A provide a reasonable pressure drop to be used in the orifice equation. The test conditions and discharge coefficients are given in Tables C-1 and C-2 for the tests with and without external thermocouples, respectively. The discharge coefficient for each orifice size, averaged over all the test runs are presented in the following table.

| Orifice Size (mm) | Average Discharge Coefficient |
|---|---|
| 0.8 | 0.628 |
| 1.6 | 0.626 |
| 3.454 | 0.647 |
| 4.496 | 0.609 |
| 6.299 | 0.624 |

Although orifice flange pressure taps would be required to evaluate accurate discharge coefficients, the above method provides valuable information for sizing orifices for the second phase of testing.

TABLE C-1

ORIFICE DISCHARGE COEFFICIENTS FOR TEST RUNS WITH EXTERNAL THERMOCOUPLES

| Run No. | Nominal Orifice DIA. (mm) | Orifice DIA at Test Conditions (mm) | ΔP Across Orifice (MPa) | Orifice Inlet Fluid Density $Kg/m^3$ | Volumetric Flow Rate l/sec | Orifice Discharge Coefficient |
|---|---|---|---|---|---|---|
| 11 | 3.454 | 3.47 | 5.55 | 747.5 | -- | -- |
| 13 | 3.454 | 3.47 | 5.6 | 647.4 | 0.779 | 0.626 |
| 12 | 3.454 | 3.47 | 4.67 | 721.9 | 0.691 | 0.642 |
| 10 | 3.454 | 3.47 | 4.64 | 754.3 | 0.694 | 0.661 |
| 14 | 3.454 | 3.47 | 4.7 | 748.7 | 0.680 | 0.641 |
| 11A | 3.454 | 3.47 | 4.83 | 751.1 | 0.691 | 0.644 |
| 11B | 3.454 | 3.47 | 4.6 | 749.6 | 0.677 | 0.646 |
| 17 | 4.496 | 4.516 | 5.7 | 655.6 | 1.249 | 0.591 |
| 20 | 4.496 | 4.516 | 6.16 | 652.9 | 1.325 | 0.602 |
| 15 | 4.496 | 4.516 | 5.34 | 755.4 | 1.220 | 0.641 |
| 21 | 6.299 | 6.327 | 3.96 | 747.9 | 2.019 | 0.623 |
| 23 | 6.299 | 6.327 | 4.6 | 750.6 | 2.175 | 0.625 |
| 3 | 0.8 | 0.8 | 8.91 | 999.4 | 0.0425 | 0.632 |
| 1 | 0.8 | 0.8 | 1.33 | 996.5 | 0.17 | 0.653 |
| 8 | 1.6 | 1.608 | 5.83 | 681.7 | 0.164 | 0.618 |
| 7 | 1.6 | 1.608 | 5.12 | 749.9 | 0.147 | 0.62 |
| 6 | 1.6 | 1.608 | 4.86 | 752.0 | 0.144 | 0.625 |
| 24 | 3.454 | 3.47 | 4.88 | 748.3 | 0.708 | 0.655 |

TABLE C-2

ORIFICE DISCHARGE COEFFICIENTS FOR TEST RUNS WITHOUT EXTERNAL THERMOCOUPLES

| Run No. | Nominal Orifice DIA. (mm) | Orifice DIA at Test Conditions (mm) | ΔP Across Orifice (MPa) | Orifice Inlet Fluid Density $Kg/m^3$ | Volumetric Flow Rate l/sec | Orifice Discharge Coefficient |
|---|---|---|---|---|---|---|
| 11 | 3.454 | 3.47 | 5.07 | 753.1 | 0.731 | 0.665 |
| 13 | 3.454 | 3.47 | 5.95 | 648.5 | 0.796 | 0.621 |
| 12 | 3.454 | 3.47 | 5.2 | 720.9 | 0.711 | 0.625 |
| 10 | 3.454 | 3.47 | 5.27 | 755.1 | 0.731 | 0.654 |
| 14 | 3.454 | 3.47 | 5.25 | 756.0 | 0.725 | 0.65 |
| 11A | 3.454 | 3.47 | 5.14 | 756.0 | 0.719 | 0.652 |
| 11B | 3.454 | 3.47 | 5.25 | 752.5 | 0.731 | 0.654 |
| 17 | 4.496 | 4.516 | 5.65 | 653.0 | 1.254 | 0.595 |
| 20 | 4.496 | 4.516 | 5.58 | 651.7 | 1.257 | 0.599 |
| 15 | 4.496 | 4.516 | 5.18 | 750.3 | 1.175 | 0.624 |
| 21 | 6.299 | 6.327 | 4.38 | 748.8 | 2.155 | 0.633 |
| 23 | 6.299 | 6.327 | 5.2 | 751.7 | 2.28 | 0.616 |
| 3 | 0.8 | 0.8 | 9.32 | 1000.0 | 0.0425 | 0.618 |
| 1 | 0.8 | 0.8 | 1.43 | 996.0 | 0.0164 | 0.61 |
| 8 | 1.6 | 1.608 | 6.55 | 679.3 | 0.176 | 0.622 |
| 7 | 1.6 | 1.608 | 5.68 | 748.7 | 0.159 | 0.634 |
| 6 | 1.6 | 1.608 | 5.82 | 751.9 | 0.161 | 0.639 |
| 24 | 3.454 | 3.47 | 5.21 | 749.3 | 0.750 | 0.673 |

# APPENDIX D

## ACTUAL TEST CONDITIONS

TABLE D-1

ACTUAL TEST CONDITIONS FOR TESTS WITH EXTERNAL THERMOCOUPLES

| Run No. | Primary System Pressure (MPa) | Initial Test Section Pressure (MPa) | Primary System Fluid Temp. (K) | Test Section Inlet Density ($Kg/m^3$) | Test Section Inlet Quality | Test Section Flow Rate (Kg/sec) | Average Test Section Inlet Fluid Velocity (m/sec) |
|---|---|---|---|---|---|---|---|
| 11 | 12.4 | 6.83 | 558.6 | 742.1 | 0 | -- | -- |
| 13 | 12.75 | 6.98 | 600.5 | 179.3 | 0.161 | 0.504 | 7.52 |
| 12 | 11.7 | 6.93 | 571.8 | 381.8 | 0.048 | 0.499 | 3.49 |
| 10 | 11.93 | 7.16 | 555.6 | 754.3 | -0.009 | 0.523 | 1.86 |
| 14 | 11.9 | 7.15 | 558.0 | 741.8 | -0.001 | 0.509 | 1.84 |
| 11A | 12.06 | 7.18 | 557.5 | 742.7 | -0.012 | 0.519 | 1.87 |
| 11B | 11.68 | 7.01 | 558.0 | 741.8 | -0.005 | 0.507 | 1.83 |
| 17 | 13.0 | 7.15 | 598.8 | 197.1 | 0.147 | 0.818 | 11.11 |
| 20 | 13.5 | 7.25 | 599.8 | 196.3 | 0.149 | 0.865 | 11.79 |
| 15 | 12.64 | 7.2 | 555.6 | 745.8 | -0.019 | 0.922 | 3.31 |
| 21 | 11.2 | 7.12 | 557.8 | 742.1 | -0.009 | 1.51 | 5.44 |
| 23 | 11.77 | 7.07 | 557.5 | 742.7 | -0.009 | 1.632 | 5.88 |
| 3 | 9.0 | 0.086 | 304.4 | 995.4 | -- | 0.042 | 0.114 |
| 1 | 1.41 | 0.086 | 304.3 | 995.4 | -- | 0.017 | 0.046 |
| 8 | 12.97 | 7.06 | 589.7 | 233.3 | 0.111 | 0.112 | 1.28 |
| 7 | 12.4 | 7.2 | 558.5 | 740.6 | -0.004 | 0.110 | 0.40 |
| 6 | 12.05 | 7.13 | 574.8 | 743.5 | -0.014 | 0.109 | 0.39 |
| 24 | 12.12 | 7.13 | 559.0 | 739.8 | -0.006 | 0.53 | 1.92 |

TABLE D-2

ACTUAL TEST CONDITIONS FOR TESTS WITHOUT EXTERNAL THERMOCOUPLES

| Run No. | Primary System Pressure (MPa) | Initial Test Section Pressure (MPa) | Primary System Fluid Temp. (K) | Test Section Inlet Density ($Kg/m^3$) | Test Section Inlet Quality | Test Section Flow Rate (Kg/sec) | Average Test Section Inlet Fluid Velocity (m/sec) |
|---|---|---|---|---|---|---|---|
| 11 | 12.47 | 7.25 | 556.8 | 744.0 | -0.017 | 0.55 | 1.98 |
| 13 | 13.2 | 7.08 | 601.1 | 183.9 | 0.16 | 0.516 | 7.51 |
| 12 | 12.2 | 6.86 | 572.8 | 365.1 | 0.052 | 0.513 | 3.75 |
| 10 | 12.35 | 7.0 | 555.7 | 745.8 | -0.013 | 0.552 | 1.98 |
| 14 | 12.35 | 7.0 | 555.2 | 746.6 | -0.015 | 0.548 | 1.96 |
| 11A | 12.04 | 6.8 | 555.1 | 746.6 | -0.012 | 0.544 | 1.95 |
| 11B | 12.25 | 6.91 | 557.1 | 743.3 | -0.005 | 0.55 | 1.97 |
| 17 | 13.0 | 7.3 | 599.6 | 199.9 | 0.147 | 0.819 | 10.96 |
| 20 | 12.98 | 7.16 | 599.8 | 192.7 | 0.152 | 0.819 | 11.37 |
| 15 | 12.1 | 6.87 | 558.0 | 748.7 | 0.0 | 0.882 | 3.15 |
| 21 | 11.58 | 6.96 | 558.5 | 740.6 | -0.002 | 1.613 | 5.83 |
| 23 | 12.0 | 6.55 | 557.2 | 743.2 | 0.006 | 1.713 | 6.17 |
| 3 | 9.4 | 0.086 | 302.5 | 996.0 | -- | 0.042 | 0.113 |
| 1 | 1.51 | 0.086 | 302.7 | 995.9 | -- | 0.016 | 0.044 |
| 8 | 13.47 | 6.82 | 590.6 | 216.6 | 0.122 | 0.119 | 1.47 |
| 7 | 12.68 | 6.92 | 559.2 | 711.8 | 0.002 | 0.119 | 0.45 |
| 6 | 12.7 | 6.81 | 557.5 | 742.7 | -0.001 | 0.122 | 0.44 |
| 24 | 12.34 | 7.0 | 558.9 | 740.0 | -0.002 | 0.562 | 2.03 |